

**DEVELOPMENT AND APPLICATION  
OF A PHYSICAL MODEL  
FOR THE ESTIMATE OF THE  
RATE AND PROBABILITY  
OF EARTHQUAKE OCCURRENCE**

**FLAMINIA CATALI**

*Dipartimento di Sismologia e Tettonofisica  
Istituto Nazionale di Geofisica e Vulcanologia*

catalli@ingv.it

**PhD THESIS**

**GEO/10 GEOFISICA DELLA TERRA SOLIDA**

ALMA MATER STUDIORUM  
UNIVERSITÁ DI BOLOGNA

Dipartimento di Fisica  
Settore di Geofisica

**Submitted: March 2007**



**TITLE OF THE THESIS:**

*DEVELOPMENT AND APPLICATION OF A PHYSICAL MODEL  
FOR THE ESTIMATE OF THE RATE AND PROBABILITY OF  
EARTHQUAKE OCCURRENCE*

**PhD STUDENT:**

Flaminia Catalli

**CHAIRPERSON**

Prof. Michele Dragoni

**SUPERVISING PROFESSOR**

Prof. Maria Elina Belardinelli

**SUPERVISORS**

Dr. Massimo Cocco

Dr. Rodolfo Console



*Nature does not reveal her secrets easily*

D. Vere-Jones, *Forecasting earthquakes and earthquake risks* (1995)



# Contents

<b>Introduction</b>	<b>1</b>
<b>1 The RSM: new insights from a theoretical point of view</b>	<b>7</b>
1.1 First aims and initial hypothesis . . . . .	7
1.2 An elastic model of the rectangular source . . . . .	9
1.3 A primary approach to the RSM . . . . .	13
1.4 An application of the RSM to a rectangular fault . . . . .	18
1.5 Temporal behavior of the triggered seismicity . . . . .	21
1.6 Discussion, match points and open questions . . . . .	25
<b>2 A more realistic version of the model</b>	<b>31</b>
2.1 The new practical version of the model . . . . .	31
2.2 The Coulomb Failure Function . . . . .	32
2.3 To model a sequence . . . . .	34
2.4 The parameters of the model and the maximum likelihood method	36
2.4.1 The relation between the reference seismicity and the shear stress rate . . . . .	38
2.5 From expected seismicity rate to probability of occurrence . . . . .	41
2.6 Discussion on the growing points . . . . .	42
<b>3 Application of the RSM to the 1997 Colfiorito seismic sequence</b>	<b>43</b>
3.1 The seismic sequence . . . . .	43
3.2 Fixing the input parameters . . . . .	46
3.3 Performing the best value of $A\sigma$ with the maximum-likelihood method . . . . .	50
3.4 Modeling seismicity rate changes . . . . .	54
3.4.1 The role of the $A\sigma$ value . . . . .	59
3.4.2 The role of the effective friction coefficient value . . . . .	60
3.4.3 The role of the reference seismicity rate . . . . .	60
3.4.4 Considering stress heterogeneity on the fault . . . . .	64
3.5 Modeling temporal behavior . . . . .	66
3.6 Probability estimates . . . . .	71

---

3.7	Discussion and conclusions . . . . .	77
<b>4</b>	<b>Unifying the epidemic and the rate-state models</b>	<b>81</b>
4.1	Stochastic model for earthquake clustering . . . . .	82
4.2	The Epidemic Rate-and-State (ERS) model . . . . .	84
4.3	Testing the ERS model through the Japanese seismicity . . . . .	87
4.4	Testing the ERS model through the seismicity of California . . . . .	93
4.5	Discussion on the ERS model achievements and final remarks . . . . .	97
	<b>Final remark and speculations on the future</b>	<b>101</b>
	<b>Curriculum Vitae</b>	<b>117</b>

# List of Figures

1.1	Slip distribution on the source defined in equation (1.1). . . . .	11
1.2	Conventions adopted for the reference system and for the parameters of the fault's orientation. . . . .	12
1.3	Shear stress [MPa], $\sigma_{12}$ , parallel to the slip direction for a strike-slip fault projected on the fault plane ( $x_1x_3$ ), $x_2 = 0.2$ km. . . . .	13
1.4	Distribution of the triggered seismicity against time for different values of induced shear stress. . . . .	15
1.5	Distribution of the number of expected events in four different cases: (a) for a positive value of earthquake shear stress; (b) for a negative value; (c) the sum of the two previous cases and (d) the integral of (c) over time. . . . .	17
1.6	Representation of the total number of induced events in different arbitrary slices around the principal fault after different intervals of time. . . . .	22
1.7	Analogous of figure (1.6). This histogram represents the distribution farther from the fault at longer intervals time. . . . .	23
1.8	Spatial distribution of the density of induced events at $t=0.01, 1$ and 100 years. . . . .	24
1.9	Comparison between the temporal distribution of the cumulative number of induced events closer from the source corresponding to synthetic data and the best fits obtained by the Omori law. . . . .	26
1.10	As figure 1.9 but for the events farther from the source. . . . .	26
3.1	Description of the main events characterizing the region . . . . .	44
3.2	Description of the main events characterizing the 1997 Umbria-Marche seismic sequence. . . . .	47
3.3	Temporal behavior of the studied seismicity during the time interval of the whole sequence. . . . .	48
3.4	Smoothed seismicity of the previous 11 years before the Colfiorito sequence. . . . .	50
3.5	Trend of the log-likelihood ratio ( $\ln(L_D/L_P)$ ) versus the $A\sigma$ values. . . . .	53

---

3.6	Trend of the total number of expected events under the RSM versus $A\sigma$ values. . . . .	53
3.7	Trend of the log-ratio between the expected rates for the RSM and the Poisson model respectively on the hypocentral coordinates of the catalog. $A\sigma = 0.04 MPa$ . . . . .	55
3.8	Expected seismicity rate changes . . . . .	57
3.9	Expected seismicity rate changes . . . . .	58
3.10	The role of $A\sigma$ on rate estimate . . . . .	61
3.11	The role of $A\sigma$ on rate estimate . . . . .	62
3.12	The role of $\mu$ on rate estimate . . . . .	63
3.13	Smoothed seismicity of the previous 16 years before Colfiorito . .	64
3.14	Expected seismicity rate at different times considering past events.	65
3.15	Three examples of maps calculated introducing stress heterogeneity on the fault. . . . .	67
3.16	Trend of the modeled temporal behavior for different values of $A\sigma$	68
3.17	Trend of the modeled temporal behavior for different values of $A\sigma$	69
3.18	Trend of the modeled temporal behavior for $A\sigma = 0.04 MPa$ . . .	70
3.19	Trend of the modeled temporal behavior for different values of $A\sigma$ for a long time period. . . . .	72
3.20	Trend of the modeled temporal behavior for different values of $A\sigma$ for a long time period. . . . .	73
3.21	Reference map for the evaluation of the probabilities of earthquake occurrence. The map refers to September 26 <sup>th</sup> (09:39 UTM) with $A\sigma = 0.04 MPa$ and $\mu = 0.05$ . . . . .	74
3.22	Trend of the probability versus $A\sigma$ . . . . .	77
4.1	Smoothed seismicity of Japan and of the surrounding area during the years 1970-2003. . . . .	87
4.2	Log-performance factors achieved by the ETAS-b and ERS models respectively, against the Poisson one. . . . .	92
4.3	Modeled rate density expected before the October 19 <sup>th</sup> , 1996 with the ERS model. . . . .	94
4.4	Log-performance factors achieved by the ETAS-b and ERS models respectively, against the Poisson one. . . . .	96

# List of Tables

1.1	Source parameters used in numerical applications. . . . .	12
1.2	Constitutive parameters used in equation (1.5). . . . .	14
1.3	Values of the parameters used in the numerical applications of the RSM. . . . .	16
1.4	Relations between fault parameters and total aftershock production around it, $N_{tot}$ . . . . .	20
1.5	Relations between fault parameters and total aftershock production around it, $N_{tot}$ . . . . .	20
1.6	Relations between fault parameters and total aftershock production around it, $N_{tot}$ . . . . .	20
1.7	Results obtained for the best-fit of the sets of data reported in figure (1.6) by the relation (1.10). $\sigma$ indicates the standard deviation of the cumulative number of events. . . . .	25
2.1	Parameters of the model. . . . .	36
3.1	Information of the main events occurred in the studied area used for CFF computations. . . . .	45
3.2	Outcomes of the maximum-likelihood method applied to search the best value of $A\sigma$ . . . . .	52
3.3	Estimated values of $A\sigma$ for aftershocks sequences reported by various authors. . . . .	54
3.4	Evaluated probabilities in selected areas varying $A\sigma$ . . . . .	75
3.5	Evaluated probabilities in selected areas varying $\tilde{\mu}$ . . . . .	76
4.1	Best fit values of the parameters of models ETAS-a, ETAS-b and ERS obtained on the learning period of the Japanese catalog. . . . .	89
4.2	List of the 28 target events and their occurrence rate density under the Poisson, ETAS-b and ERS models respectively. . . . .	91
4.3	Best fit values of the parameters of models ETAS-a and ERS obtained on the learning period of the Californian catalog. . . . .	95



# Introduction

Natural hazards are assuming ever greater social and economic importance, both in regional and in global scale. The earthquake hazard still stands out as one of the most intractable. Nevertheless, aftershocks hazard assessment is critical for the whole society; in particular in real-time, for emergency planners in the immediate aftermath of a destructive earthquake, in order to intervene and plan information for media and for the population, when the information need is greatest. Early warning procedures, based on the real-time, can play an important role in reducing the negative impact of such catastrophic events on densely populated areas and in mitigating the damage to structures and lifelines.

Our goal in this work has been to perform a physical model, and its transcription in a numerical code, that could be a significant and practical contribution to seismic hazard and early warning systems. We have exploited the most recent progresses in the physical and statistical description of the phenomenon of clustering with the aim to develop and test a robust and original procedure for earthquake forecasting.

We have been interested therefore to perform a physical model that could describe both spatially and temporally the earthquake interactions. For this goal we have integrated two principal ingredients: the Coulomb Failure Function (CFF) model and the Rate-and-State Model (RSM).

The CFF approach is one of the physical models mainly used for time-independent seismic hazard estimates in the last years with encouraging results. The combination of the CFF model with the RSM (and so with a time dependent friction law) allows to extend the forecast of potential areas of increased seismicity (via CFF) with aftershock decay rates, i.e. a temporal forecast of activity changes.

The RSM is nowadays considered one of the most powerful tool to evaluate probability changes in the expected seismicity rates, being both physically based and statistically testable.

The CFF model takes into account the static stress changes (or triggers) that occur instantaneously and permanently and that are the main cause of earthquake interactions. It is based on the hypothesis that coseismic stress increases promote, while stress decreases inhibit, failure on active faults, depending on

their mechanical state expressed by the static friction coefficient. Several phenomenological studies have confirmed the reality of static stress change triggering, as we will discuss in section (2.2). But the CFF model alone can not explain two important phenomena of earthquake triggering: the possibility that even small stress changes could provoke changes in seismicity rates and the delay that often elapses between the stress change and the failure.

The *Dieterich* (1994) model, based on rate-and-state friction theory, can justify both these behaviors, as we will deepen in chapter (1) and (3). Briefly, the explanations are both in the effect of the frictional response of the fault to the applied perturbation, imaging the fault as a part of an infinite population of patches close to failure. The closer the fault to failure, the smaller stress change needed and the shorter the time delay. In this way, the phenomenon of triggering is not considered as a threshold process (*Ziv and Rubin*, 2000; *Ogata*, 2005). It represents primarily a clock-advance failure, rather than a creation of new earthquakes (*Toda et al.*, 2005).

We will discuss and generalize the RSM both from a purely theoretical prospective (chapters (1) and (2)), as many other authors have made (*Gomberg et al.*, 2000, 2001; *Ziv and Rubin*, 2003; *Gomberg et al.*, 2005b; *Console and Catalli*, 2006), and through an application to a real case study (chapter (3)), as *Gross* (2001); *Toda and Stein* (2003); *Toda et al.* (2005) and *Catalli et al.* (2006) have also discussed.

Developing a RSM we faced with a few critical, challenging open questions related to such a model. The most difficult was to define and estimate a realistic, complete and reliable reference seismicity rate (see chapter (3) for details).

In the RSM the reference seismicity has a fundamental role. *Toda et al.* (2005) argued that even small stress increases can immediately activate sites of high background seismicity because it can amplify the expected rate. They also observed that the background seismicity can mitigate the expected rates too. The choice of the reference rate can therefore influence the good comprehension of the outcomes. Let us mention, for example, that the ability to observe seismicity rate declines (i.e. stress shadows) is hampered by low background rate, because the rate must be high enough, before the perturbing earthquake, to measure a decrease (*Ziv and Rubin*, 2003; *Gomberg et al.*, 2005a; *Marsan*, 2006).

In the RSM one needs to define a *reference seismicity* that not necessarily has to be identified exactly with the *background*. For *background* seismicity we mean the seismicity rate of previous years when unperturbed, i.e. in absence of any triggers<sup>1</sup>.

For our purposes we will represent the reference seismicity as a smoothing of

---

<sup>1</sup>Frequently the two terms *background seismicity rate* and *reference seismicity rate* are used indifferently to indicate the same concept, also in this work. We will highlight the difference when important during the text.

the whole seismicity of the previous years before the sequence (see chapters (2) and (3)). We therefore consider it as spatially variable but time independent. Nevertheless, few open questions remain to deepen: is it correct or unimportant to represent the seismicity rate as stationary and time independent (see *Hainzl and Ogata (2005)*; *Lombardi et al. (2006)*; *Lombardi and Marzocchi (2007)*)? How long the time window has to be to correctly define it without including the effects of the long-lasting sequences (see *Marsan (2003)*; *Marsan and Nalbant (2005)*; *Console and Catalli (2006)*)?

Finally, let us observe that the problem of the reference seismicity rate does not concern only a more precise definition of it, but sometimes, as in the case that we will face, the lack of sufficient data in the region does not permit to properly evaluate it.

The RSM involves several parameters to be assessed and this represents another challenge of such type of modeling. Our greatest effort during the work was to reduce the number of free parameters to one,  $A\sigma$  (the constitutive source parameter). In the literature many authors have suggested possible ranges for  $A\sigma$  (see chapter (3) for details). We will demonstrate that this parameter can highly affect the final results. We try therefore to find its best value through a statistical tool in chapters (2) and (3).

The phenomenon of triggering has been modeled not only by physical process, as we have just discussed above, but also by statistical ones. From a statistical viewpoint the so-called epidemic model (the Epidemic Type Aftershock Sequences model, the ETAS), introduced by *Ogata (1988)*, and its variations, have become fairly well known in the seismological community. Tests on real seismicity, and comparison with the plain time-independent Poissonian model, through likelihood-based methods, have reliably proved its validity.

In an epidemic system, no earthquake is claimed to be fully linked to any other earthquake in particular, but rather to all previous events and to the background seismicity, with different weights. A purely stochastic model as the ETAS, however, ignores the physical interpretation of earthquakes.

During our work on the RSM we have tried to unify such physical model with the ETAS one, with the aim to test a new hybrid model (an Epidemic Rate and State one, the ERS model) which unifies in itself physical and statistical laws. In this way we have tested the performance of the application of the rate-and-state laws in a pure epidemic process, verifying the simplifications needed in such a case.

Stress transfer, and so rate changes, leads to changes in probability of earthquake occurrence. To put in practical use the scientific knowledge on triggering it is more comprehensible for common people to speak about probability changes. More scientifically, the need to formulate models for earthquake occurrence in probabilistic terms arises also from the growing recognition of the

several difficulties in managing early warning procedures against earthquakes. *Vere-Jones* (1995) recognizes three major obstacles: i) the complexity of earthquake formation; ii) extensive and reliable data on triggering phenomena are expensive to collect, and take a long time to accumulate; iii) processes which have their origin some tens of kilometers below the Earth's surface are not directly observable. These difficulties demonstrate the impossibility to treat the earthquake occurrence and interactions in deterministic terms. Therefore, predictions should be formulated in terms of probability, i.e. the expectation in the time-space-magnitude domain, of the occurrence of an earthquake.

To date, just some attempts have been made in providing information on earthquake predictions to the society: for the recurrence of large earthquakes over periods of tens of years (*Working Group on California Earthquake Probabilities*, (2003), for details visit <http://pubs.usgs.gov/of/2003/of03-214/>); of aftershocks over period of days (*Wiemer*, 2000); in some places as time-dependent shaking maps (e.g. see *Cramer et al.* (2000)).

Such critical information requires studies of its credibility before being disseminated to the public. The contrary can provoke incidents which could discredit the scientific basis of the predictions (see *Vere-Jones* (1995)). Several authors have stressed the need of testings and validations.

*Parsons* (2005) explored the variability, parameter sensitivity, and limitations of the time-dependent approach. He used simple statistical tools to asses how large a stress change must be to significantly change the probabilities. He shows that we should be confident in the probability estimates only when the perturbing stress change is large relative to the tectonic stress rate and when the fault is well characterized.

This is consistent with the results of *Kagan et al.* (2005), who found that for southern California seismicity the impact of stress transfer from large earthquakes on recurrence of other faults is almost weak. They question whether this may be an observational limitation rather than a physical consequence.

*Reasenberget al.* (2003) emphasized the importance of considering a variety of probability models, combining estimates with appropriate weighting.

With regard to the tests against observations, authors as *Kagan and Jackson* (2000); *Console and Murru* (2001) and *Papadimitriou et al.* (2001) presented different approaches for testing the forecasting effectiveness of their models.

Finally, we would remember that some authors have suggested that spatially varying aftershock probabilities can be computed without calculating Coulomb stress changes.

*Wiemer* (2000) and *Wiemer et al.* (2002) proposed that observations of the initial portion of aftershocks sequences could be used to directly estimate the probabilities of later events.

*Felzer et al.* (2003) suggested that forecasts of late aftershocks based on earlier

events outperformed similar forecasts based on the main shock induced stress perturbation.

The next frontier in hazard assessment is to move away from static (stationary Poissonian) models towards time-dependent ones. In this context, we will estimate probabilities from time-dependent rate changes due to Coulomb stress variations. To objectively validate the robustness of the model we believe that it is necessary: i) testing and comparing the outputs against observations (not used in the derivation of the model), both qualitatively and statistically, as we have tried to do in chapter (3); ii) analyzing the impact of the free parameters on final results to be not led into unrealistic outcomes (we have stressed this point in chapter (3)); iii) objectively comparing the model against few others.

The last point represents to us the future challenge we are going to tackle in the context of the SAFER (Seismic eArly warning For EuRope) project (visit [www.saferproject.net](http://www.saferproject.net)).

The future aim is therefore to validate our procedure, testing the model among several others in the Euro-Med region, instead of individual test. We believe that such validation and quantitative hypothesis testing is the key to advance the presented procedure and earthquake science in general and to put aside the dangers of basing operational decisions on only partially tested hypothesis.



# 1

## The rate-state model for earthquake nucleation on a rectangular fault: a deepening and new insights from a theoretical point of view

Since the beginning of this work, our attention has been focused on the *Dieterich* (1994) model for earthquake nucleation and interaction, based on rate-and-state friction theory introduced by *Ruina* (1983) and *Dieterich* (1986, 1992, 1994). The original and significant characteristic of this model (for now on called RSM), is that it seems capable to physically justify the phenomenon of earthquake triggering in terms of space and time, considering the physical properties of the faults.

Here we would like to revisit the model from a purely theoretical prospective, seeking new insights. We also look for a relationship between the source parameters of an earthquake and the rate of all other subsequent events. For such a purpose we initially performed a numerical code that assumes very simplifying hypothesis. In this whole chapter we refer to this code. In the follow of the work a few of such hypothesis will be generalized to build a more complex and useful tool.

### 1.1 First aims and initial hypothesis

Our main goal in this chapter is to observe the spatio-temporal variation of the seismicity rate after a shear stress change, introducing in the algorithm a rate-state model approach. In particular, we try to identify a physically based relationship between the magnitude of the causative earthquake and the number of its aftershocks. We thus consider that a seismic events modify the stress field around the causative fault.

Some recent studies put in evidence that sudden stress variations, even of small magnitudes, can produce large variations of the seismicity rate. It is recognized as a phenomenon of triggering on faults that are already loaded by tectonic stress and in close-to-failure condition.

The seismicity rate increases in general where the shear stress change is positive, according to the Coulomb model (*Mendoza and Hartzell*, 1988; *Boatwright*

and Cocco, 1996; Stein *et al.*, 1997; Gomberg *et al.*, 1998, 2000; Harris, 1998; King and Cocco, 2001; Stein, 1999; Toda and Stein, 2000; Kilb *et al.*, 2002; Belardinelli *et al.*, 2003; Nostro *et al.*, 2005). These studies were able to give a physical interpretation for earthquake interaction observed in specific real cases, but they were not suitable to justify the time behavior of failure rates.

In particular, the Coulomb stress change criterion does not allow to model the hyperbolic time decay of the aftershock rate after a mainshock, known as the Omori law. In this simple model all the impending earthquakes would be clock-advanced by a constant time that depends on the stress change and on the loading rate but does not depend on the physical properties of the fault (Gomberg *et al.*, 1998). The experience shows that the Earth does not rather behave in this way. The most popular empirical description of the phenomenon is the Omori law, stating that the aftershock rate decays in time as  $t^{-1}$ . Moreover, above mentioned studies, based on Coulomb criterion, can not explain why the failure is often delayed from the occurrence of the stress change. Furthermore, they were not adequate for the general application of the model in predictive way, using only the information contained in a seismic catalog. Therefore, among the various theories modeling the Omori law, we have taken in consideration the one that assumes the rate-and-state friction law of faults.

We consider in the modeling only the static stress changes created by an earthquake. We have not considered, even without rejecting them in principle, other hypotheses that predict a time variation in stress, like viscoelastic relaxation or the diffusion of fluids in the crust.

The rate-state model for earthquake nucleation seems capable of substantially explaining all the phenomenology we are interested to. In this model a promoted failure does not occur instantaneously at the exceeding of a threshold stress as for the Coulomb-Amonton criterion, but follows a more complex non-linear time history with different phases. This time history depends on the physical properties of the fault.

Basing our work on the classical theory of the elasticity, we start from the formulation of the stress released by a rectangular fault with uniform stress-drop in a full space (see for details *Catalli (2006)*); then we apply the rate-state model (*Dieterich, 1994*) obtaining the complete time and space distribution of the seismicity induced by a given earthquake.

For modeling an extended source, in this chapter as in *Catalli (2006)*, we sum the different contributions of a number of point sources.

It is important to remark also that for present purposes we neglect the interaction between subsequent events, supposing that only the first event perturbs the stress field. We also neglect the effect of the free surface of the Earth.

In this preliminary study we focus our attention on the behavior of induced seismicity in space (specifically on the fault plane) and time and its relationship

with the fault parameters.

The results of simulations are analyzed to find out the scaling relationships existing between the free parameters of the model and the expected seismicity. These relationships will allow the validation of the model by real observations summarized in any seismic catalog.

Before going on, we want clearly enumerate the hypothesis we make in this preliminary version of the code:

- the effect of the free surface is neglected;
- only the static stress change is considered;
- a uniform stress drop is imposed on the source plane (but a non uniform dislocation);
- we do not consider the heterogeneity of the stress drop on the fault;
- the extended source is modeled as a certain number of acting point sources;
- we deal just with shear stress changes (we do not consider changes in normal stress);
- no interactions between events are regarded;
- all parameters of the model are arbitrarily fixed.

Though this first simple theoretical approach, we believe to preserve the capability of modeling the stress transfer from a seismic source to another that we are interested to analyze here. Several of these hypothesis have been generalized in the progress of the work aiming to a more versatile and detailed tool to make a more realistic forecast.

## **1.2 An elastic model of the rectangular source**

We will analyze the role of a finite, rectangular source in stress transfer and rate change. Therefore in this section we need to define an elastic model for such a source.

Suppose that a fault is embedded in a homogeneous, isotropic, elastic medium where the stress tensor  $\sigma$  is uniform. At a particular moment, the fault slips generating an earthquake, and suppose that the earthquake fully releases the component of the traction parallel to the slip vector across the fault. We call  $\Delta\sigma$  (the stress drop) the uniform negative change of traction on the fault.

It is well known that the slip distribution on a fault in similar conditions is not uniform. The slip distribution will satisfy the theory of the elasticity at the

new equilibrium, and it will be zero on the edges of the fault. It is also well known that the shear stress on the fault plane outside the edges of the fault increases significantly.

The analytical solution for the slip distribution on a fault at the equilibrium does not exist except that for very simple geometries, such as a rectangular fault of constant width and infinite length (*Knopoff*, 1957) and for a circular fault (*Keilis-Borok*, 1959; *Udias*, 1999). As mentioned by *Kostrov and Das* (1998), the analytical solution is not known even for a geometry as simple as a rectangular shape of width  $W$  and length  $L$ .

In the literature it is possible to find the computation of the stress field generated by an ideal rectangular fault with uniform slip in an infinite homogeneous space or half-space (*Chinnery*, 1961; *Iwasaki and Sato*, 1979; *Okada*, 1985, 1992). However this is not a realistic model since it implies the com-penetrability of the medium at the edges of the slip region. For this reason, here we make use of a non uniform slip distribution that is approximatively compatible with a uniform stress drop on the fault.

To calculate the static displacement, stress and strain, we start from the Somigliana Tensor and we make use of the double couple point source elastic theory (*Catalli*, 2006). Our model of an extended source is drawn heuristically from that of a rectangular fault infinitely extending in one direction and from that of a circular fault, and it is characterized by a slip distribution as:

$$\Delta u = \frac{\Delta\sigma}{\mu} \sqrt{\frac{\left[\left(\frac{W}{2}\right)^2 - x^2\right] \left[\left(\frac{L}{2}\right)^2 - y^2\right]}{\frac{LW}{4}}}, \quad (1.1)$$

defined for  $-W/2 \leq x \leq W/2$  e  $-L/2 \leq y \leq L/2$ , where  $x, y$  are the coordinates on the fault plane whose origin is coincident with the center of the rectangle,  $\Delta\sigma$  is the stress drop and  $\mu$  the shear modulus (rigidity) of the elastic medium. Figure 1.1 illustrates the behavior of the slip distribution on the source defined in equation (1.1). Equation (1.1) satisfies the condition of zero slip on the edges of the rectangle. This slip distribution is of a form very similar to that obtained numerically by *Kostrov and Das* (1998) with the finite differences method. Its analytical form is similar to the solution for a circular fault. Moreover, for a fault of square shape ( $W = L$ ) it achieves a seismic moment consistent with those obtained analytically for two circular faults, respectively inscribed and circumscribed to the square.

*Bonafede and Neri* (2000) have shown that, when imposing a unidirectional traction release in the strike or dip direction, a minor component of slip is present, over the fault plane, even in the direction perpendicular to the released traction. We have neglected this component.

For our numerical applications we discretize the continuous slip distribution of equation (1.1) with a set of point sources densely and uniformly distributed

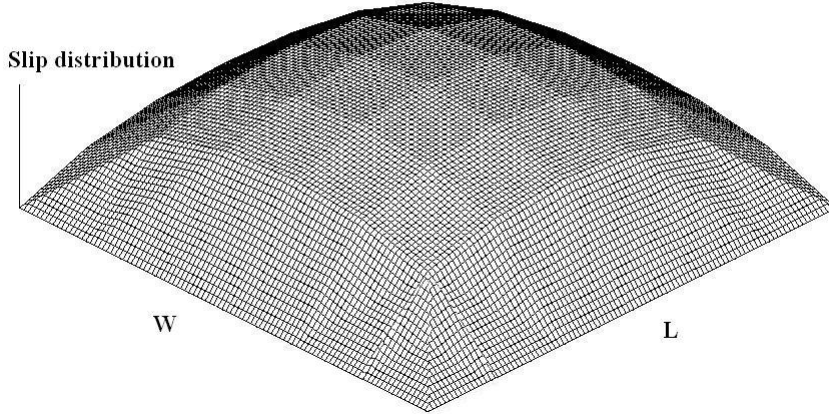


Figure 1.1: Slip distribution on the source defined in equation (1.1).

on the fault (*Catalli, 2006*). The more numerous the point sources, the more accurate the approximation.

In our numerical simulations, we arbitrarily, but without loss of generality, suppose that the fault is on the  $x_1, x_3$  plane. See figure (1.2) for the conventions we adopted for the reference system <sup>1</sup>. Let us notice that some fault parameters are connected among each other; in particular, the scalar moment  $M_0$  is defined through the relation:

$$M_0 = \mu \overline{\Delta u} W L = \frac{\pi^2}{16} \mu \Delta u_{max} W L = \frac{\pi^2}{32} \Delta \sigma (W L)^{3/2}, \quad (1.2)$$

where  $\overline{\Delta u}$  is the average slip on the fault and the maximum slip,  $\Delta u_{max}$ , is defined as:

$$\Delta u_{max} = \frac{\Delta \sigma \sqrt{L W}}{\mu \cdot 2}. \quad (1.3)$$

We also assume that the magnitude  $M$  is proportional to the logarithm of the seismic moment  $M_0$  (measured in  $Nm$ ) according to the *Kanamori and Anderson (1975)* relation:

$$\log_{10} M_0 = 9.1 + 1.5M. \quad (1.4)$$

<sup>1</sup>We briefly note that about the conventions in the reference system we found several mistakes in the texts we consulted, as *Udias (1999)*, *Aki and Richards (1980)* and *Stein and Wysession (2002)*. This mistakes, apparently trivial, could generate not negligible errors in the final results. We believe that figure (1.2) represents the solution to these questions.

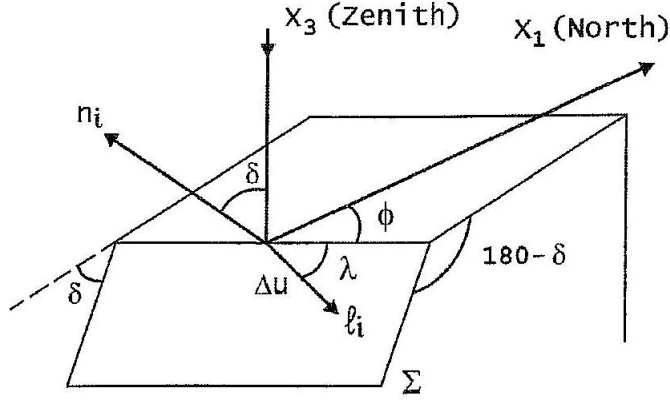


Figure 1.2: Conventions adopted for the reference system and for the parameters of the fault's orientation. The  $x_3$  axis is positive toward the Nadir direction. The strike is positive in clockwise; the dip and strike are positive in counterclockwise.

Table 1.1: Source parameters used in numerical applications.

Parameter	Value
Strike, dip and rake	0, 90, 0 degree
Dimension of the fault	(10 × 6) km
Spacing on the fault	0.1 km
Dimension of the grid	(30 × 30) km
Spacing on the grid	0.5 km
Magnitude	6

In this work, for sake of simplicity we make the assumption that all the aftershocks have the same focal mechanism of the causative earthquake. For the numerical applications in this chapter we make use of parameter values reported in table (1.1).

In figure (1.3) we can observe the major component of the stress field in such case,  $\sigma_{12}$ , that is the component parallel to the slip. Note that this figure shows the stress change and not its absolute value. The figure shows also that the shear stress  $\sigma_{12}$  is maximum near the edges of the fault, in particular along the slip direction  $x_1$ , and decreases with increasing the distance from the fault. Inside the fault the stress change is negative and approximately equal to the imposed value of  $-\Delta\sigma$ .

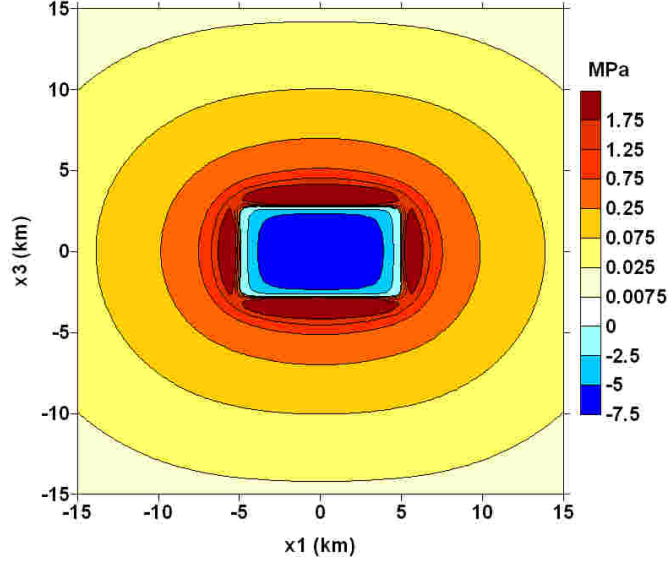


Figure 1.3: Shear stress [MPa],  $\sigma_{12}$ , parallel to the slip direction for a strike-slip fault projected on the fault plane ( $x_1x_3$ ),  $x_2 = 0.2$  km.

### 1.3 A primary approach to the RSM

We assume that the time-dependent behavior of the seismicity, triggered by a shear stress change in a population of faults, is described by the RSM introduced by *Dieterich* (1992, 1994), where the constitutive friction law proposed by *Ruina* (1983) and *Dieterich* (1986) is used.

The RSM model describes the seismicity rate changes as frictional failures on a distribution of nucleation patches that have been perturbed by a stress change; all these patches, constituting the population, are in different moments of their cycle-life, more or less close to failure, in a critical state. It is obviously a statistical simplification for describing a non deterministic phenomenon.

According to this model the rate  $R$  of earthquakes due to a  $\Delta\tau$  shear stress perturbation is given by:

$$R = \frac{r \frac{\dot{\tau}}{\dot{\tau}_r}}{\left[ \frac{\dot{\tau}}{\dot{\tau}_r} \exp\left(\frac{-\Delta\tau}{A\sigma}\right) - 1 \right] \exp\left(\frac{-t}{t_a}\right) + 1} \quad \dot{\tau} \neq 0, \quad (1.5)$$

whose various parameters are defined in table (1.2). Note that equation (1.5) does not account for the magnitude of the earthquakes, for the distribution of which we assume the classical Gutenberg-Richter frequency-magnitude relationship. However, both  $R$  and  $r$  refer to the number of earthquakes in a specific magnitude range.

Table 1.2: Constitutive parameters used in equation (1.5).

Symbol	Description
$r$	reference seismicity rate
$\dot{\tau}$	shear stressing rate
$\dot{\tau}_r$	reference stressing rate
$\Delta\tau$	earthquake shear stress change
$A$	fault constitutive parameter describing the direct effect of friction
$\sigma$	normal stress
$t$	time
$t_a$	characteristic time for seismicity to return to the steady state
$t_c$	characteristic time over which $\mathcal{R}(t)$ is maximum and constant

The main novelty of this model is that the expected seismicity depends not only on the amplitude of the stress perturbation  $\Delta\tau$ , but also on the physical constitutive properties of the fault, expressed by the temporal evolution of the friction coefficient and the effective normal stress, as well as on the reference seismicity  $r$ .

We have just observed that the major advantages of the application of the RSM are the capability to explain the temporal decay of the seismicity and to justify the variations of time delays between subsequent events (*Gomberg et al.*, 2000, 2005a).

*Dieterich* (1994) has shown that the characteristic time,  $t_a$  (the time at which the rate returns back to the reference value), is related to the stress rate,  $\dot{\tau}$ , of the area by the relation:

$$t_a = \frac{A\sigma}{\dot{\tau}}. \quad (1.6)$$

Here and in the following we make the assumption  $\dot{\tau} = \dot{\tau}_r$ . The interpretation of this assumption is that the primary earthquake does not change the long-term stress rate due to the tectonic driving forces in the environment.

It is easily understandable from (1.5) that the integral of  $R$  over infinite time diverges. This is due to the fact that the limit of  $R$  for  $t \rightarrow \infty$  is the reference rate  $r$ . Therefore, we prefer to deal with the net triggered seismicity rate  $\mathcal{R} = R - r$ .

The plot of  $\mathcal{R}$  versus time for different values of  $\Delta\tau$  is shown in figure (1.4) (see also *Dieterich* (1994)). It shows that the initial value of the triggered seismicity rate, immediately after the triggering event, is proportional to the exponential of the stress variation, but the time period over which  $R(t)$  is maximum and relatively constant decreases exponentially by the same factor for increasing shear stress change. This time period,  $t_c$ , in substantial agreement with *Dieterich* (1994), can be obtained computing the intersection between  $\mathcal{R}(t = 0)$  and the

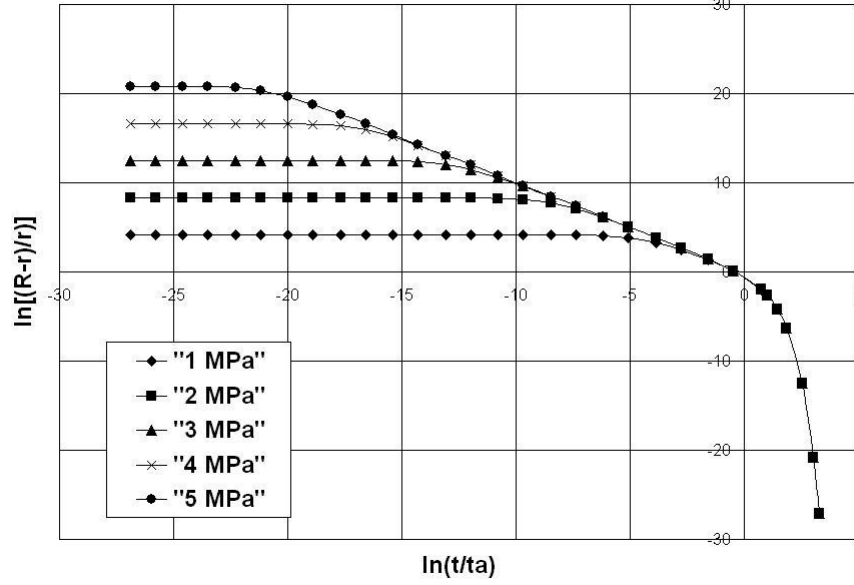


Figure 1.4: Distribution of the triggered seismicity against time for different values of induced shear stress. Other parameters are fixed arbitrarily.

straight line corresponding to the limit of  $\mathcal{R}$  when  $\Delta\tau \rightarrow \infty$ :

$$t_c = -t_a \ln \left[ 1 - \exp \left( -\frac{\Delta\tau}{A\sigma} \right) \right]. \quad (1.7)$$

The difference with the result of *Dieterich* (1994) is that we have preferred to make use of  $\mathcal{R}$ , rather than  $R$ , and we ignore the case  $\dot{\tau} = 0$  which we judge not realistic in the case study of earthquake interaction. Such time period,  $t_c$  ranges from few hours for a variation of  $\Delta\tau = 5MPa$  to nearly one year for  $\Delta\tau = 1MPa$  (we refer to table (1.3) for parameter values imposed).

Thus we can state that there are two critical times introduced by the RSM involved in the temporal trend predicted,  $t_a$  and  $t_c$ , both detectable in figure (1.4).

Figure (1.4) finally shows that the total duration of the triggered seismicity is the same for any stress change, but the shape of the decay is different for different  $\Delta\tau$ .

For the identification of the temporal behavior of  $\mathcal{R}$  the tuning of the parameter  $A\sigma$  plays a fundamental role because it is involved both in the computation of seismicity rate response to CFF, (1.5), and in definition of the two characteristic times, (1.6) and (1.7). In this chapter we fix an arbitrarily value of  $A\sigma$  leaving to chapter (3) a more detailed analysis of the complex role of this parameter in the model.

Table 1.3: Values of the parameters used in the numerical applications of the RSM.

Parameter	Value
$r$	$4\text{events}/(1\text{y} \cdot 1000\text{km}^2)$
$\dot{\tau}$	$5 \text{ KPa/y}$
$\dot{\tau}_r$	$5 \text{ KPa/y}$
$A$	0.008
$\sigma$	$30 \text{ MPa}$
$t_a$	$48 \text{ y}$

Let us note that, with respect to the Omori law, such kind of temporal behavior, predicted by the RSM, has a more complex meaning.

*Dieterich* (1994) has affirmed the substantial agreement of this model with Omori law; but, the trends illustrated in figure (1.3) are clearly sensible to the different values of stress change, somewhat that the Omori law does not take into account.

The empirical trend expected by the Omori law is a sort of a general mean of the various temporal decays observed during a sequence of events. We will face again and deepen this aspect in chapter (3), when we will analyze the temporal behavior of the results obtained applying the model to a real case study.

The integration of  $\mathcal{R}$  over infinite time leads to the not completely trivial result that the total number of triggered events in an area of constant stress change is proportional to  $\Delta\tau$ :

$$\int_0^\infty \mathcal{R}(t)dt = \frac{rt_a}{A\sigma} \Delta\tau = \frac{r}{\dot{\tau}} \Delta\tau. \quad (1.8)$$

This relationship, predicted by the friction model, had just been observed for Landers aftershocks also by *Gross and Kisslinger* (1997).

We consider the integral over time of the triggered seismicity rate  $\mathcal{R}$ , once for a positive  $\Delta\tau$ , and then for a negative  $\Delta\tau$  of the same size, and we sum the two functions. We obtain a quantity that initially has a positive increase and then tends back to zero (see figure (1.5)). This result can be interpreted as a sort of conservative law of the seismicity by saying that the expected total number of aftershocks generated in a place close to a fault can be balanced, at long range, by the total number of those events that are inhibited by the stress drop in a place internal to the fault, if the stress drops are equal in absolute value. It seems to us that this circumstance has been ignored, so far, in all previous studies on this subject.

As we told above, for numerical applications in this chapter we refer to table (1.3) for the parameter values which had been inferred from several geophysical

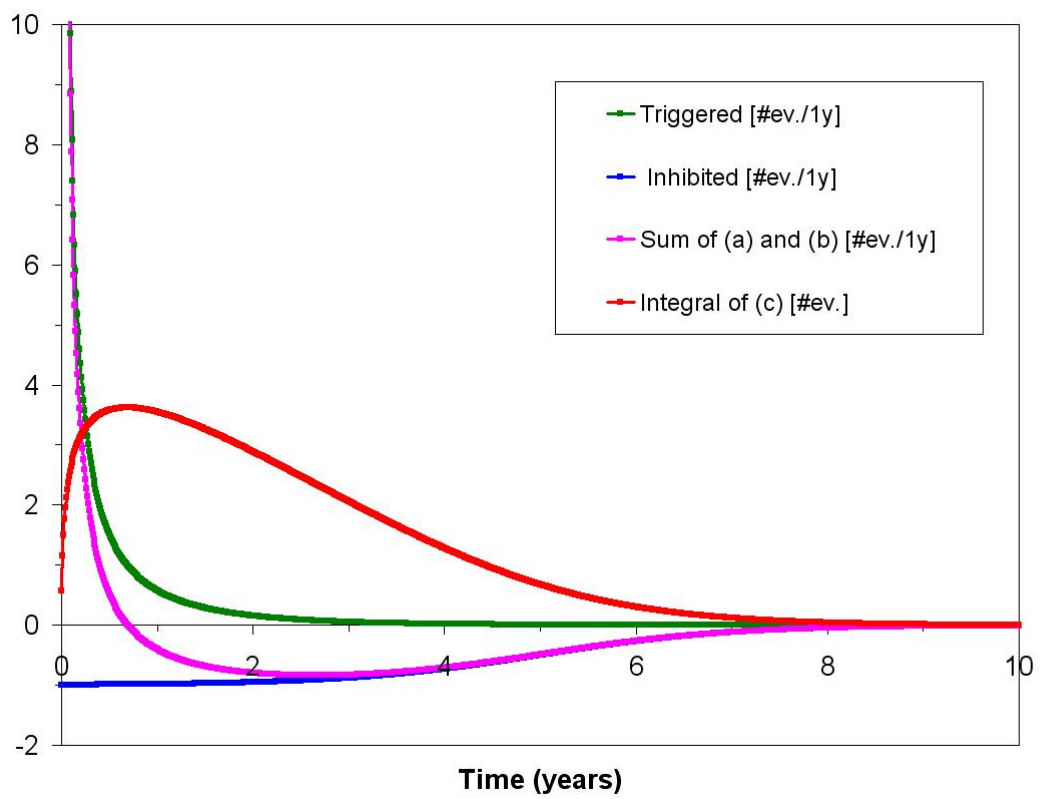


Figure 1.5: Distribution of the number of expected events in four different cases: (a) for a positive value of earthquake shear stress equal to 5 MPa, (b) for a negative value equal to -5 MPa, (c) the sum of the two previous cases and (d) the integral of (c) over time. The values of  $r$  and  $t_a$  are fixed at 1.

considerations.

The reference seismicity rate,  $r$ , is a quantity that should be known experimentally for a given area, and it is related to the average strain rate  $\dot{\tau}$  of that area. We use for  $r$  a uniform value of four events of magnitude exceeding 3.0 per year per 1000  $km^2$ , and for  $\dot{\tau}$  a value of 5  $KPa$  per year. These are simplifications of the reality where  $r$  and  $\dot{\tau}$  are not geographically uniform. These parameters seem however reasonable for an area of moderate seismicity.

The parameter  $A$  of the constitutive law has a value ranging from 0.005 to 0.015 obtained from laboratory experiments (*Dieterich*, 1994, 1995). Generally, simulations that most nearly resemble earthquakes in nature were obtained with rather small values of  $A$ , near to  $A \approx 0.001$ .

*Antonoli et al.* (2006) observed that the minimum value of  $A$  in literature is 0.003.

The value of  $A\sigma$  has been also evaluated for different sequences of earthquakes by several authors (*Harris* (1998); *Toda et al.* (1998); *Belardinelli et al.* (1999); *Stein* (1999); *Guatteri et al.* (2001); *Toda and Stein* (2003) and references therein; see table (3.3) for deepenings).

The parameter  $\sigma$  is the normal stress on the fault (of the order of some tens of  $MPa$ ). The characteristic time of aftershocks,  $t_a$ , depending on the other parameters through the relation (1.6), here assumes a value of the order of several tens of years. This value is essential to model a long term triggered seismicity, because the effect of the stress change disappears completely after a time of the order of the double of  $t_a$ .

## 1.4 An application of the RSM to a rectangular fault

*Dieterich* (1994) discussed in detail the case of a finite circular dislocation with uniform stress drop.

In this section we take into consideration a vertical, rectangular strike-slip fault embedded in an infinite, homogeneous, isotropic, elastic medium. The values assumed for the fault parameters are again those reported in table (1.1).

Assuming a constant stress drop  $\Delta\sigma$ , the scalar seismic moment  $M_0$  is proportional to the quantity  $(WL)^{3/2}$ , that can be considered a sort of equivalent source volume. Scaling  $W$  and  $L$  by a given factor,  $M_0$  scales accordingly, referring to equation (1.2), and also the shape of the stress distribution in space scales by the same factor according with the elastostatic theory.

Assuming that the reference seismicity rate is given as the number of events per unit volume and time, and integrating over the space, we find that the number of events triggered by the earthquake is thus proportional to the source volume, i.e. to the seismic moment  $M_0$ , or to  $10^{\frac{3}{2}M}$ , where  $M$  is the magnitude. But in this study we analyze only those aftershocks occurring on the fault plane

neglecting off-fault seismicity and assuming that this is the plane of weakness optimally oriented with respect to the tectonic loading stress.

The modeling of the space-time distribution of seismicity triggered by a rectangular source is straightforward, introducing in equation (1.5) the expression for the shear stress change  $\Delta\tau$  according to the theory presented in section (1.2). Let us notice again that we are here neglecting any contribution of the normal stress changes. But we can observe that on the fault plane the normal stress changes in a homogeneous and isotropic medium are likely to vanish. In this case (remaining only on the fault plane), the number of triggered events would be proportional to the fault area of the triggering event and then to  $M_0^{2/3}$ , or to  $10^M$ . If this scaling is true, one earthquake of magnitude  $M$  would have a number of aftershocks ten times larger than one earthquake of one magnitude unit smaller. Assuming, then, that the  $b$  value of the Gutenberg-Richter frequency-magnitude relation is equal to 1, it would follow that all the earthquakes of magnitude  $M$  produce the same number of aftershocks as the earthquakes of one magnitude unit smaller. This hypothesis is supported by the statistical analysis of real observations (*Utsu, 1969; Yamanaka and Shimazaki, 1990; Felzer et al., 2002; Helmstetter, 2003; Helmstetter et al., 2005*) and will be used in the following of the chapter.

A first group of numerical simulations, concerning the seismicity triggered by a rectangular fault with the RSM, have been performed to study the variation of the total number of triggered events (in space and time),  $N_{tot}$ , versus the main free source parameters: the stress drop  $\Delta\sigma$ , the linear dimensions  $L$  and  $W$  and the magnitude  $M$ . Tables (1.4), (1.5) and (1.6) show the results obtained assigning a fixed value for one of the parameters at time, and letting the others change according to equations (1.2) and (1.3). These simulations have been carried out by summation of the single contributions of the elementary cells constituting the area surrounding the fault. Only the seismicity triggered on the fault plane, but outside the fault edges, has been considered. Looking at table (1.4) one can notice that, under our hypothesis and for a constant stress drop, the total number of triggered events increases about proportionally to the fault area  $L \cdot W$ . Theoretically it should be exactly proportional to the area of the source, but in the computations there are numerical imprecisions due to the grid size approximations. These numerical simulations show, also, that the number of aftershocks is proportional to the  $2/3$  power of the scalar seismic moment (or to the exponential of the magnitude,  $10^M$ ), in agreement with the above theoretical arguments. Table (1.5) clearly shows the proportionality existing between the stress drop  $\Delta\sigma$  and  $N_{tot}$ , having fixed the linear dimensions of the fault. This is a simple consequence of the proportionality between the stress drop,  $\Delta\sigma$ , and the consequent shear stress change,  $\Delta\tau$ , at any point of the space around the source; thus, it is also an example of the proportionality expressed in equation

Table 1.4: Relations between fault parameters and total aftershock production around it,  $N_{tot}$ .  $\Delta\sigma$  is fixed at 4 MPa; the total area considered is of  $100 \times 100 \text{ km}^2$ . The source area is represented by  $L \cdot W$ .

$L \cdot W \text{ [km}^2\text{]}$	$M$	$M_0 \text{ [Nm]}$	$N_{tot}$
4	4.6	$9.9 \cdot 10^{15}$	13.4
25	5.4	$1.5 \cdot 10^{17}$	78.2
100	6.0	$1.2 \cdot 10^{18}$	263.2
225	6.4	$4.2 \cdot 10^{18}$	532.8

Table 1.5: The area of the fault is fixed at the value of  $100 \text{ km}^2$ ; the total area considered is of  $20 \times 20 \text{ km}^2$ .

$\Delta\sigma \text{ [MPa]}$	$M$	$M_0 \text{ [Nm]}$	$N_{tot}$
1	5.6	$3.1 \cdot 10^{17}$	51.8
2	5.4	$6.2 \cdot 10^{17}$	103.4
3	5.9	$9.3 \cdot 10^{17}$	155.2
4	6.0	$1.2 \cdot 10^{18}$	206.8
5	6.1	$1.6 \cdot 10^{18}$	258.6

Table 1.6: The value of  $M$  is fixed at 6.0; the total area considered is of  $20 \times 20 \text{ km}^2$ .

$L \cdot W \text{ [km}^2\text{]}$	$\Delta\sigma \text{ [MPa]}$	$N_{tot}$
4	510.7	<i>overflow</i>
25	32.7	597.6
100	4.1	223.2
225	1.2	107.8

(1.8) between  $\Delta\tau$  and the total number of triggered events, integrated on the whole space.

The results reported in table (1.6) give credit to the hypothesis that, for a constant magnitude, the earthquakes of smaller linear dimensions generate a larger number of triggered events. Indeed, a point source would yield the largest quantity of triggered events for the same magnitude.

Let us mention, lastly, the results of a simple numerical test. We just have theoretically shown, in the previous section, that the total number of events triggered by a stress change  $\Delta\tau$  per unit area is, after a time much larger than the characteristic time  $t_a$ , identical to the number of events inhibited by a negative shear stress change  $-\Delta\tau$  (figure (1.3)). The numerical simulations about an

extended source, with parameter still shown in table (1.1), reflect this idea in a more general way. In fact, if we take the total number of aftershocks produced in a time interval of 100 years by a fault of  $100 \text{ km}^2$  on the portion of an area of  $10^4 \text{ km}^2$  external to it, we find 353.2 events, while the same computation made including the negative contribution of the area internal to fault itself gives only 15.6 events (less than 5%). The idea of an overall null balance is, then, substantially met: we can conclude that the phenomenon of clustering does not change the long term seismicity rate of a large area. This is in contrast with the opinion that trigger zones produce many more shocks than are missing from the shadows (*Toda and Stein, 2003*). We nevertheless regard for *Marsan (2003)* that put in evidence the practical difficulty to observe in nature the lack of events (the quiescence) mainly when looking at weakly active regions and short timescales.

## 1.5 Temporal behavior of the triggered seismicity

We want consider now in more detail the dependence on time of the number of triggered events predicted by the RSM considering a rectangular source. *Kagan and Jackson (1991)* and *Dieterich (1994)* found, in their empirical works, that shallow aftershocks, above a given magnitude cutoff, decay globally (for different distance intervals) in about 10 years and this time decay appears to systematically decrease with increasing depth.

In our model the behavior in different zones depends on the different values of the stress changes, that decrease with the increasing distance from the edges of the fault. It can be then noted that the plateau of the plot of the seismicity rate versus time (see figure (1.4)) has a duration that increases with the increasing distance from the source. This result depends on our assumption of considering only aftershocks on the mainshock fault plane. It can also be biased by the fact that we consider only the effect of the static stress step  $\Delta\tau$  caused by a mainshock and we neglect the interaction between other events. We also do not account for heterogeneities of frictional constitutive properties nor for the dynamic stress concentration at the crack tip. In spite of that, we believe that our model can describe a behavior not so far from reality. Therefore we keep as our reference the model of fault given in table (1.1) again.

As shown in figure (1.6), in the close neighboring of the fault (within  $0.5 \text{ km}$  from the perimeter of the fault), most of the aftershocks occur within one day after the occurrence of the inducing earthquake, and more than  $1/3$  of them occur already in the first hour. This is clearly not the case for further distance from the source: in the slice between  $0.5$  and  $8.5 \text{ km}$  from the fault, about half of the activity is exploited within about one year. The further we go apart from the source, the longer is the time interval necessary for the exploitation of the triggered activity. In fact, in the distant zones (from  $20$  to  $100 \text{ km}$  from the

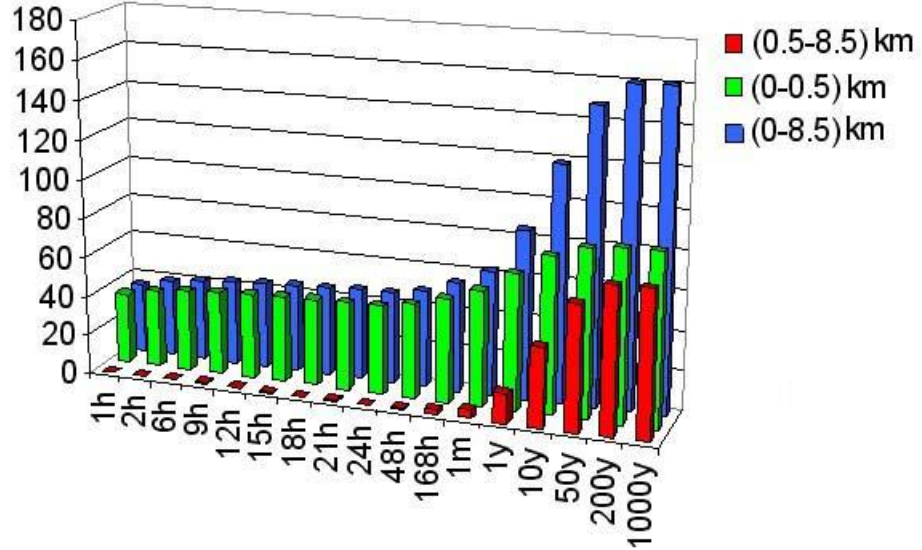


Figure 1.6: Representation of the total number of induced events (on vertical axis) in different arbitrary slices (red, green and blue columns) around the principal fault after different intervals of time (on horizontal axis). The distances of the limits of the slices are computed from the perimeter of the source and the reference magnitude in the simulation is 6.0. This histogram represents the distribution nearest to the source from shorter to longer intervals time (the time scale is purely qualitative).

fault) most of the triggered events occur longer than 20 years after the inducing earthquake (figure (1.7)).

The behavior shown in figure (1.6) and (1.7) is illustrated also by the snapshots of the spatial distribution of the seismicity rate at different times. Panels of figure (1.8) clearly show how the distribution of aftershocks resembles that of the stress change (figure (1.3)) and how the time decay is different in the different slices. These also show how shadow zones (where the seismicity is inhibited) last longer in time. We want remark again that we make the assumption that the aftershocks occur mainly on the fault plane and that these have the same focal mechanism of the causative event.

We are now interested to check if the generalized Omori law is suitable to describe the temporal behavior of  $\mathcal{R}(t)$  predicted by our model in every spatial slice and, in such case, by means of which free parameters. We refer to the generalized Omori law as to the formula describing the decay of aftershock rate

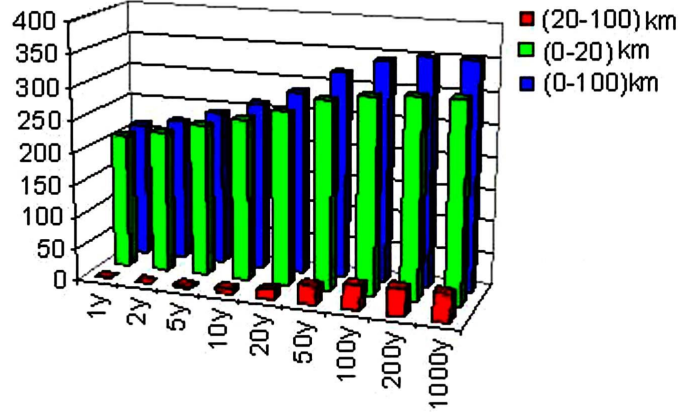


Figure 1.7: Analogous of figure (1.6). This histogram represents the distribution farther from the fault at longer intervals time.

after a mainshock (*Utsu et al.*, 1995) through three free parameters  $a$ ,  $c$  e  $p$ :

$$\mathcal{R}(t) = \frac{a}{(c+t)^p}. \quad (1.9)$$

For this purpose we make use of an algorithm for the least squares best-fit of the sets of data reported in figures (1.6) and (1.7) by the integral of (1.9) over the time:

$$y = \int_0^t \mathcal{R}(t') dt' = a \left[ \frac{(c+t)^{1-p} - c^{1-p}}{1-p} \right]. \quad (1.10)$$

The results obtained for the best-fit are shown in table (1.7). It is evident that the values of the parameters obtained are quite different from case to case (for instance, the  $c$  parameter is extremely small for the slices closest to the fault edges), and that the standard deviation  $\sigma$  of the cumulative number of events is larger for the slices that include the wider range of distances from the fault. These results show that the same set of parameters in equation (1.10) can not fit the synthetic values obtained for different zones. *Dieterich* (1994) reached a similar conclusion for a source model represented by a circular shear crack. However, his analysis was limited to the spatial variation of  $p$  parameter letting  $c = 0$ . The observation that the Omori  $p$  parameter varies spatially in real aftershocks sequences has been documented not only by *Dieterich* (1994)

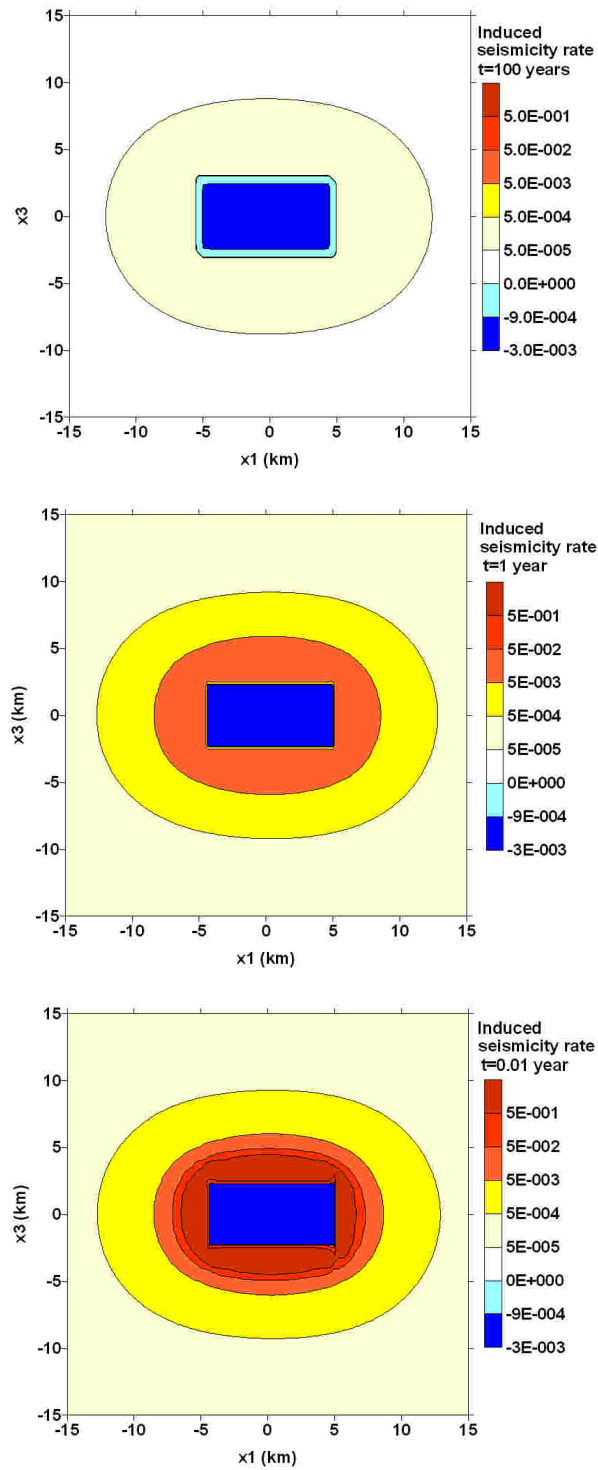


Figure 1.8: Spatial distribution of the density of induced events at  $t=0.01$ , 1 and 100 years.

Table 1.7: Results obtained for the best-fit of the sets of data reported in figure (1.6) by the relation (1.10).  $\sigma$  indicates the standard deviation of the cumulative number of events.

Slice [km]	$a [y^{p-1}]$	$c[y]$	$p$	$\sigma$
(0 ÷ 0.5)	$3.24 \pm 0.17$	$0.37 \cdot 10^{-7} \pm 0.2 \cdot 10^{-6}$	$1.02 \pm 0.02$	1.86
(0 ÷ 8.5)	$11.0 \pm 0.76$	$0.23 \cdot 10^{-7} \pm 0.2 \cdot 10^{-6}$	$0.91 \pm 0.032$	9.16
(0.5 ÷ 8.5)	$83.7 \pm 70.0$	$3.1 \pm 1.96$	$1.44 \pm 0.19$	3.3
(0 ÷ 20)	$34.3 \pm 8.0$	$0.13 \cdot 10^{-1} \pm 0.019$	$1.14 \pm 0.077$	9.22
(0 ÷ 100)	$36.8 \pm 9.1$	$0.15 \cdot 10^{-1} \pm 0.023$	$1.12 \pm 0.08$	10.8
(20 ÷ 100)	$(12.5 \pm 10.9) 10^3$	$61.0 \pm 5.43$	$2.8 \pm 0.96 \cdot 10^{-3}$	0.45

but also in a number of papers (*Wiemer and Katsumata, 1999; Wiemer, 2000; Enescu and Ito, 2002; Wiemer et al., 2002; Wiemer and Wyss, 2002*). *Wiemer et al.* (2002) reported a case of significantly different  $c$  values in the northern and southern Hector Mine aftershock volume, respectively. *Enescu and Ito* (2002) in their study of aftershock activity of the 2000 Western Tottory earthquake found  $c$ -values very close to 0 except for larger magnitude earthquakes, arguing that this feature could result from incompleteness of data, or might also reflect the complexity of the rupture process.

The situation is illustrated also by the plots of figures (1.9) and (1.10), showing the graphical comparison between the synthetic data and the relative theoretical approximation for different slices.

## 1.6 Discussion, match points and open questions

In the development of this first version of the model some approximations have been made. Three of the most important are **(a) having neglected the singularity introduced by the free surface of the Earth; (b) having neglected the dishomogeneity of the stress drop on the fault**, and consequently the very complicated pattern of slip (this must certainly have influence on the aftershock pattern: some aftershocks may even occur inside the fault, where the gradient of slip is high); **(c) having neglected the interaction between subsequent events**.

We will observe in the next chapter (2) that approximations (a) and (c) have been surpassed in the ongoing of the work. About hypothesis (b), we will deepen in chapter (3), section (3.4.4), that using the sum of a number of point sources as a solution for an extended source, at certain scales, we can generate a sort of numerical dishomogeneity that could simulate the dishomogeneity of the stress

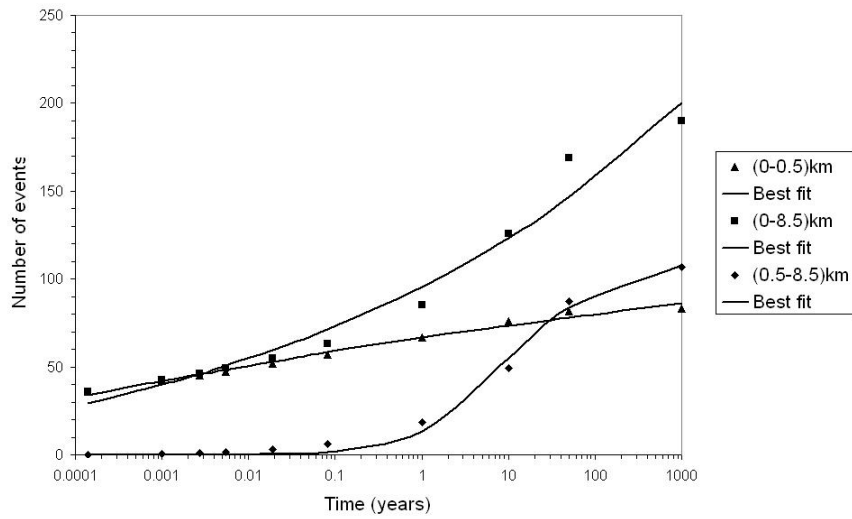


Figure 1.9: Comparison between the temporal distribution of the cumulative number of induced events closer from the source corresponding to synthetic data and the best fits obtained by the Omori law.

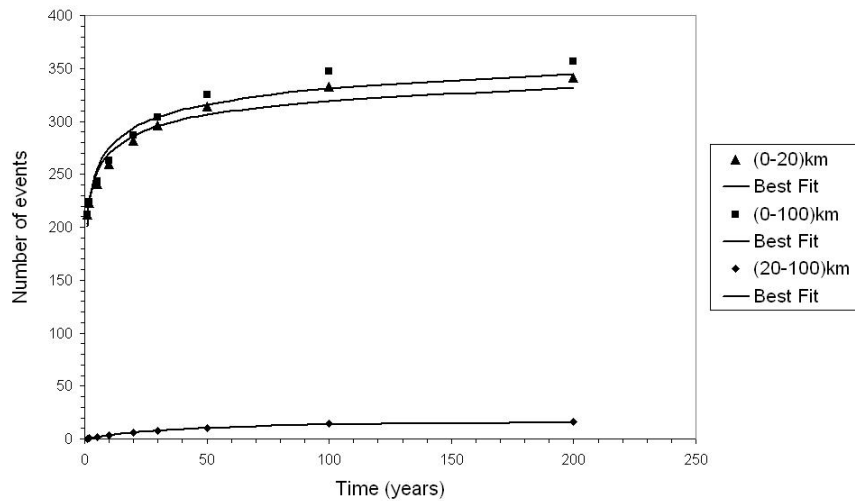


Figure 1.10: As figure 1.9 but for the events farther from the source.

on the fault. We will exploit this phenomenon to analyze the role of the stress heterogeneity in earthquake interactions.

In spite of these approximations, the first step of our modeling, concerning the stress change in the medium following an earthquake, has given results comparable to those of previous papers as, for instance, *Chinnery* (1961), *Nostro et al.* (1997), *King and Cocco* (2001), as *Catalli* (2006) has just delved into. This substantial agreement, though the simplifications introduced in this specific case of rectangular source, supports the validity of our methodology.

Neglecting the interaction among seismic events and using the rate-and-state model of *Dieterich* (1994) entails that the total number of triggered events per unit area is proportional to the shear stress change. Nevertheless, the time constant by which the rate of events decreases has a large variability, ranging from a fraction of hour for a shear stress change of several *MPa*, up to tens of years for stress variations smaller than 1 *MPa*.

A first set of simulations carried out with a model of rectangular fault, based on the hypothesis that most of the aftershocks occur on the same plane of the fault, has lead to the relationship between the main source parameters and the number of triggered events. The simulations lead to the conclusion that many earthquakes of small magnitude can produce, in total, a number of aftershocks comparable to that of fewer larger earthquakes. Our model predicts, in fact, that, for a constant stress drop, the number of triggered events is roughly proportional to the seismic moment at the power of  $2/3$ , or equivalently to  $10^M$ , as observed in various occasions.

*Helmstetter* (2003) and *Helmstetter et al.* (2005) suggest that this behavior can be related to the fractal structure of the spatial distribution of the seismicity and to the nature of earthquake interactions.

For a constant stress drop we also observe that the total number of triggered events is proportional to the area of the fault; on the other way, if the linear dimensions of the fault are kept constant, the number of triggered events is proportional to the stress drop.

An important aspect of the model concerns the time-space behavior of the triggered seismicity. The simulations show that the application of the RSM through equation (1.5) has as a consequence something more complicate than the conventional Omori law for the temporal decay of aftershock rate. In fact, the seismicity is expected to be intense (in accordance to the stress change) and have a maximum constant value close to the fault edges of the primary earthquake, but the time necessary for the starting of decay is shorter. On the contrary, the seismicity expected at larger distances (up to 10 times the linear dimensions of the fault) is weak, but the time necessary for the decay from the maximum value is longer (even some tens of years).

We can conclude that the temporal behavior of aftershock rate varies in space.

Moreover, the model predicts that the total long term production of aftershocks, including wider areas, is not negligible respect to the short term production. In this respect, the regional background seismicity could be interpreted as a sort of noise, or memory, due to the superposition of the effect of many older earthquakes.

The time decay described by the popular Omori law could be interpreted as an apparent average result of the contribution from the various areas on the plane containing the primary fault.

The RSM (Dieterich, 1994), used in our algorithm for the time distribution of the seismicity produced by a dislocation on a rectangular fault, has allowed just a partial justification of the Omori law, getting over it.

We outline the following main conclusions obtained from the simulations:

- The seismic activity is very intense during the first few hours or days after the occurrence time of the primary earthquake, in the rectangular slice close to the edges of the fault.
- The immediate decay of this intense activity is followed by a period of time during which the activity at larger distance (of the order of the linear dimensions of the fault) is nearly constant. For longer time (several years) the total number of triggered events in the external zone becomes comparable with that of the most internal one.
- The number of events triggered over a long time scale at distances larger than the fault linear dimensions is significantly large.
- The seismic activity inside the fault drops to negligible values at the occurrence of the primary earthquake and returns to normal values only after a time much longer than the characteristic time (several tens of years in our simulations); for a long time range the number of events inhibited inside the fault is comparable to that of the events triggered outside: the net balance can be considered null; the seismicity rate changes in space and time, but it does not have influence on the rate averaged over very large intervals of space and time.

In light of the consequences derived from our model, both positive and negative perturbations of the seismic activities, resulting from the interactions among earthquakes, would last for a time of the order of decades. In this respect, it seems unrealistic to define and observe what is specifically called *background seismicity* of an area. Nevertheless, we will see that it is necessary to define in some way this quantity if we are interested in applying the model to a real case.

Now then we are going to verify in several different cases that this matter about the choice of the reference seismicity is a controversial and crucial open question.

We can conclude that this first version of the model here analyzed, in spite of its very simple conception, gives a physical justification both to the very popular phenomenon of short term earthquake clustering (aftershocks and foreshocks in strict sense) and to that of the long term induction and quiescence, also observed in various occasions.



## 2

# A more realistic version of the model for applications to real case studies

In chapter (1) we have presented a first group of results on earthquake triggering obtained with the RSM. As we have highlighted, for this first approach to the RSM we used an algorithm with several strict hypothesis. But our final target is to perform an useful and versatile tool for earthquake forecasting. That is why in this chapter we present a new version of the model where the most part of the preliminary rigid hypothesis have been generalized.

### 2.1 The new practical version of the model

In section (1.1) we listed the restrictions we had made in the early stage of the modeling. In the next paragraphs we are going to generalize and discuss the most part of these restrictions. We anticipate here the most significant, new skills we included in the new version of the algorithm:

- we include the effect of the free surface of the Earth, imaging a 3-D half space;
- dislocations brought by extended sources are calculated using *Okada (1992)*'s solutions;
- the slip on the source is heterogeneous (when known);
- we take into account changes both in shear and normal stress considering the Coulomb Failure Function (hereinafter CFF);
- we regard to the interactions between the main events (to simulate a sequence).
- we reduce to one the free parameter of the model and we optimize its value with the maximum log-likelihood method;
- we introduce the possibility to evaluate, from the expected seismicity rate, the probability of occurrence in a space-time-magnitude window.

Only two hypothesis still hold steady: (a) we continue to ignore the dynamic stress variations and (b) we do not consider the heterogeneity of the stress drop on the fault.

Although we will use in this study only static stress changes, it is important to emphasize that the RSM can be applied to any arbitrary, complex stress perturbation.

According to *Marsan (2006)* and *Helmstetter and Shaw (2006)*, we do not ignore that the spatial heterogeneity of the stress field can explain in more detail the phenomenon of triggering; we decided to not consider this complexity in our model for seek of simplicity. However we will discuss this topic also later, in chapter (3), presenting some simple examples regarding the introduction of stress heterogeneity in the modeling.

Thereby, in the follow of our study we consider a 3-dimensional half space where stress changes are calculated using the numerical procedure proposed by *Okada (1985, 1992)*. This means that we now imagine the source plane as a whole and not as a discrete sum of point sources.

With the precise aim to apply the model to real cases and match these at the highest degree, now the slip on the fault is not imposed arbitrarily but comes from real information.

Let us discussing the other changes in more details.

## **2.2 The Coulomb Failure Function and its inclusion in the RSM**

The spatial evolution of seismicity during different seismic sequences has been commonly interpreted in terms of fault interaction caused by coseismic stress transfer.

The CFF model has been proposed as a robust tool to model fault interaction and earthquake triggering. It is based on the hypothesis that coseismic stress increases promote, while stress decreases inhibit, failure on active faults depending on their mechanical state expressed by the static friction coefficient (see *King et al. (1994)*; *Harris (1998)*; *King and Cocco (2001)* and references therein).

This model has been extensively applied and tested in numerous papers published in the literature, as that of *Stein et al. (1997)*; *Gomberg et al. (2000)*; *Kilb et al. (2002)*; *Nostro et al. (2005)*; *Steacy et al. (2005)*, among many others. Many recent papers have pointed out the role of stress transfer in earthquake occurrence by showing the correlation between the Coulomb stress changes and the seismicity rate changes (*Stein, 1999*; *Toda and Stein, 2003*; *Toda et al., 2005*), as well as with locations of main shocks (*Nostro et al., 2005*; *Steacy et al., 2005*).

We calculate the CFF, i.e. the capability of the mean to crack, caused by an earthquake dislocation in a homogeneous half-space using the 3-D algorithm

proposed by *Nostro et al.* (1997).

We consider here two different models for evaluating the CFF: the *constant apparent friction model* and the *isotropic poroelastic model* (*Beeler et al.*, 2000; *Cocco and Rice*, 2002).

*Cocco and Rice* (2002) affirmed that it is not possible a priori to decide the correct physical model between the two. They highlighted however the differences that could exist between the results of the two models, remarking that the isotropic poroelastic one implies a clearly choice of the time window. They concluded that the appropriate choice has to be made in function of the particular case study.

We are interested to verify if differences in expected seismicity rate could appear with the two different solutions introduced in the RSM.

We calculate the Coulomb stress change through the well-known general expression:

$$\Delta CFF = \Delta\tau + \mu(\Delta\sigma + \Delta P), \quad (2.1)$$

where  $\Delta\tau$  is the shear stress change calculated along the slip direction on the assumed fault plane,  $\Delta P$  is the pore pressure change,  $\mu$  is the friction coefficient and  $\Delta\sigma$  is the effective normal stress change (positive for extension).

The *constant apparent friction model* involves that  $\Delta P$  is proportional to the normal stress changes:

$$\Delta P = -B\Delta\sigma, \quad (2.2)$$

where  $B$  is the Skempton coefficient. Therefore, Coulomb stress changes are calculated through the widely used expression (see *Harris* (1998); *Cocco and Rice* (2002) and references therein):

$$\Delta CFF = \Delta\tau + \mu'\Delta\sigma, \quad (2.3)$$

where  $\mu' = \mu(1 - B)$  is the apparent friction coefficient.

To the other end, the *isotropic poroelastic model* provide, for changes in pore pressure, that:

$$\Delta P = -B\frac{\Delta\sigma_{kk}}{3}, \quad (2.4)$$

where  $\Delta\sigma_{kk}$  is volumetric normal stress change. Thus, the CFF in this case is calculated as:

$$\Delta CFF = \Delta\tau + \mu\left(\Delta\sigma - B\frac{\Delta\sigma_{kk}}{3}\right). \quad (2.5)$$

But stress changes alone can not explain the temporal evolution of seismicity, such as the Omori decay of aftershocks or the seismicity migration to which we are interested. As we have just stated in the previous chapter, in order to model both the spatial pattern of seismicity and the temporal decay of the rate of earthquake production, the fault constitutive properties have to be taken

into account. Thus, we want couple CFF changes with the RSM introducing in equation (1.5) the variations in CFF in place of  $\Delta\tau$ . In this case we would strongly remark the necessity, previously confirmed only by *Linker and Dieterich* (1992), *Dieterich* (2000, 1994); *Harris* (1998), to correct the value of the friction coefficient  $\mu = \tau/\sigma$ . In fact, for the nucleation solution the correct friction coefficient is:

$$\tilde{\mu} = \frac{\tau}{\sigma} - \alpha, \quad (2.6)$$

where  $\alpha$  is the constitutive parameter for the evolution of the state with normal stress acting. It seems to us that this necessary correction there was not treated with sufficient clarity, or even ignored, in recent papers concerning the coupling of CFF and RSM (we refer in particular to the works of *Toda and Stein* (2003); *Toda et al.* (2005)); therefore, in the next chapter, we are also going to investigate the role of  $\alpha$  in seismicity rates computations (section (3.4.2)). Let us note that this correction is valid and necessary both for positive and negative normal stress variations; in fact, as *Linker and Dieterich* (1992) stated that a sudden variation in  $\sigma$  results as a sudden change in the state that is symmetric with regard to increases versus decreases in  $\sigma$ . Thus, a pulse in normal stress produce no net variation in the state.

Therefore, when we introduce the CFF changes in the RSM, we have to consider the  $\alpha$  correction both in the constant apparent friction model:

$$\Delta CFF = \Delta\tau + \tilde{\mu} (1 - B) \Delta\sigma, \quad (2.7)$$

and in the isotropic poroelastic model:

$$\Delta CFF = \Delta\tau + \tilde{\mu} \left( \Delta\sigma - B \frac{\Delta\sigma_{kk}}{3} \right). \quad (2.8)$$

Observe that in (2.7) we correct  $\mu$  and not  $\mu'$  because it is  $\mu$  that multiplies the effective normal stress in equation (2.1). Adopting reasonable values for the parameters, as  $\mu = 0.75$ ,  $B = 0.45$  and  $\alpha = 0.25$ , in equation (2.7) the final apparent friction coefficient, that multiplies  $\Delta\sigma$ , is equal to 0.27 (not far from the 0.2 often assumed as in *King and Cocco* (2001)) and in equation (2.8) it is equal to 0.5.

## 2.3 How to model a sequence of stress perturbations with the RSM

To model the effect of repeated stress perturbations, we use the expression of seismicity rate  $R$  as a function of the state variable  $\gamma$  at the reference shear

stressing rate  $\dot{\tau}_r$ , proposed by *Dieterich* (1994) (see also *Toda and Stein* (2003) and *Toda et al.* (2005)):

$$R = \frac{r}{\gamma \dot{\tau}_r}, \quad (2.9)$$

where  $r$  is the reference seismicity of the considered area;  $\gamma$ , the state variable, evolves with time and stressing history. *Dieterich* (1994) shows that, under a constant stressing rate, the state variable is at the steady state and takes the value:

$$\gamma_0 = \frac{1}{\dot{\tau}_r}. \quad (2.10)$$

We have assumed that the stressing rate does not change before and after the main shock, being equal to  $\dot{\tau}_r$ , as we have just observed in the previous chapter. This implies that, in absence of any stress perturbation, the seismicity rate given by (2.9) is at the steady state and  $R = r$  (i.e.  $\gamma = \gamma_0$ ).

According to *Dieterich* (1994) the rate  $R$  can be interpreted as a statistical representation of the expected rate of earthquake production in a given magnitude range.

An applied stress perturbation to the fault population modifies the seismicity rate through the evolution of the state variable given by:

$$\gamma_n = \gamma_{n-1} \exp\left(\frac{-\Delta CFF}{A\sigma}\right), \quad (2.11)$$

where  $\gamma_{n-1}$  and  $\gamma_n$  are the values of the state variable before and after the applied stress change respectively. Let us note again that here we represent the coseismic stress perturbation in terms of a Coulomb stress change, CFF, calculated as described in the (2.2).

The same *Dieterich* (1994, 2000) showed that the evolution of state variable is governed by the following law:

$$d\gamma = \frac{1}{A\sigma} [dt - \gamma dCFF]. \quad (2.12)$$

The effect of a stress perturbation caused by an earthquake occurred nearby is to drop the state variable, so that the fault slips at higher rate. This produce a higher seismicity rate. After that, a decrease of the seismicity rate begins, according to the critical time  $t_c$ , as reported in equation (1.7). When the rate decreases, the state variable increases. The temporal evolution of  $\gamma$  is given by:

$$\gamma_{n+1} = \left(\gamma_n - \frac{1}{\dot{\tau}_r}\right) \exp\left(\frac{-\Delta t \dot{\tau}_r}{A\sigma}\right) + \frac{1}{\dot{\tau}_r}, \quad (2.13)$$

where  $t$  is the time step.

## 2.4 The parameters of the model and the maximum likelihood method

To compute the elastic stress perturbations we need to fix the source parameters as the focal mechanism, the magnitude, the linear dimension and the slip distribution, which are evaluable from real observations. To the other hand, three are the own parameters of the RSM to be assigned: the reference seismicity  $r$ , the reference shear stress  $\dot{\tau}_r$  and the fault constitutive parameter  $A\sigma$ , as table (2.1) highlights. The two critical times,  $t_a$  and  $t_c$ , are inferred from the previous parameters. Let us remember again that we hypothesize that  $\dot{\tau}/\dot{\tau}_r = 1$ .

Before going on, we feel now the need to spend some more words clarifying what we specifically mean for the *reference seismicity* instead of the *background seismicity* rates. Let us begin observing that for the RSM  $r$  represents the seismicity rate related to the reference shear stressing rate  $\dot{\tau}_r$ , and any other restrictions are imposed for its evaluation by *Dieterich* (1994). Therefore, for seeking of more clarity, we would precisely define the two different ways we consider to interpret  $r$ . The widely used in literature is the *background seismicity rate*: a spatially variable, time independent  $r$  that should be evaluated in a fixed time window on a *declustered catalog* (or on a catalog which is believed not to contain aftershock sequence). Even if this representation is the most common in literature, it is also further from reality because long lasting, secondary triggering make very difficult to identify a catalog without aftershock sequences. The second way to interpret  $r$  is as a simple *reference seismicity rate*: it is always evaluated in a fixed time window but on an *undeclustered* catalog.

In the follow of this work we will assume  $r$  as a reference seismicity rate.

Table 2.1: Parameters of the model.

Parameter	Description	Estimate by
$(\varphi, \delta, \lambda); m; L; W; \Delta u$	source parameters	real observations
$r$	reference seismicity rate	smoothing previous seismicity
$\dot{\tau}_r$	reference shear stress rate	an approximate relation within $r$
$A\sigma$	fault constitutive parameter	a likelihood best fit

Then we compute the reference seismicity rate by smoothing the whole seismicity (without declustering) of the previous years before the beginning of the studied sequence, according to the algorithm proposed by *Frankel* (1995). In this way, the reference seismicity rate is assumed spatially variable, but time independent and consequently the process stationary.

The reference seismicity is a crucial variable in any fault population model, which plays a very important role, as observed for example by *Toda et al. (2005)* studying the RSM. The choice of the background is also determinant in trying to define and observe the quiescence of seismicity, as observed by *Ziv and Rubin (2003)*; *Gomberg et al. (2005a)*; *Marsan (2006)*. Because of its importance, we would leave some open questions to be deepened in the future progress of the work, as: is it really correct to assume the reference seismicity as time independent and stationary<sup>1</sup>? In any case, how long the time window has to be to correctly estimate a smoothed reference background? And how to exclude the possibility that long-lasting sequences could contaminate such an estimate (mainly if we really want to estimate the *background*)? Some answers to these questions have been recently published by various authors.

*Hainzl and Ogata (2005)* and *Lombardi et al. (2006)* affirm that in volcanic areas, that is for short time periods, the background seismicity shows a time dependence and a non stationary behavior. They speak about the background as commonly interpreted by ETAS modelers (for details on ETAS model see chapter (4)): for them the background coincides with the rate of spontaneous events, without the presence of any cluster. We then can deduce that for the reference seismicity the time dependence is even more accentuated.

Moreover, *Lombardi and Marzocchi (2007)* observes a non stationarity in the time distribution of large worldwide earthquakes, over longer time windows too.

Finally, *Marsan (2003)*; *Marsan and Nalbant (2005)*; *Console and Catalli (2006)* cope with the difficulty to extrapolate a background seismicity from real data.

We have to observe that several problems could arise in selecting a reference seismicity if there are insufficient data relatively to the selected area.

The reference seismicity rate and the reference shear stress rate are not independent in a specific area. That idea was just discussed in *Console et al. (2006)*. Here we propose a more practical and rigorous version of the final relation between the reference seismicity and the reference shear stress, as revised by *Catalli et al. (2006)*. Let us note that to correctly apply such relation for estimate  $\dot{\tau}$  now it is necessary to deal with a reference seismicity rate (as we do) instead of the background rate, because the shear stressing rate refers to the tectonic seismic moment released by all the earthquakes.

---

<sup>1</sup>To clarify the different meanings between a *time independent* and a *stationary* process we send to *Lombardi and Marzocchi (2007)* and reference therein

### 2.4.1 The relation between the reference seismicity and the shear stress rate

Here we aim to explicitly motivate the approximate relationship between the reference seismicity rate  $r$  and the stressing rate  $\dot{\tau}_r$  of an area, presented for the first time by *Console et al.* (2006) and then revised by *Catalli et al.* (2006). We start from the Gutenberg-Richter relationship:

$$N(m) = 10^{a-bm} = N_0 10^{-b(m-m_0)}, \quad (2.14)$$

which defines the number of earthquakes  $N(m)$  with magnitude larger of a general value  $m$ ;  $a$  and  $b$  are the well known free parameters of that law<sup>2</sup> and  $N_0$  is the number of seismic events with magnitude larger than a given threshold  $m_0$ .

The seismic moment is related with the magnitude through the *Kanamori and Anderson* (1975) relationship (1.4) that we can write again as:

$$M_0(m) = M_0^* 10^{1.5(m-m_0)}, \quad (2.15)$$

where  $M_0^*$  is the seismic moment of an earthquake of magnitude  $m_0$ .

The number of earthquakes  $\Delta N$  comprised in a magnitude interval  $[m, m_0]$  is given by:

$$\Delta N(m) = N_0 - N = N_0 [1 - 10^{-b(m-m_0)}]. \quad (2.16)$$

Consequently, the number of earthquakes in a magnitude interval  $[m_0, m_{max}]$  is:

$$\Delta N = N_0 - N(m_{max}) = N_0 [1 - 10^{-b(m_{max}-m_0)}] \approx N_0, \quad (2.17)$$

which does not substantially differ from  $N_0$  even for small magnitude intervals.

According to the Gutenberg-Richter relation (2.14), the increment in the number of expected earthquakes for an infinitesimal increment of magnitude is given by:

$$\frac{d\Delta N}{dm} = b \ln(10) N_0 [10^{-b(m-m_0)}]. \quad (2.18)$$

The total seismic moment  $M_0^{tot}$  associated with the  $\Delta N$  earthquakes having magnitudes comprised in the interval  $[m_0, m_{max}]$  is:

$$\begin{aligned} M_0^{tot} &= \int_{m_0}^{m_{max}} M_0(m) \frac{d\Delta N}{dm} dm \\ &= b \ln(10) N_0 M_0^* \int_{m_{max}}^{m_0} 10^{(1.5-b)(m-m_0)} \\ &= b N_0 M_0^* \frac{1}{1.5-b} (10^{(1.5-b)(m_{max}-m_0)} - 1). \end{aligned} \quad (2.19)$$

---

<sup>2</sup> $a$  is equal to the natural logarithm of the number of events of magnitude 0 and  $b$  is the inverse of the slope of the predicted trend.

From this equation we can easily derive an expression for  $N_0$ :

$$N_0 = \frac{M_0^{tot}}{M_0^*} \frac{(1.5 - b)}{b} \frac{1}{(10^{(1.5-b)(m_{max}-m_0)} - 1)}, \quad (2.20)$$

that will be useful in the following.

We evaluate in practice, and thus we define here, the seismicity rate of reference as:

$$r = \frac{\Delta N}{\Delta T S_{tot}}, \quad (2.21)$$

where  $S_{tot}$  is the areal finite element we selected as the area of reference and  $\Delta t$  is the time window in which the  $\Delta N$  earthquakes occurred. According to equation (2.17), the previous one becomes:

$$r = \frac{1}{\Delta T S_{tot}} \frac{M_0^{tot}}{M_0^*} \frac{1.5 - b}{b} \frac{1}{(10^{(1.5-b)(m_{max}-m_0)} - 1)}. \quad (2.22)$$

We now assume that the selected group of  $N$  earthquakes occurs in a seismogenic volume  $V$  and we use the *Kostrov* (1974) approach to express the average stress tensor  $\bar{\sigma}_{ij}$  associated with the moment tensor  $M_{0ij}^k$  of these selected earthquakes:

$$\bar{\sigma}_{ij} = 2G\bar{\epsilon}_{ij} = \frac{1}{V} \sum_{k=1}^{\Delta N} M_{0ij}^k, \quad (2.23)$$

where  $\bar{\epsilon}_{ij}$  is the strain tensor and  $G$  is the rigidity. Considering that the tectonic load  $\sigma_{tect}$  is given by the shear stress components, we can write the following simplified expression:

$$M_0^{tot} = \sigma_{tect} V = \dot{\tau} \Delta T V \cong \dot{\tau} \Delta T W_{seis} S_{tot}, \quad (2.24)$$

where we have expressed the seismogenic volume as the product of the thickness of the seismogenic layer,  $W_{seis}$ , and the reference area. The substitution of this relation in equation (2.22) implies that we consider a seismogenic volume  $V$  large enough to contain an appropriate number of earthquakes, but at the same time small enough to image seismicity rate changes on a map view. This approximation is commonly performed when computing and plotting seismicity rates in maps.

Performing simple algebraic computations we finally obtain our desired relationship:

$$\dot{\tau} \cong \frac{r M_0^*}{W_{seis}} \frac{b}{1.5 - b} (10^{(1.5-b)(m_{max}-m_0)} - 1). \quad (2.25)$$

\*\*\*

We have so reduced the free parameters of the model to one,  $A\sigma$ , overcoming a drawback of the RSM consisting of poorly constrained parameters. We have just discussed the state of the art in the specific literature concerning  $A\sigma$  (in section (1.3)). And we also have just said that we can consider it as a unique parameter because it appears almost always as a multiplication. In section (1.3) we highlighted that in literature one can find a wide range of the values corresponding to  $A\sigma$ . For instance, *Harris* (1998) evaluated  $A\sigma$  for a specific aftershocks sequence found a value range ranging from 0.0012 to 0.6 *MPa*.

In our procedure we perform the best value of  $A\sigma$  from a maximum-likelihood best fit, testing the model with real seismicity of the studied area. The algorithm also compares it with a plain time-independent Poissonian model. This procedure for evaluating a free parameter is that used also by *Console and Murru* (2001); *Console et al.* (2003, 2006) and previously introduced by *Ogata* (1998). It consists in searching for the maximum of the log-likelihood function of a realization of  $N$  seismic events described by a catalog  $\{x_j, y_j, t_j, m_j; j = 1, \dots, N\}$ :

$$\ln(L) = \sum_{j=1}^N \ln[\lambda(x_j, y_j, t_j, m_j)V_0] - \int_X \int_Y \int_T \int_M \lambda(x, y, t, m) dx dy dt dm, \quad (2.26)$$

where

$$V_0 = \int_X \int_Y \int_T \int_M dx dy dt dm$$

is a coefficient whose dimensions are equal to those of the inverse of the rate density  $\lambda(x_j, y_j, t_j, m_j)$ . The rate density  $\lambda$  in this case corresponds to the rate of seismicity  $Re^{-\beta m}$  corrected by the Gutenberg-Richter law. The second term at the right-hand side of equation (2.26), that expresses the expected total number of triggered events ( $N_{tot}$ ), should be computed on the total space-time-magnitude volume spanned by the catalog.

The effort we made to fix all the parameters from physical observations, through a catalog information, and to evaluate the free parameter  $A\sigma$  with the maximum-likelihood method is a first important step to comply with the recognized need of a statistical validation of the forecasting models through the comparison between the predictions and the observed seismicity. This is a common need arisen from the recent development of earthquake interaction models as observed by *Marsan and Nalbant* (2005), *Wiemer et al.* (2005) and many others.

But, we have here to acknowledge that our using of the likelihood method for the moment is just a retrospective exercise. We so have to face up not only to the inadequacies of this test but also to the fallacy of prior knowledge in testing procedure. We are conscious that there is only one honest test and this is a prospective test. Nevertheless, throughout the application of the maximum likelihood method we have understood some important characteristics of our model and its application, that we will explain in detail in section (3.3).

The biggest problem of the likelihood test is that it places far too much weight on the least probable event. Let us make a simple thought case. Consider two forecast models, A and B, which are intended to forecast the occurrence of 100 future earthquakes. Model A successfully forecasts 99 events placing the probability of their occurrence equal to 1; but it also assigns probability 0 to the last event. Evaluating equation (2.26), one finds that  $\ln(L) = -\infty$  and so one would be led to reject the forecast as a failure. Model B assigns 0 probability to all the 100 events. The log likelihood values is again equal to  $-\infty$ . The statistical test then indicates that the two models perform the same (both failure), despite the fact that model A is a far better than model B and it provides much more information.

The above fallacy of the likelihood method in real applications has to face up to the problem of the localization errors: the combination of the two could easily leads to misleading results.

## 2.5 From expected seismicity rate to probability of occurrence

Our final goal in this study is to achieve a practical, useful and versatile tool to make forecasting. In the viewpoint that we can forecast seismicity behavior in real time with a good level of reliability, the easiest way to communicate with the society is to produce probability maps. We so introduced in the code the possibility to evaluate the probability of occurrence in a space-time-magnitude window.

It must be considered that the process we treat is a non stationary and with memory process. It is non stationary for its dependence to the time flow and it is with memory because it is connected with the past seismicity trough the reference seismicity. Nevertheless, we found in the literature (see *Vere-Jones* (1995) and references therein) the justification to can use also in this case the follow common relation, often associated with the plain time poissonian process, to calculate the probability:

$$P(\Delta S, \Delta T, m \geq \bar{m}) = 1 - \exp(-N), \quad (2.27)$$

where  $P(\Delta S, \Delta T, m \geq \bar{m})$  is the probability that almost one event of magnitude equal or major of a magnitude of reference  $\bar{m}$  occurs in the space-time window characterized by  $\Delta S$  and  $\Delta T$ ;  $N$  is the cumulative number of expected event in the same window calculated as:

$$N(m \geq \bar{m}) = 10e^{-b(\bar{m}-m_0)} \int_{V(x,y,t)} R(t, m \geq m_0) dV, \quad (2.28)$$

where  $R$  is the rate calculated with the RSM.

## 2.6 Discussion on the growing points

In this chapter we have not only generalized the most part of the strict hypothesis we made at the beginning, but we have deepened some key aspects of the proposed procedure and we have also overcome some important limits.

Let us retrace in order the most important growing points.

In other studies, coupling the RSM with the CFF, the necessity to correct the friction coefficient is not relieved with sufficient clarity, as we have observed in section (2.2) deepening this topic. We will investigate in chapter (3) what different values of  $\tilde{\mu}$  yield in the final results of expected seismicity rates and probabilities.

About picking the parameter values of the model, we have introduced some important and original novelties. First of all, we reduced to one the free parameter of the model. All the others could be fixed from real observations.

We proposed an original, physical relation to estimate the shear stressing rate from the reference seismicity in equation (2.25).

The unique free parameter,  $A\sigma$ , is a critical parameter of the RSM because it is not easily identifiable from observations and in literature very large ranges of it are proposed. So the most important change we have proposed is to apply a statistical tool, as the maximum log-likelihood method, to assess the value of  $A\sigma$ .

Finally, we have achieved now a practical and versatile model, and its arrangement in a numerical code, and we are ready to apply it to real cases needing only information from a catalog.

# 3

## Application of the RSM to the 1997 seismic sequence of Umbria-Marche, central Italy

In the previous chapter we presented a more practical version of the code relative to the RSM, generalizing the most part of the initial hypothesis.

Now that we have devised a tool able to be used in a more complex, realistic condition, we can apply it to a real case study. We have therefore selected the 1997 Umbria-Marche seismic sequence because of its peculiar characteristics regarding the spatio-temporal behavior. The presence of normal faulting aftershocks on the hanging wall of the main fault planes (i.e. on the shadows zones) and the extraordinary migration of seismicity have been interpreted in terms of fluid flow and pore pressure relaxation by *Miller et al.* (2004); *Nostro et al.* (2005); *Antonioli et al.* (2006).

Here we are interested to verify whether the RSM alone is able to justify the migration of seismicity occurred during this sequence and the presence of secondary earthquakes on stress shadows. We also perform for the first time the best fit of the unique free parameter  $A\sigma$  with the maximum log-likelihood method described in the previous chapter, finding original and unforeseen outcomes. We finally present some examples of rate and probability computations and the influence that some parameters have on them. All these results will help us to better understand the flaws and the qualities of the presented model.

### 3.1 The seismic sequence

Our main target is to model the seismicity rate changes during the 1997-1998 seismic sequence that struck the Umbria-Marche region, Central Apennines, Italy (see figure (3.1) and table (3.1)). Six main shocks of the 1997 sequence ruptured normal faults, consistently with the extensional tectonics active in this sector of the Apennines, and thousands of aftershocks followed in the next 40 days. Their focal mechanisms are shown in figure (3.1), together with those of the two largest events occurred in the region in the previous 20 years (the 1979 Valnerina and the 1984 Gubbio earthquakes) and that of the April 3<sup>rd</sup> 1998, the Gualdo Tadino earthquake, which occurred after the sequence at the northwestern edge of the

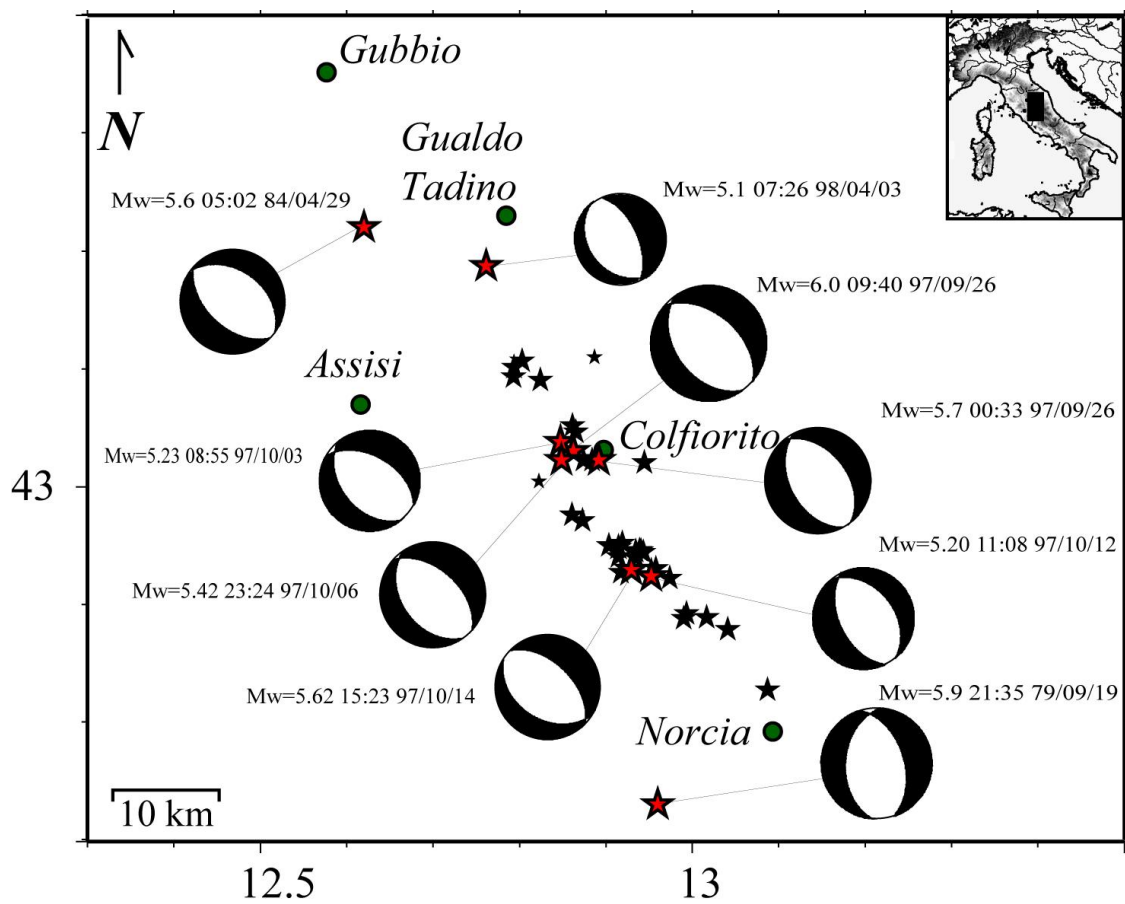


Figure 3.1: Description of the main events characterizing the region

Table 3.1: Information of the main events occurred in the studied area used for CFF computations.

Date	Lon	Lat	L [km]	W [km]	Dep [km]	$M_w$	$\phi$ [deg]	$\delta$ [deg]	$\lambda$ [deg]
79/09/09, 21:35	12.96	42.73	11	11	6.27	5.9	315	70	218
84/04/29, 05:02	12.34	43.13	7.5	4.0	6.5	5.6	135	35	270
97/09/03, 22:07	12.88	43.02	2.5	2.5	4.0	4.72	137	30	272
97/09/26, 00:33	12.89	43.02	7	7	5.7	5.69	152	46	277
97/09/26, 09:40	12.86	43.03	12	7	5.7	5.85	144	42	280
97/10/03, 08:55	12.85	43.04	5	5	4.82	5.21	141	43	286
97/10/06, 23:24	12.85	43.02	6	6	5.51	5.53	170	40	280
97/10/12, 11:08	12.95	42.92	5	5	4.83	5.29	154	51	267
97/10/14, 15:23	12.93	42.93	9	6	5.98	5.61	122	38	260
97/10/16, 12:00	12.89	43.04	1.5	1.5	0.94	4.8	287	80	175
98/04/03, 07:26	12.76	43.19	4.8	4.8	6.06	5.1	142	30	254

activated seismogenic volume. See also table (3.1) for details.

The seismic sequence began on September 3<sup>rd</sup> with a  $M_w$  4.7 foreshock, the black focal mechanism on figure (3.2a).

The two largest events of the sequence,  $M_w$  5.7 and 6.0 respectively, struck the Colfiorito area on September 26<sup>th</sup> (within 9 hours from each other) and ruptured two normal faults with opposite rupture directivity (*Hernandez et al.*, 2004), see the red focal mechanisms in figure (3.2a). They were followed by other four moderate magnitude ( $5 < M_w < 6$ ) earthquakes, which also ruptured normal fault segments in the subsequent 18 days.

On October 16<sup>th</sup> a strike slip earthquake,  $M_w$  4.3, the gray focal mechanism in figure (3.2a), ruptured a nearly NS shallow structure inherited by previous tectonics (*Collettini et al.*, 2005). The analysis of seismicity pattern (*Chiaraluce et al.*, 2003) and the local tectonic setting from structural geology (*Collettini et al.*, 2005) suggest that the NS inherited compressional structures were reactivated during the 1997-98 seismic sequence with strike slip earthquakes and the inversion of the slip direction. This finding is consistent with coseismic stress changes caused by the normal faulting main shocks (*Nostro et al.*, 2005).

The progressive activation of fault segments, whose elongations range between 5 and 12 km, made up a broad,  $\approx 45$  km long, NW-trending fault system (figure (3.2a)).

The geometry of each segment is quite simple and consists of planar faults, dipping toward SW with an average dip of 40°- 45° (*et al.*, 1998; *Chiaraluce et al.*, 2003), down to 8 km depth.

The largest magnitude earthquakes of the sequence nucleated at the base of the seismogenic volume (5 – 6 km).

The aftershock focal mechanisms are consistent with the extensional kinematics: 70% of these reveals normal faulting and 24% is associated to left-lateral strike slip events (see *Chiaraluce* (2004) and also the inset in figure (3.2a). The aftershock fault plane solutions are very similar to the focal mechanism of their associated main shock.

For all the main earthquakes we use the CMT focal mechanisms proposed by *Ekstrom et al.* (1998), except that for the October 6<sup>th</sup> 1997 event for which we use the focal mechanism calculated by *Chiaraluce et al.* (2003) from P-wave polarity data (the green focal mechanism in figure (3.2a) (see *Nostro et al.* (2005) and *Chiaraluce et al.* (2003) for a detailed discussion).

The migration of seismicity toward the southeast, where the two main shocks of October 12<sup>th</sup> and 14<sup>th</sup> nucleated, is extraordinary and clearly visible on the space-time diagram shown in figure (3.2b): the seismicity migrated at nearly 1 km/day or 0.04 km/h.

*Chiaraluce et al.* (2003) pointed out the presence of normal faulting aftershocks on the hanging wall of the main shock fault planes and the lack of seismicity on the footwall.

Each main shock had its own aftershock sequence (see figure (3.3)) with a temporal decay well described by an Omori-like power law. Nevertheless, figure (3.3) reveals a particular temporal evolution of seismicity with clear fluctuations of the rate of earthquake production during the sequence not only associated with the occurrence of a main shock. The black stars in figures (3.2b) and (3.3) indicate the locations of the earthquakes with  $M_l$  ranging between 3.8 and 4.8, while in figure (3.3) the occurrence of the main shocks is indicated by color-coded triangles.

Our goal is now to model the rate of earthquake production in terms of coseismic elastic stress changes and a rate and state dependent friction law to account for the constitutive behavior of faults.

### 3.2 Fixing the input parameters

In order to compute elastic stress perturbations we use the same source parameters for the foreshock and for the six mainshocks ( $M_w > 5.2$ ) used by *Nostro et al.* (2005), which are listed in table (3.1) with few modifications. We also list in table (3.1) the source parameters of the 1979 Valnerina and 1984 Gubbio mainshocks (the two largest events in the area preceding the 1997 sequence) and of the Gualdo Tadino ( $M_w$  5.1) shock, that occurred on April 3rd 1998. The source parameters of the 1979 Valnerina and 1984 Gubbio earthquakes are taken from *Dechamps et al.* (1983) and *Westaway et al.* (1989), respectively. In some

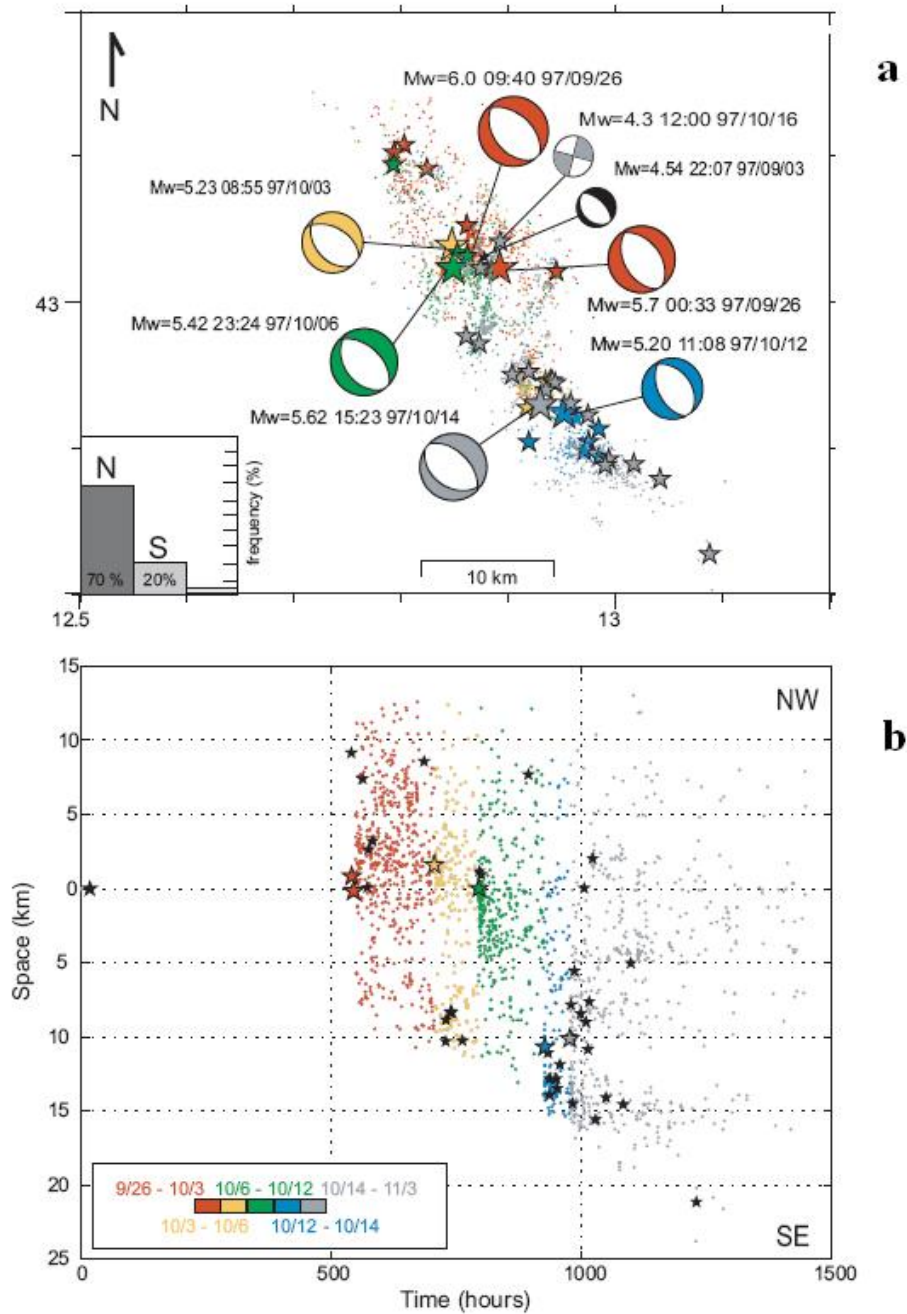


Figure 3.2: Description of the main events characterizing the 1997 Umbria-Marche seismic sequence. In panel (a): focal mechanisms and epicenter (the stars) of the 8 main events with their aftershocks (the dots). In panel (b): a diagram emphasizing the space-time migration of the seismicity.

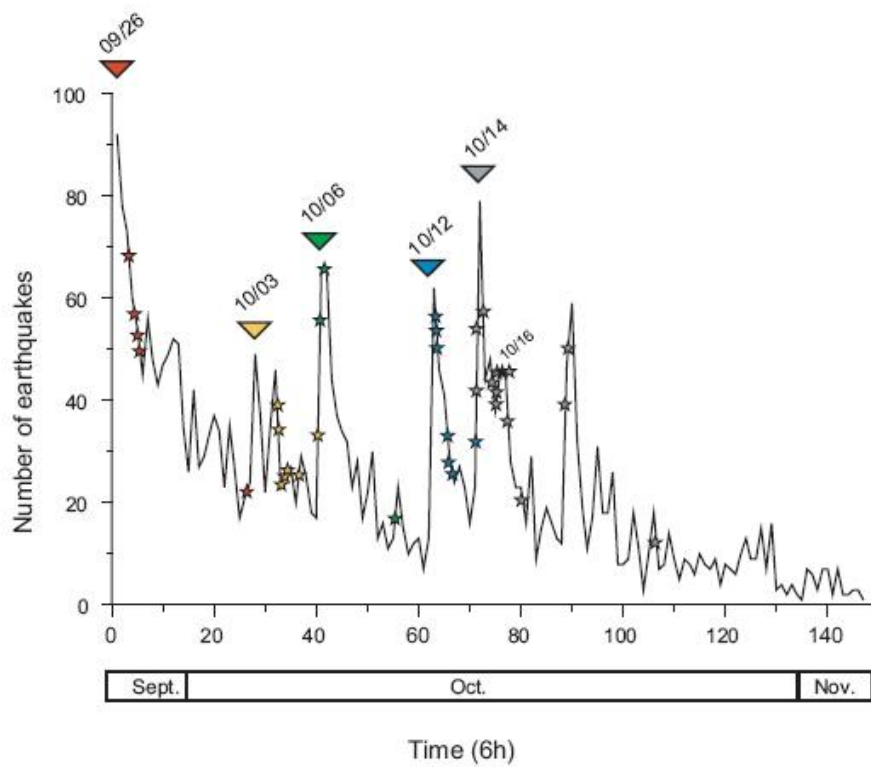


Figure 3.3: Temporal behavior of the studied seismicity during the time interval of the whole sequence.

simulations we have used more than nine mainshocks as interacting events; in these cases we used the fault geometry proposed by *Chiaraluce et al.* (2003) and *Chiaraluce* (2004) selecting all the events with  $M_l > 3.8$ . Except for the nine main shocks listed in table (3.1), the source dimensions were extrapolated from the seismic moment assuming a square source. The moment magnitudes for these events have been inferred from the local magnitude,  $M_l$ , using the scaling relation:

$$M_w = 0.812 \cdot M_l + 1.145, \quad (3.1)$$

as proposed by *Gasperini and Ferrari* (2000).

We have used the non-uniform slip distributions on the fault plane for the three largest events of the sequence (the two events of September 26<sup>th</sup> and the October 14<sup>th</sup> earthquake) obtained by *Hernandez et al.* (2004) inverting GPS, DInSAR and strong motion data which are the only available in the literature. Following *Nostro et al.* (2005) we use a uniform slip distribution for the other mainshocks and the fault geometry proposed by *Chiaraluce et al.* (2003) and *Chiaraluce* (2004) for all the largest magnitude earthquakes of the sequence  $M_l > 3.8$ .

When the event focal mechanism is not available, we use an average focal mechanism obtained by averaging strike, dip and rake angles of all the normal faulting aftershocks with  $M_l > 3.8$ : the resulting values are for strike, dip and rake respectively 149°, 46°, 267°. These values represent also the mean focal mechanism we used for projecting all our maps (unless other specifications are provided).

In order to estimate the reference seismicity rate  $r$  we smooth the seismicity of the previous 11 years on the considered area, as described in chapter (2). Figure (3.4) shows the smoothed seismicity from 1986 to 1996. For this purpose we selected all the events with magnitude greater than 2.0 and depth included in the range 0 – 20 km, using the catalog elaborated by *Chiarabba et al.* (2005), which reports seismicity from 1981 to 2002. For mapping the hypocenters of the 1997 seismic sequence we rather use the accurate locations obtained by *Chiarabba and Amato* (2003) from their 3-D tomographic study of the area; this catalog includes events from September 26<sup>th</sup> to November 8<sup>th</sup> 1997 and it does not contain the early aftershocks of the first October 26<sup>th</sup> main shock (occurred at 00:33 UTM).

Let us observe that the reference seismicity we have found smoothing the seismicity of the previous 11 years, which is showed in figure (3.4), presents very low values and very light variations. This result could be correlated with the quiescence observed by *Murru et al.* (2004) in this region from the 1994 till the begin of the sequence. Such low mean value of the reference seismicity will lead up to high values of the characteristic time  $t_a$ , which we will discuss in the next section.

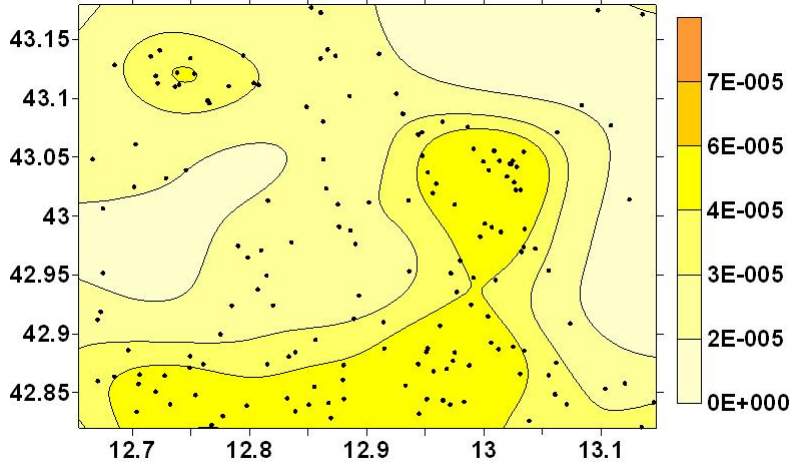


Figure 3.4: Smoothed seismicity of the previous 11 years before the Colfiorito sequence. The color scale represents the number of events with  $m \geq 2.0$  per 1 day and  $1 \text{ km}^2$ . The used correlation distance is  $5 \text{ km}$  (Frankel, 1995).

### 3.3 Performing the best value of $A\sigma$ with the maximum-likelihood method

In the previous section we have described the choice of the various parameters involved in the model that can be fixed from real observations. We remember that, from the reference seismicity  $r$ , we are also able to fix the value of the reference shear stress  $\dot{\tau}_r$  through the physical relation (2.25), as we discussed in section (2.4). The estimated values of  $\dot{\tau}_r$  range between  $7 \cdot 10^{-6} \div 7 \cdot 10^{-4} \text{ MPa/year}$ , selecting  $W_{seis} = 8 \text{ km}$ ,  $m_0 = 2.0$ ,  $m_{max} = 6.0$  and  $b$  fixed by fitting the Gutenberg-Richter relation for real seismicity. This range of values for  $\dot{\tau}_r$  is lower with respect to the range proposed by *Toda et al.* (2005), i.e. approximately  $10^{-4} \div 10^{-2} \text{ MPa/y}$  (derivable from their values of  $A\sigma = 0.05 \text{ MPa}$  and  $t_a = 7 \div 66 \text{ years}$ ). But one has to consider that Italy has much less seismicity than California, where *Toda et al.* (2005) evaluated  $\dot{\tau}_r$ ; moreover, we smoothed seismicity in a time window without big events, that release most of the slip. We then figure that our estimate of  $\dot{\tau}_r$  is underestimated of factor 10. In this region one can also estimate a value of  $\dot{\tau} \approx 1.7 \cdot 10^{-3} \text{ MPa/y}$  from the strain-rate value provided by *Serpelloni et al.* (2005) by the analysis of continuous and survey-mode GPS observations collected between 1991-2002 (*Team Task 4.7-S2* (2005-2007), oral communication). For the moment we neglect the inadequacy of our estimate.

So we now have to set the value of the unique free parameter that remains unknown:  $A\sigma$ . To this goal we used the procedure described in the last part

of section (2.4), scanning the period 1997-2000 of the catalog elaborated by *Chiarabba et al. (2005)*.

We examined a range of  $A\sigma$  values from 0.001 to 1.0  $MPa$ , that is the largest range we found in literature (see *Harris (1998)*). In table (3.3) we show some values of  $A\sigma$  estimated for aftershock sequences in the literature by various authors.

In table (3.2) are listed some outcomes of the method applied to the selected range of  $A\sigma$ . The log-ratio value of the likelihoods under the Dieterich and the Poisson model respectively,  $\ln(L_D/L_P)$ , can help us not only to find the best value of the parameter, searching for its maximum, but also to highlight the range of  $A\sigma$  where we expect that the RSM is better than the Poisson model. This range is characterized by a value of  $\ln(L_D)$  larger than  $\ln(L_P)$ , that is a positive value of their difference. So we can deduce from table (3.2) that from the value of  $A\sigma = 0.01 MPa$  we are in a reasonable range of  $A\sigma$  values. The upper limit could be evaluated observing the behavior of the total number of expected events by the RSM versus  $A\sigma$ , see figure (3.6). We in fact would like to match as closely as possible the observed value in the analyzed time interval, i.e. 1881 events recorded in the catalog during the time window 1997-2000, with  $m > 2.0$  and depth  $0.0 < z < 20.0 km$ . We so reasonably can exclude all the values that take  $N_{tot}$  to tend to zero.

We found as the best fit for  $A\sigma$  the value of 0.04  $MPa$ , as one can see in table (3.2) and in figure (3.5). The value  $A\sigma = 0.04 MPa$  maximizes in fact  $\ln(L_D)$  and  $\ln(L_D/L_P)$ . It is very close to the value obtained by *Toda and Stein (2003)* and used by *Toda et al. (2005)*. But, this value of  $A\sigma$  leads to an estimate of the characteristic time  $t_a$ , by equation (1.6), that seems unrealistic for the studied area:  $100 < t_a < 5000 years$ . We rather expect for this region a characteristic time of about some tens of years up to a few hundreds.

In the previous section we have anticipated our expectation to find high values of  $t_a$ , considering the quiescence observed by *Murru et al. (2004)* and also visible in our reference seismicity estimate, but the result is beyond our expectations. We are facing again the open and burning question of which is the correct and best choice of the background or reference seismicity. We wonder whether in this case it is correct to assume our estimate of the background accepting all the effects. In other respects, we could recognize in this controversial result a possible bias of the model. This bias could rise up when we try to estimate  $\tau_r$  by equation (2.25), as we have just observed at the beginning of this section. The real problem could be the estimate we have made of the reference seismicity  $r$ . With a smooth of the previous 11 years before the beginning of the sequence we do not consider the *real* reference seismicity of the region, underestimating both the regional seismicity and the reference shear stress consequently.

Because of the lack of data in this region before the 1997, to overdraw our

Table 3.2: Some outcomes of the maximum-likelihood method applied to search the best value of  $A\sigma$ . In the columns there are in order: the examined values of  $A\sigma$ ; the first term of equation (2.26), i.e. the sum of the expected rates on the catalog points; the total number of events expected with the RSM; the log-likelihood under the RSM and finally the log-likelihoods ratio considering the log-likelihood under the Poisson model,  $\ln(L_P)$ , as a reference term. Under the Poisson model the sum of the expected rates on the catalog points, the total number of predicted events and the log-likelihood value are constants, respectively:  $-20344$ ,  $4$ ;  $46.3$  and  $-20390.7$ .

$A\sigma$ [MPa]	$\sum \ln[\lambda(x_j, y_j, t_j, m_j)V_0]$	$N_{tot}$	$\ln(L_D)$	$\ln(L_D/L_P)$
0.0010	-30707.1	2197.6	-32904.6	-12514.0
0.0050	-19263.4	3283.4	-22546.7	-2156.1
0.0100	-16500.3	3430.0	-19930.3	460.3
0.0200	-15937.0	3329.4	-19266.4	1124.3
0.0300	-16041.2	3093.3	-19134.5	12560.2
0.0310	-16059.3	3068.5	-19127.8	1262.9
0.0320	-16074.2	3044.3	-19118.5	1272.1
0.0330	-16088.1	3020.6	-19108.7	1282.0
0.0340	-16102.8	2996.6	-19099.4	1291.2
0.0350	-16118.9	2969.2	-19088.1	1302.6
0.0360	-16118.9	2969.2	-19088.1	1302.6
0.0370	-16155.3	2913.2	-19068.6	1322.1
0.0380	-16172.8	2886.1	-19058.9	1331.7
0.0390	-16192.6	2859.4	-19052.0	1338.7
<b>0.0400</b>	-16215.4	2833.2	-19048.6	<b>1342.0</b>
0.0410	-16242.0	2807.7	-19049.7	1341.0
0.0420	-16272.5	2782.5	-19055.0	1335.7
0.0430	-16303.4	2757.9	-19061.3	1329.4
0.0440	-16336.7	2732.6	-19069.4	1321.2
0.0450	-16372.1	2706.5	-19078.6	1312.1
0.0460	-16406.4	2680.1	-19086.5	1304.2
0.0470	-16438.9	2653.7	-19092.5	1298.1
0.0480	-16470.4	2627.7	-19098.2	1292.5
0.0490	-16501.0	2601.1	-19102.1	1288.6
0.0500	-16530.7	2574.9	-19105.6	1285.1
0.0600	-16816.6	2339.7	-19156.3	1234.3
0.0700	-17085.5	2147.9	-19233.4	1157.2
0.0800	-17323.1	1988.1	-19311.2	1079.4
<b>0.0900</b>	-17531.5	<b>1850.0</b>	-19381.5	1009.2
0.1000	-17713.5	1727.8	-19441.3	949.3
0.5000	-19574.2	190.3	-19764.5	626.1
0.9000	-19902.8	86.5	-19989.3	401.3

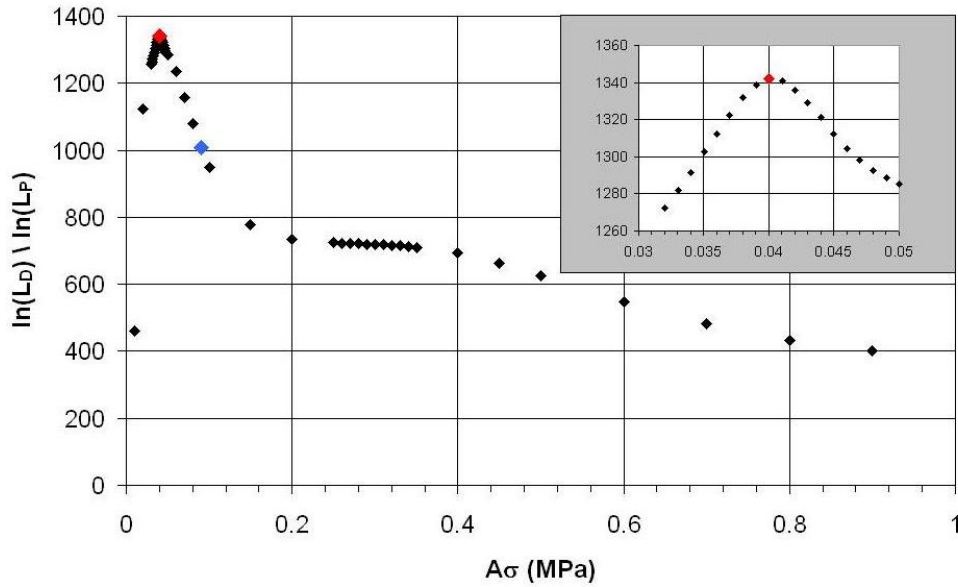


Figure 3.5: Trend of the log-likelihood ratio ( $\ln(L_D/L_P)$ ) versus the  $A\sigma$  values. Only the positive values of the y-axis are plotted. The red symbol shows the value of the parameter ( $A\sigma = 0.04 \text{ MPa}$ ) that maximizes  $\ln(L_D)$ ; instead, the blue symbol ( $A\sigma = 0.09 \text{ MPa}$ ) shows the value that corresponds to the total number of expected events closest to the effective observed value 1881. The inset is a zoom around the best-fit value.

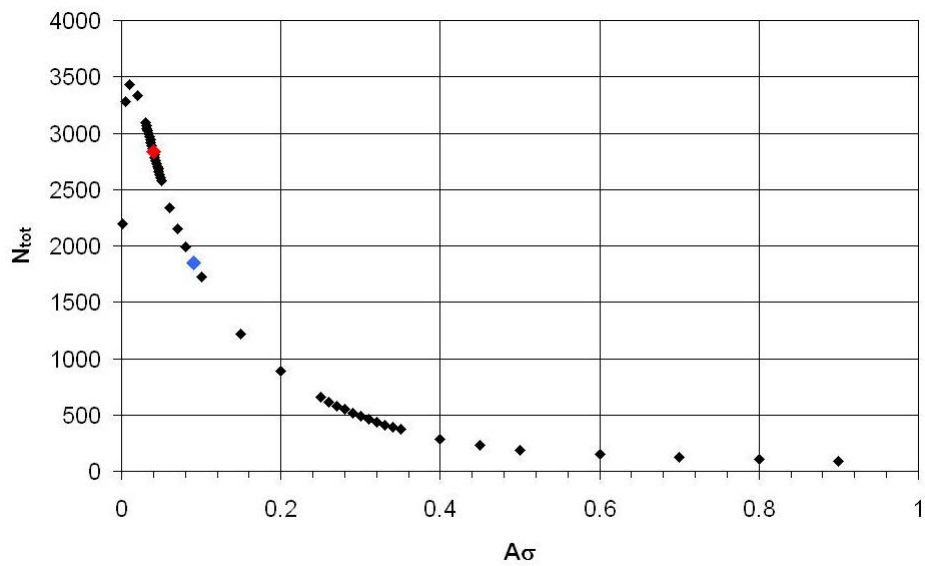


Figure 3.6: Trend of the total number of expected events under the RSM versus  $A\sigma$  values.

Table 3.3: Estimated values of  $A\sigma$  for aftershocks sequences reported by various authors. Some other authors focusing on this topic are *Gross and Kisslinger (1997)*; *Stein et al. (1997)*; *Gomberg et al. (2000)* and *Hardebeck (2004)*.

$A\sigma$ [MPa]	Comment	Reference
0.0012-0.6	For the San Francisco bay area	<i>Harris (1998)</i>
0.08-0.09	For the 1980 Irpinia earthquake	<i>Belardinelli et al. (1999)</i>
0.01-0.75	For the 1995 Kobe earthquake	<i>Guatteri et al. (2001)</i>
0.035±0.015	For the 1995 Kobe earthquake	<i>Toda et al. (1998)</i>

smooth to a larger time window, including big events for a better estimate of  $r$ , we have validated the result obtained with the likelihood test arbitrarily, fixing a priori a more reasonable value of  $\dot{\tau}_r \approx 10^{-3}$  MPa/year (consequently  $r = 0.6$  events of  $m \geq 2.0$  per year and per  $km^2$ , uniform on the area, and  $t_a \approx 40$  years) and we have repeated the likelihood test finding the same best value for  $A\sigma$ . The maximum log-likelihood value in this case is however 869 units lower than the case with the spatially variable reference seismicity, evidencing the advantage of this solution.

This exercise, to repeat the estimate of  $A\sigma$  in a different condition finding the same result, shows also the robustness of its best value in this application though the problems we still have to solve in our procedure. Therefore we will use  $A\sigma = 0.04$  MPa for the rest of this study.

To show how this choice for  $A\sigma$  is justified by the likelihood method and reasonable, we plot in figure (3.7) the histogram of the difference between the logarithms of the expected rates on the catalog points for the RSM and the Poisson model respectively,  $\ln[\lambda^D((x_j, y_j, t_j, m_j))] - \ln[\lambda^P((x_j, y_j, t_j, m_j))]$ , having sorted these differences in increasing order. Positive values of the ordinates in this histogram denote the that the rate expected according to the RSM is larger than the Poisson rate. Figure (3.7) shows that the distribution does not have a random behavior, but it is in favor of a positive value of the logarithmic ratio, so pointing to a clear correlation between the increase on the seismicity and the rate expected by the time dependent RSM with respect to the time independent Poisson rate.

### 3.4 Modeling seismicity rate changes

We now have all necessary information (all those listed in table (2.1)) to model rate changes, as we described in section (2.3).

We decided to use for our simulation the spatially variable reference seismicity

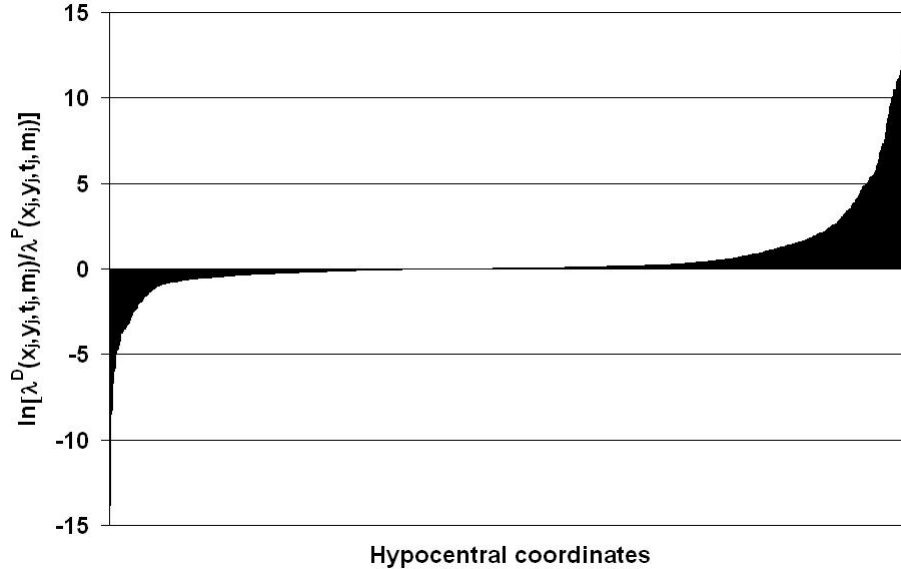


Figure 3.7: Trend of the log-ratio between the expected rates for the RSM and the Poisson model respectively on the hypocentral coordinates of the catalog by *Chiarabba et al.* (2005).  $A\sigma = 0.04$  MPa.

of figure (3.4), even if we have to retain the bias that this choice produces in estimating  $\hat{\tau}$  and then  $t_a$  (see previous section). The effect that we are going to detect in the view maps of expected rate is just in term of the characteristic time  $t_a$ : the bigger the values of  $t_a$ , the longer the lasting of the CFF effects. But, we believe that, for our present purposes, it does not affect the comprehension of the model and its application. We remember also that the model including the space variable reference seismicity gives a better value of the likelihood probability than that with a constant background.

The first step is computing the Coulomb stress changes, as explained in section (2.2). We used both the constant apparent friction and the isotropic poroelastic model to compute the CFF variations. We found that their effects on the rate estimates are almost the same, therefore here we will show only the outcomes related to the isotropic poroelastic model (2.8). We have resolved stress perturbations onto the average focal mechanism ( $\varphi = 149^\circ$ ,  $\delta = 46^\circ$  and  $\lambda = 267^\circ$ ) and at a mid-depth of the seismogenic volume (4.5 km). Two exceptions have been made for September 26<sup>th</sup> and October 16<sup>th</sup> strike slip event: for the first the CFF was computed at deeper depth (6.0 km); for the second the CFF was resolved at a shallower depth (1.0 km) and for a strike-slip focal mechanism. We have calculated the expected seismicity rate changes just before the time of occurrence of the nine mainshocks. The results are shown in figures (3.8) and (3.9).

The color scale is planned considering the mean value of the reference seismicity ( $\approx 3 \cdot 10^{-5}$ ) as a benchmark: below there is the inhibited rate of seismicity (gray colors); above there is the favorite rate (other colors). Let us remember the fixed values of  $\tilde{\mu} = 0.5$  and  $A\sigma = 0.04 \text{ MPa}$  used for these computations.

In each panel of figures (3.8) and (3.9) the black stars indicate the locations of the causative earthquakes and the blue stars the locations of the subsequent promoted main shock. The black dots represent the distribution of the seismicity in the time period comprised between the two subsequent main shocks (i.e. the seismicity comprised between the last mainshock occurred and the future one, represented by the blue star) and for a depth range comprised between 0 and 20 km.

In temporal order, the first panel of figure (3.8) shows the seismicity rate changes caused by the September 3<sup>rd</sup> foreshock and confirms that the first main shock of September 26<sup>th</sup> (00:33 UTM) occurred in an area of enhanced rate of earthquake production.

Panel 2 displays the seismicity rate changes after the occurrence of the foreshock and the first main shock of September 26<sup>th</sup>. Also in this case the second main shock of September 26<sup>th</sup> (09:40 UTM) occurred in an area of enhanced Coulomb stress and of seismicity rate increase. The subsequent main shocks in this time interval are located in areas characterized by an increase in the rate of earthquake production, but aftershocks are located in a seismicity shadow.

Panels 3 and 4 of figure (3.8) and panels 1 and 2 of figure (3.9) illustrate the seismicity rate changes calculated immediately before the four normal faulting main shocks occurred on October 3<sup>rd</sup>, 6<sup>th</sup>, 12<sup>th</sup> and 14<sup>th</sup>, respectively.

Panel 3 of figure (3.9) shows the seismicity rate changes immediately before the occurrence of the October 16<sup>th</sup> strike slip earthquake and in this case Coulomb stress changes are resolved onto the strike-slip aftershocks which followed that event (black solid dots in the figure).

Finally, panel 4 of figure (3.9) shows the seismicity rate changes at the end of the seismic sequence, immediately before the April 3<sup>rd</sup> 1998 normal faulting earthquake occurred in the north termination of the study area. These computations precisely confirm the results obtained by *Nostro et al.* (2005) in terms of elastic stress interactions. Only one main shock out of the nine considered here is located in a stress shadow (panel 3 of figure (3.8)), represented in our simulations by a decrease in the rate of earthquake production. This result is not surprising because, as clearly demonstrated by *Nostro et al.* (2005), the October 3<sup>rd</sup> main shock is located in a stress shadow caused by the previous large earthquakes ( $M_w > 5.0$ ), or on the same fault segment which ruptured during the September 26<sup>th</sup> (09:40 UTM) main shock, but within the high slip patch. Panel 3 of figure (3.8) clearly shows also a wide area of seismicity shadow on the hanging wall of the main shock fault plane. This is consistent with the stress shadows

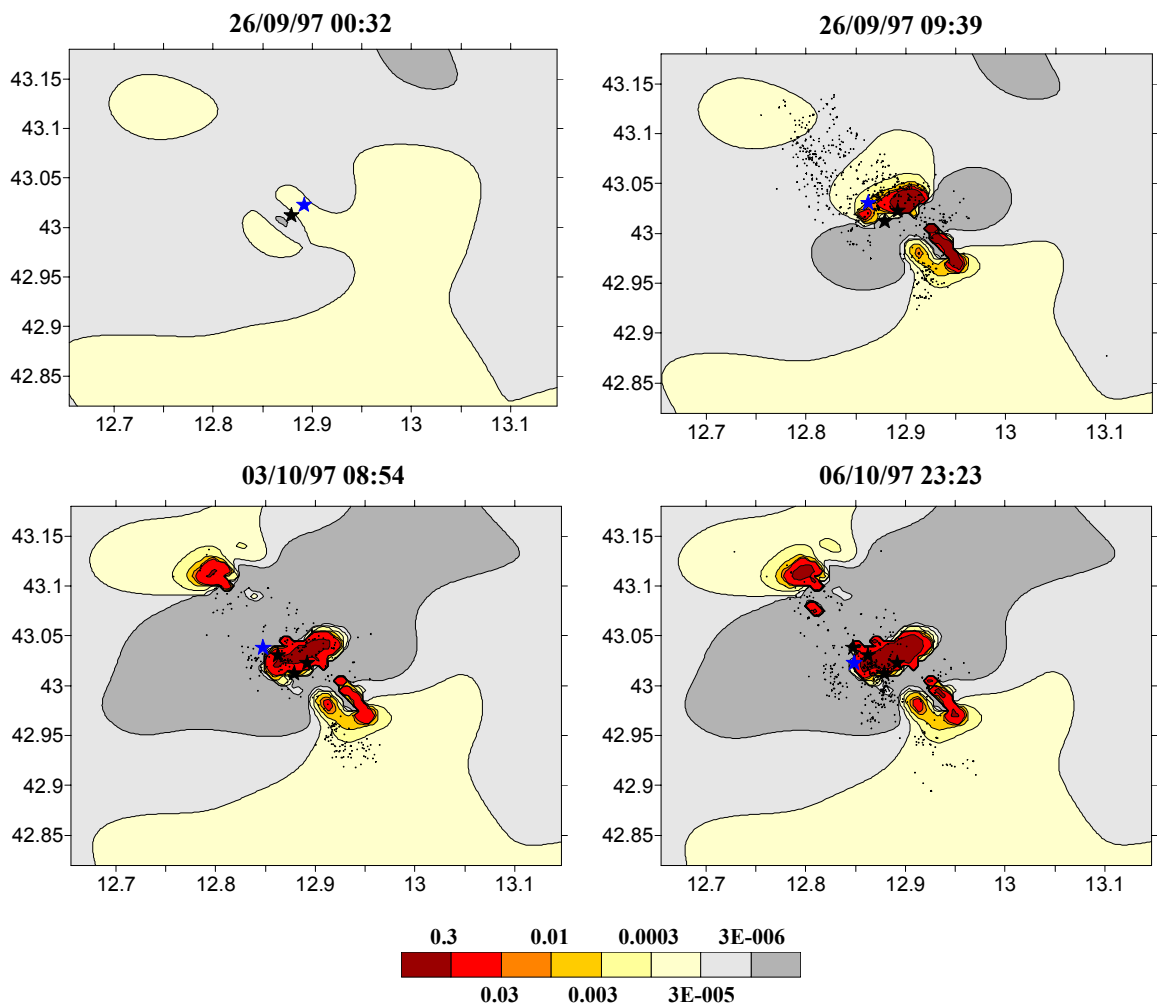


Figure 3.8: Expected seismicity rate changes with the RSM during the 1997-1998 Umbria-Marche sequence.

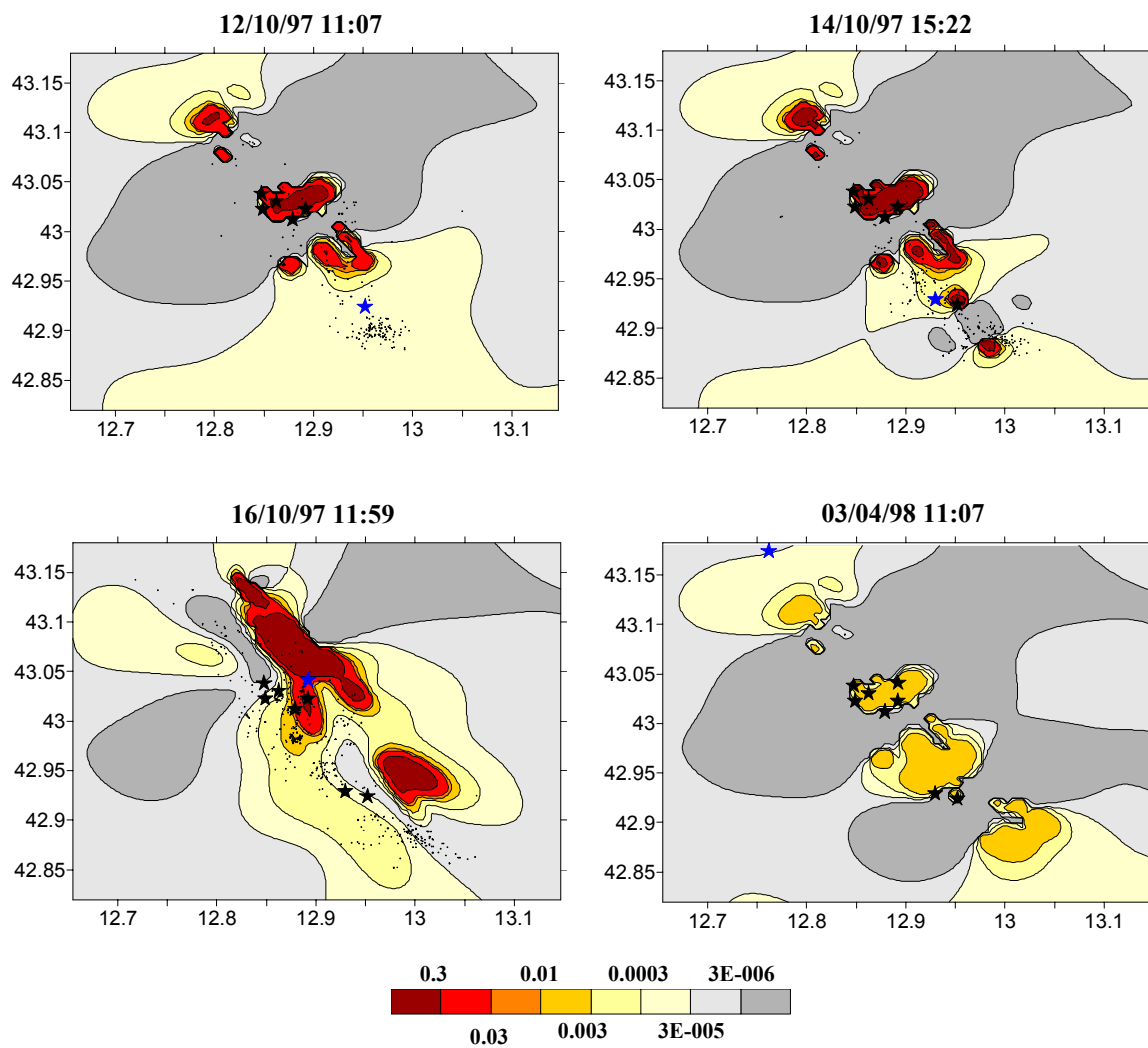


Figure 3.9: Expected seismicity rate changes with the RSM during the 1997-1998 Umbria-Marche sequence.

obtained by *Nostro et al.* (2005). Most of the aftershocks located here, as those shown in panel 2 of figure (3.8) or panel 2 of figure (3.9), have normal faulting mechanisms (*Chiaraluce et al.*, 2003) and therefore they cannot be triggered by elastic Coulomb stress changes on the hanging wall of the normal faulting main shocks. Also in *Chiaraluce* (2004) is shown that the problem of the presence of secondary seismicity on the hanging wall of normal faulting faults is mainly enhanced for September 26th (00:33 UTM) and October 14th events, as we have just observed.

Several recent papers (*Marsan*, 2006; *Helmstetter and Shaw*, 2006) have suggested that the stress heterogeneity can suppress seismicity shadows. This might represent an explanation to the presence of normal faulting earthquakes on the hanging wall of the causative faults discussed above. In the section (3.4.4) we will propose a first simple approach to consider the effect of the stress heterogeneity on the expected seismicity.

Other studies proposed that small magnitude earthquakes can trigger other small (and large) magnitude events (*Felzer et al.*, 2002, 2003; *Marsan and Nalbant*, 2005); thus, multiple triggering, that we have not considered in our simulations, could also explain the lack of expected seismicity on the hanging wall of the normal faults which ruptured during the main shocks of the 1997 Colfiorito sequence. In order to test this hypothesis we have also tried to compute the seismicity rate changes caused by 47 earthquakes with  $M_l > 3.8$ . The results (very similar to those shown in figures (3.8) and (3.9), so we decided not to show them here) reveal that including the moderate magnitude aftershocks ( $M_l > 3.8$ ) does not remove or reduce the seismicity shadows where real seismicity is registered.

### 3.4.1 The role of the $A\sigma$ value

We have discussed a lot about the choice of the fault parameter  $A\sigma$ . It does not have a trivial role in the RSM. It is involved both in the feedbacks of the CFF variations and in the temporal behavior of rates. In fact, it appears two times in equation (1.5): in the exponent with the stress changes and implicitly in the temporal exponent because of its relation with  $t_a$ .

We are now interested in showing how it can influence the rate computations and so stress again the importance of rigorously performing this parameter, as we have tried to do with the likelihood method.

In figures (3.10) and (3.11) is shown the effect of different values of  $A\sigma$  (0.01, 0.04, 0.09 and 0.34 MPa) for two cases of rate computations, for September 26<sup>th</sup> (07:26 UTM) and April 4<sup>th</sup> 1998.

In figure (3.10) is emphasized the role of  $A\sigma$  connected more strictly with the influence of stress changes in rate estimations. The lower  $A\sigma$ , the higher the weight of CFF on rates (in terms of the portion of the area influenced by the perturbation), both for positive and negative rates. Let us highlight how with

the highest value of  $A\sigma$  we have used, 0.01 MPa, the stress shadow above the first event of September 26<sup>th</sup> even disappears. Observe also that for increasing  $A\sigma$  the positive rate changes seem to decrease, focusing (with higher values) in smaller zones, up to almost disappear.

In figure (3.11) is rather emphasized its role in controlling temporal behavior through the relation (1.6). For this purpose we show the rate situation at the time of the last event of the Colfiorito sequence. Also in this case one can observe an important role of  $A\sigma$  in controlling the outcomes. For increasing  $A\sigma$ ,  $A\sigma = 0.01; 0.04; 0.09; 0.34$  MPa, the model expects positive rate changes which vary of the order of ten between the different values of such parameter. However, as in the previous figure, for increasing  $A\sigma$  the total area which presents rate variations from the reference seismicity decreases more and more.

So, it is clear from these examples how different choices of  $A\sigma$  can lead to very different results and conclusions. Even the presence of an expected stress shadow could be influenced by  $A\sigma$ .

We can so conclude that  $A\sigma$  has an important weight in seismicity rates computing. Therefore we believe that one should mind its role in calibrating the model.

### 3.4.2 The role of the effective friction coefficient value

In section (2.2) we have just highlighted the necessity to introduce the  $\alpha$  correction when we calculate the CFF for the nucleation solution in the RSM. It seems to us that the authors who worked on this topic do not make precise this point. We want therefore investigate here how important is the weight of this correction in rate estimates.

Figure (3.12) shows the expected rates calculated on September 26<sup>th</sup> (09:40 UTM) and on April 4<sup>th</sup> 1998 selecting  $\alpha = 0.25$  (i.e. the effective coefficient of friction  $\tilde{\mu} = 0.5$ ) and  $\alpha = 0.00$  ( $\tilde{\mu} = 0.75$ ). One can see that both in the first and in the second example the value of  $\tilde{\mu}$  influences the result up to 10% in the areas of maximum rate changes. This is more evident in the map relative to April 4<sup>th</sup> 1998, when the general rate change is lower.

We can conclude that the weight of  $\mu$  in expected rate changes is visibly lower than that of  $A\sigma$  shown before, but we believe it is however correct to take it into account.

### 3.4.3 The role of the reference seismicity rate

Because the background seismicity rate plays an important role in the computations of rates of earthquake production (*Toda et al.*, 2005), we have also estimated the reference seismicity rate by smoothing earthquakes in a larger time window (the largest for which we have data), extending it to sixteen years (1981-1996,

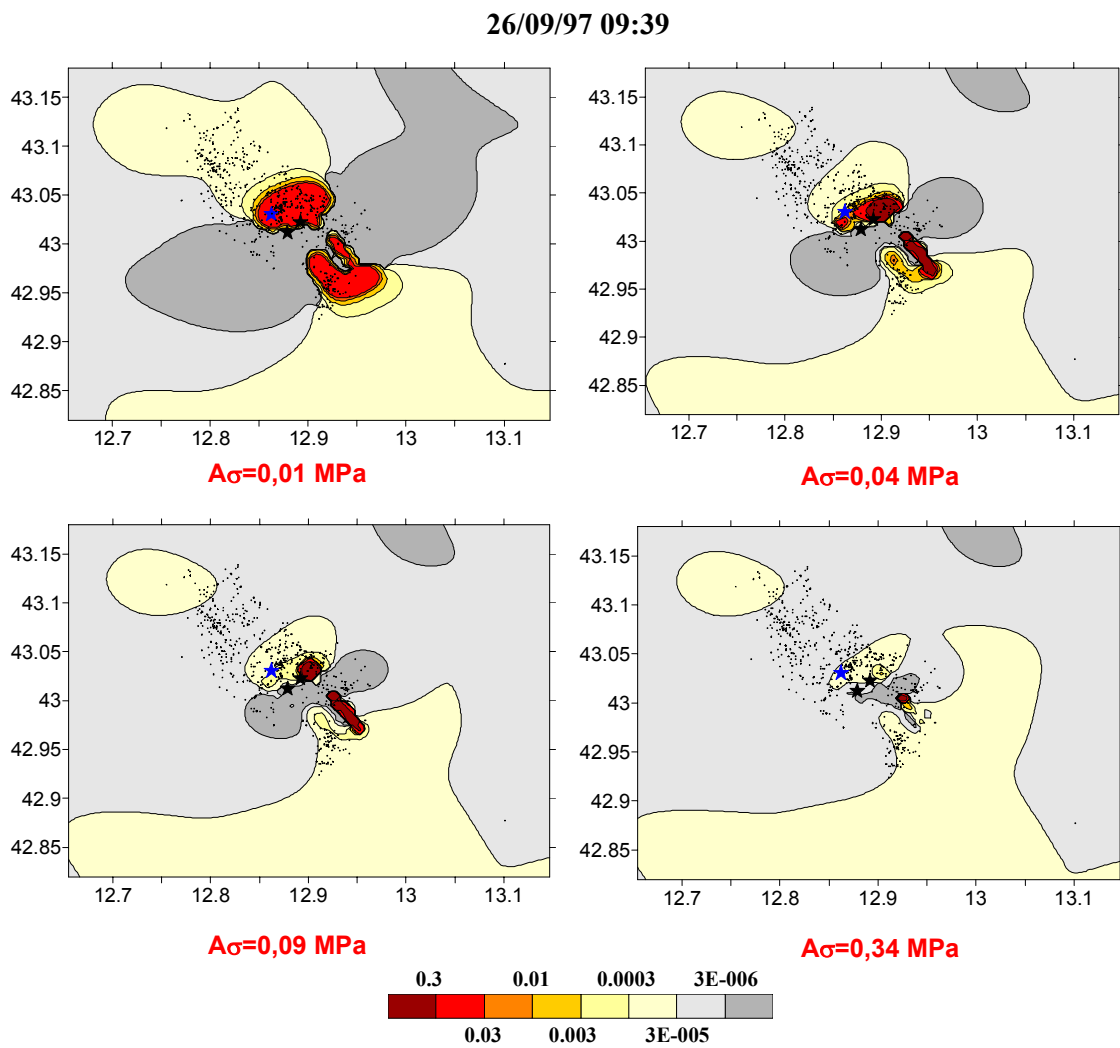


Figure 3.10: Expected seismicity rates at the time of September 26<sup>th</sup> (09:40 UTM) for four different values of  $A\sigma$ .

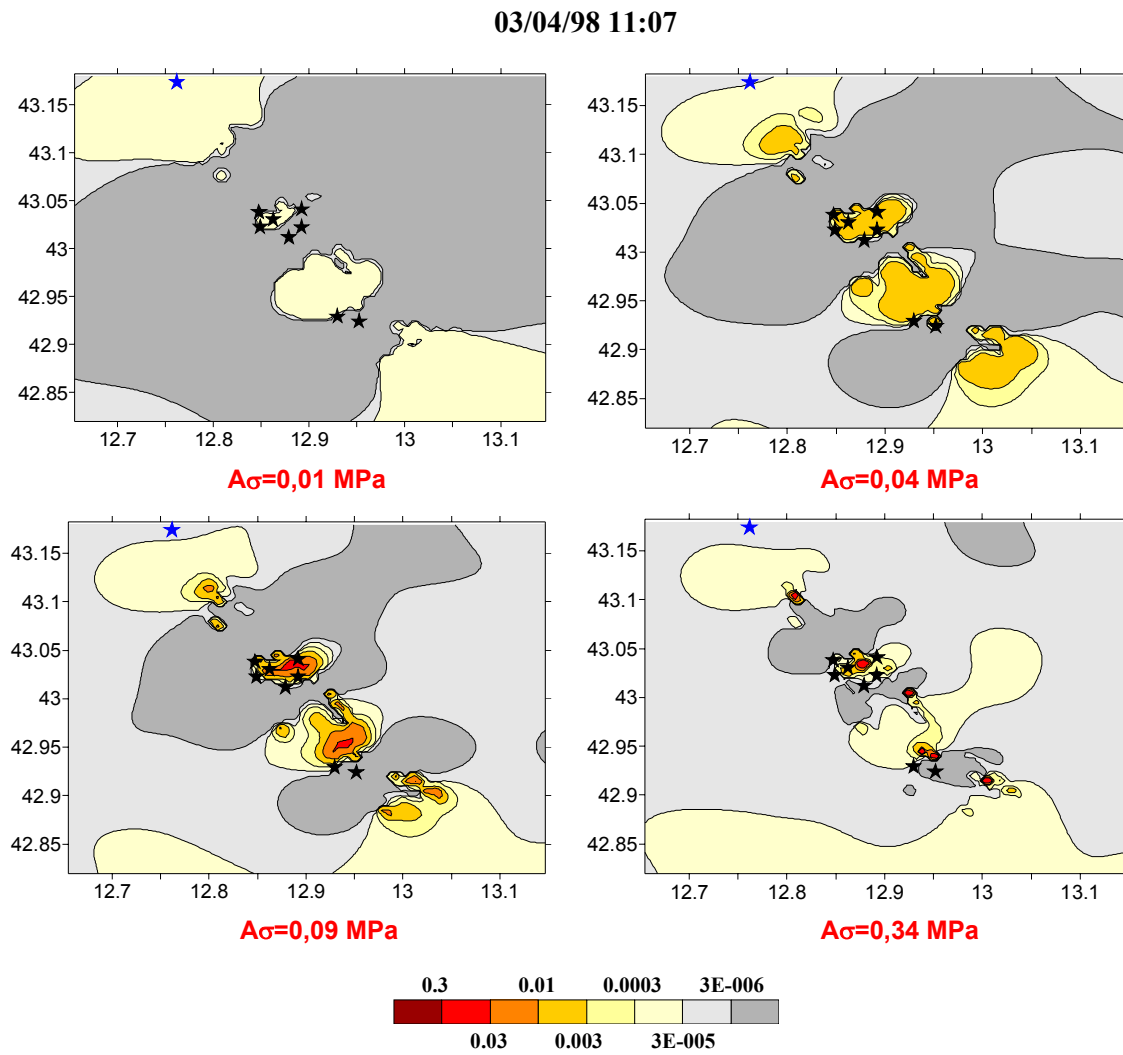


Figure 3.11: Expected seismicity rates at the time of April 4<sup>th</sup> 1978 for four different values of  $A\sigma$ .

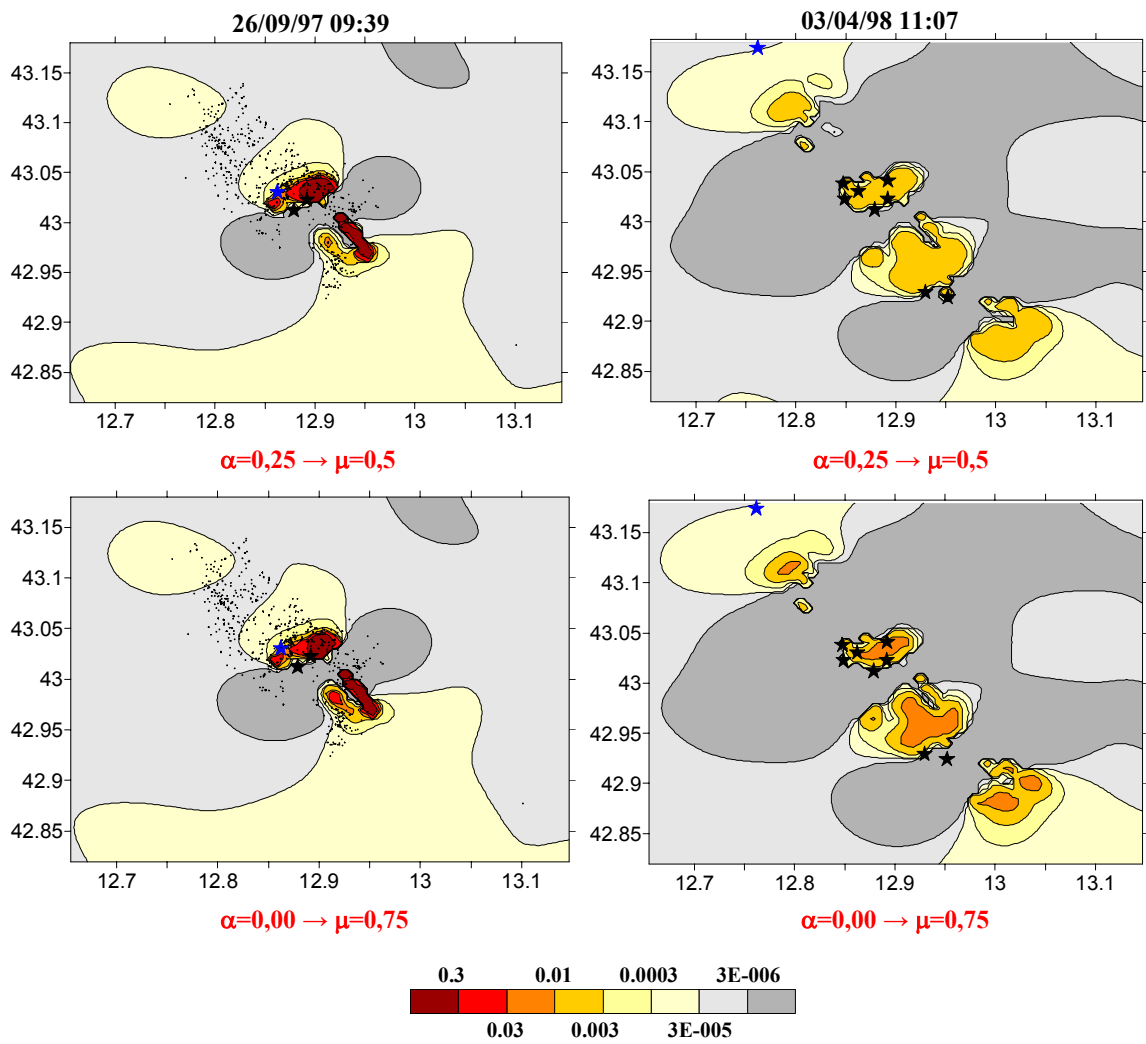


Figure 3.12: Expected seismicity rates at the time of September 26<sup>th</sup> (09:40 UTM) and of April 4<sup>th</sup> 1998 for two different values of  $\mu$ .

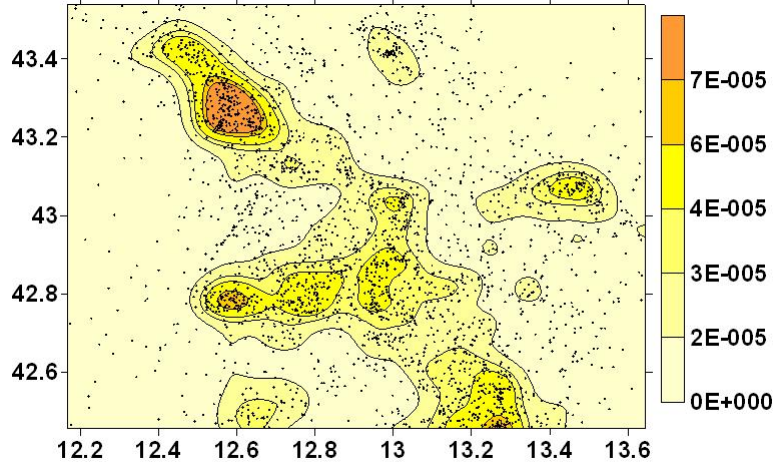


Figure 3.13: Smoothed seismicity of the previous 16 years before the Colfiorito sequence. The color scale represents the number of events with  $m \geq 2.0$  per 1 day and  $1 \text{ km}^2$ . The used correlation distance is  $5 \text{ km}$ .

so at least the 1984 Gubbio event affects the computed reference rate), and for a larger area, which now includes the epicenters of the two big past earthquakes of the area (events 1 and 2 of table (3.1), namely Valnerina 1979 and Gubbio 1984). This different reference seismicity is shown in figure (3.13).

Our main purpose is trying to justify the presence of seismicity detected on seismicity shadows. The results of the new computations of rates are shown in figure (3.14). The upper panels of figure (3.14) refer to the time of the two past events of Valnerina and Gubbio. The lower panel refers to October 3<sup>rd</sup> 1997 event. Let us observe that the influence of the two past earthquakes of Valnerina, 1979, and Gubbio, 1984, still lasts after 18 and 13 years respectively. This map clearly shows that, also changing the reference rate, it does not reduce or eliminates the seismicity shadow previously observed, so the problem remains unwarranted. We cannot exclude that this is due to the lack of completeness of the catalog at small magnitudes. Let us more observe that, even with this background choice, the value range of  $\dot{\tau}_r$  remains unrealistic (too low values) and consequently also the value range of  $t_a$  (too high), as we observed in the previous section.

#### 3.4.4 Considering stress heterogeneity on the fault

We have previously observed that *Marsan* (2006) and *Helmstetter and Shaw* (2006) have suggested that the stress heterogeneity can suppress seismicity shadows. They model the distribution of small scale stress change  $\tau$  by a Gaussian law

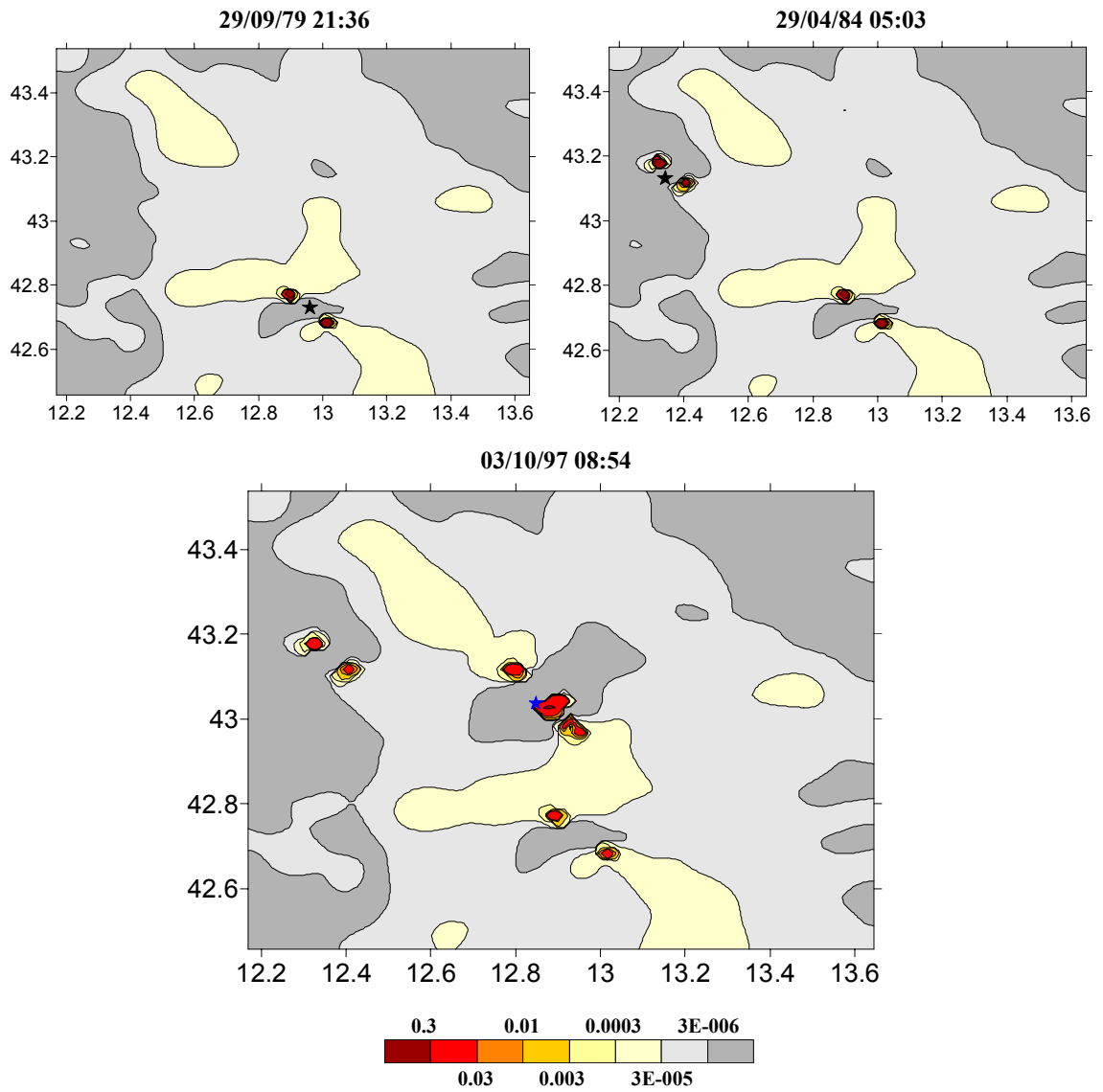


Figure 3.14: Expected seismicity rate at different times. The two past events of Valnerina and Gubbio are now considered among the causative events. The color scale represents the number of events per 1 day and 1  $km^2$ .

with mean  $\bar{\tau}$  and standard deviation  $\sigma_{\tau}$ , explaining several delayed quiescence otherwise not justified by data.

We have also had the possibility to observe that stress heterogeneity has an important role in reducing expected stress shadows where real seismicity is present, as in particular we have highlighted in figure (3.8), panels 2 and 3, and in figure (3.9), panel 2.

Our possibility to observe this phenomenon has grown out of testing the new version of the code that we have developed during the work (see section (2.1) in chapter (2)) in comparison with the first rawer version of it (chapter (1), section (1.1)). In fact, testing the results of the two codes at the same time and folding them, we can conclude that the fundamental difference is not due to the solution extended to the semispace nor in the variable slip distribution adopted, but it is due to the solution assumed for the finite source.

Using the sum of a number of point sources as a solution for extended source, instead of *Okada* (1992) solution, at certain scales we generate a sort of numerical dishomogeneity that could resemble the stress heterogeneity on the fault. So, using this solution for the rectangular sources in the half space, with all previously fixed parameter values, we obtain the maps shown in figure (3.15). The three panels of figure (3.15), compared with the relative panels 2 and 3 of figure (3.8) and panel 2 of figure (3.9), clearly show that the effect of introducing the stress heterogeneity is to reduce the stress shadows otherwise unjustified.

Let us finally observe that however the October 3<sup>rd</sup>, 1997, event still remains in a stress shadow.

### 3.5 Modeling temporal behavior

We have also examined the temporal behavior of the modeled seismicity, analyzing again the role of different values of  $A\sigma$ , and comparing the expected trends with the real temporal behavior of the registered events. Figures (3.16) and (3.17), (3.19) and (3.20) show the fits of the modeled temporal trends of the rate of earthquake production for such different values of  $A\sigma$ , over short and long periods respectively.

Figures (3.16) and (3.17) indicate that the model reproduces consecutive Omori decays as observed in a natural behavior. But the modeled seismicity presents peaks of expected rates higher than those registered in the catalog. In the four panels of figures (3.16) and (3.17) one can also observe how the different values of  $A\sigma$  influence these peaks relative to the subsequent modeled temporal decays. In fact for  $A\sigma = 0.01$  MPa the maximum number of events expected in 3 hours is greater than 800; for  $A\sigma = 0.04$  MPa it is greater then 400; for  $A\sigma = 0.09$  it is almost 300; and for  $A\sigma = 0.34$  MPa the maximum value of the expected earthquakes is dropped to about 50 events. For  $A\sigma = 0.34$  MPa

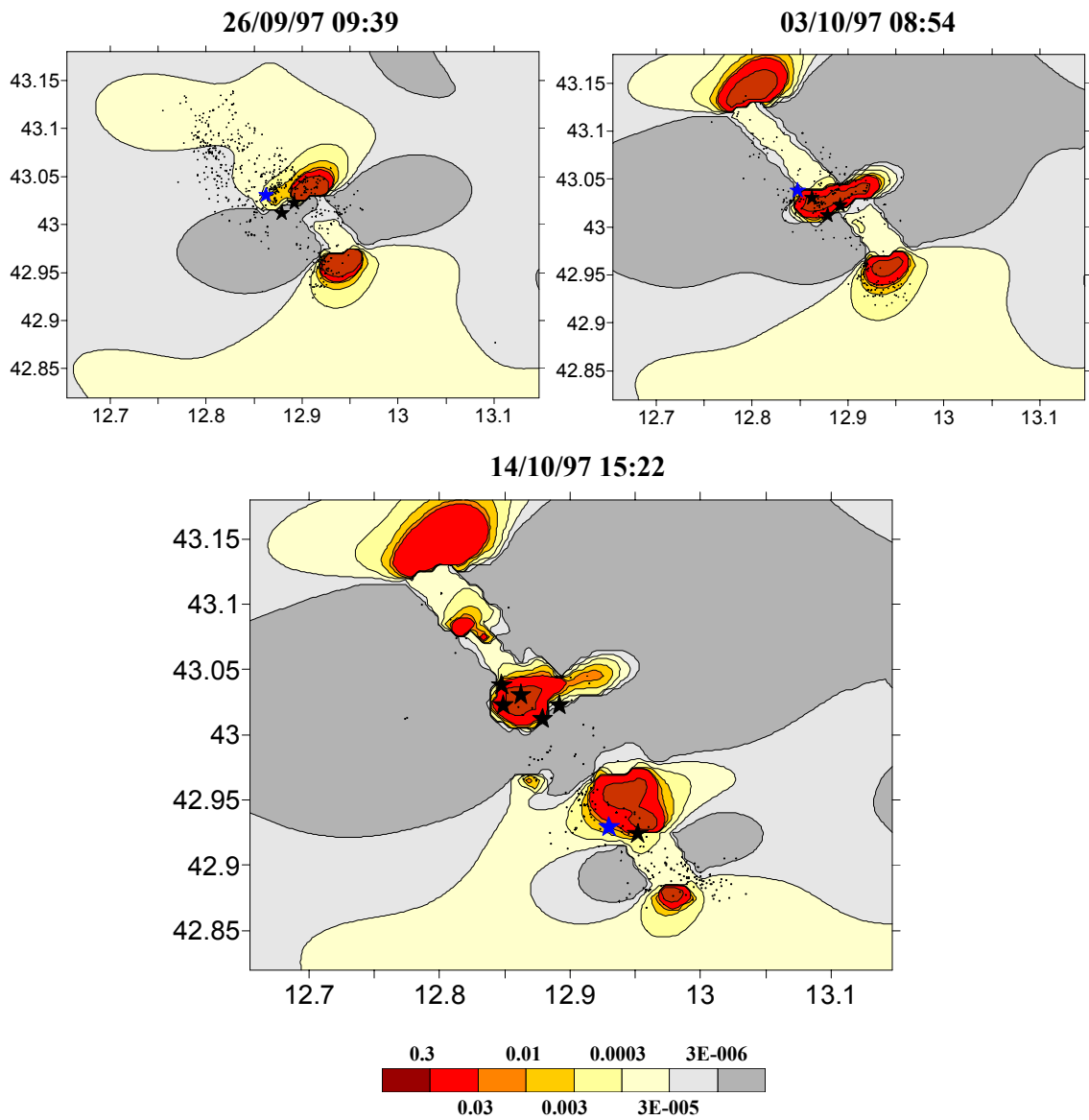


Figure 3.15: Three examples of maps calculated introducing stress heterogeneity on the fault.

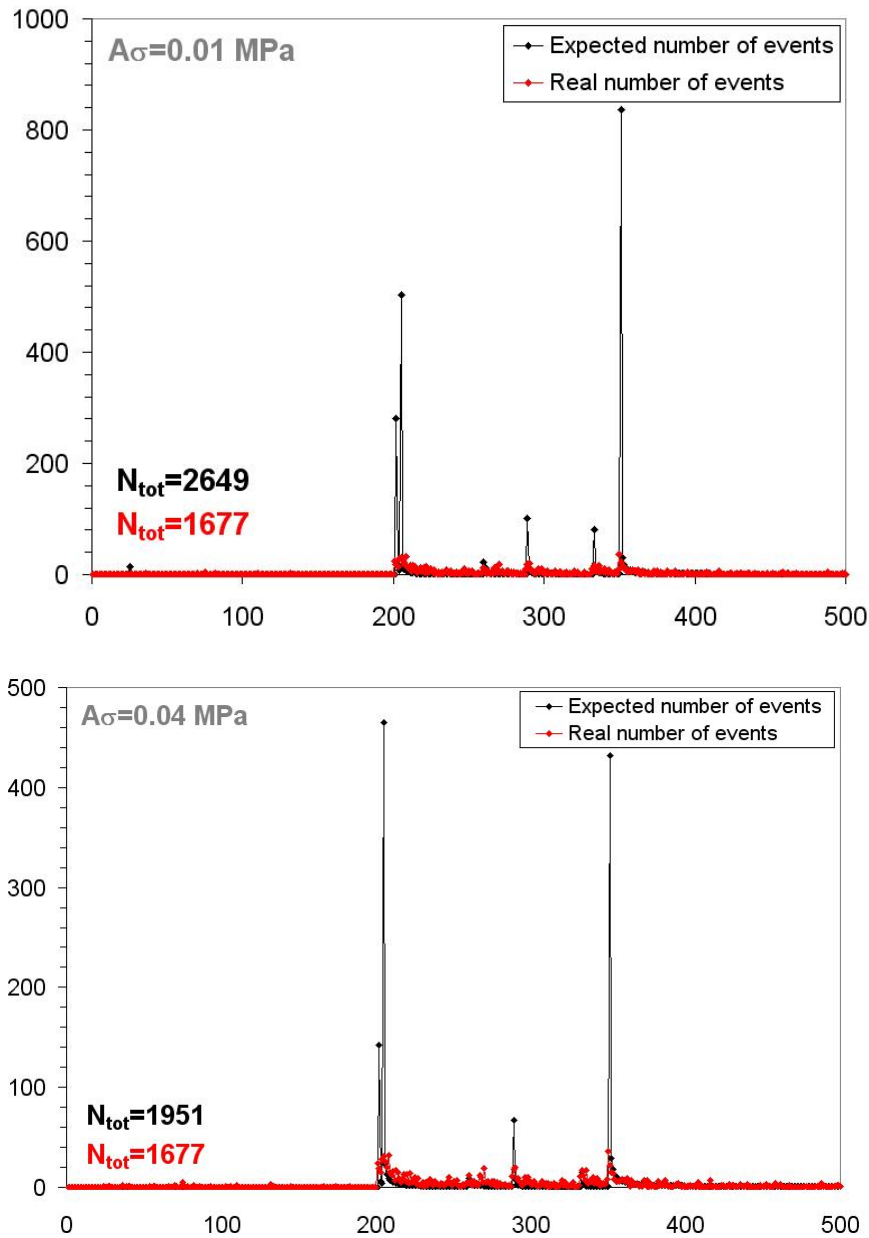


Figure 3.16: Trend of the modeled temporal behavior for different values of  $A\sigma$  compared with the observed trend. The origin time is September 1<sup>st</sup> 1997. On the x-axis time is reported in steps of 3 h. The time window then covers the whole sequence, until October 31<sup>th</sup> 1997. On the y-axis is reported the number of events, modeled or registered, in the study area ( $\approx 400 \text{ km}^2$ ).

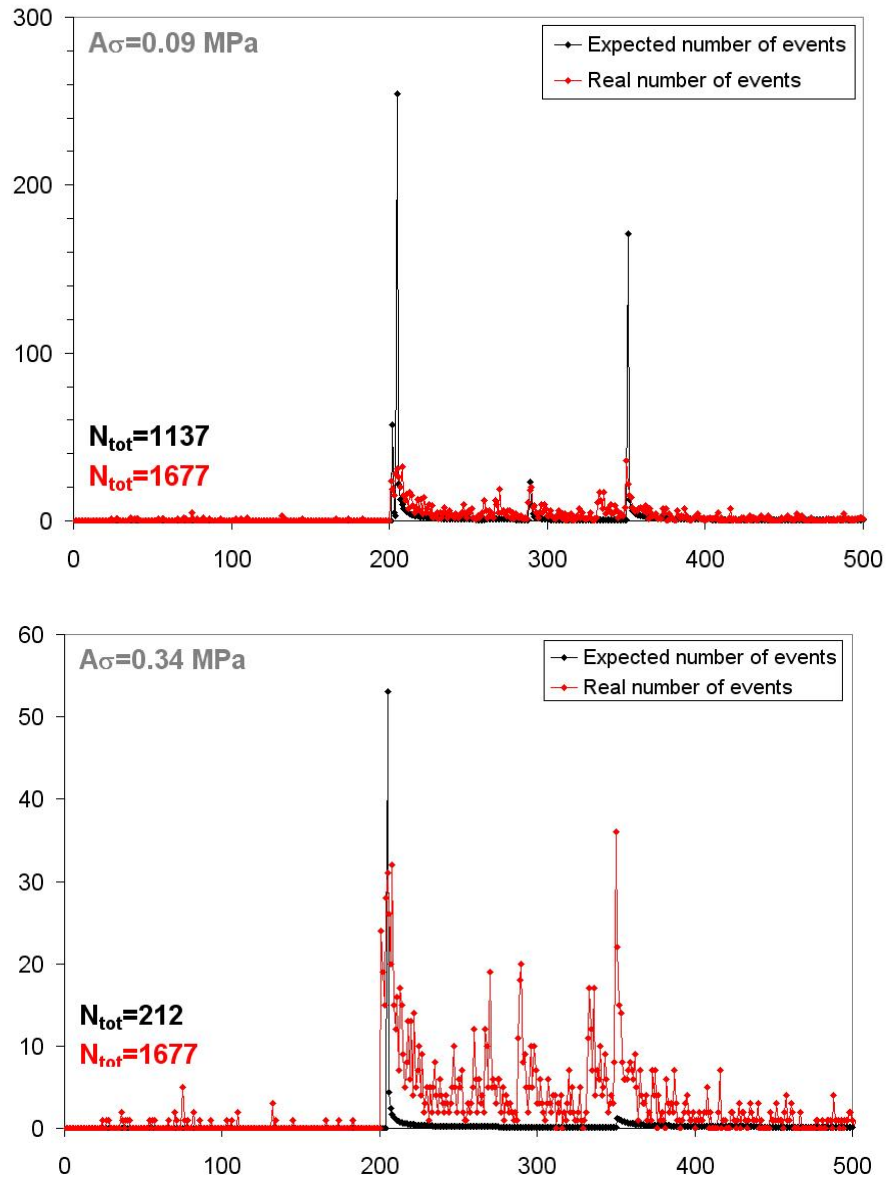


Figure 3.17: Trend of the modeled temporal behavior for different values of  $A\sigma$  compared with the observed trend. The origin time is September 1<sup>st</sup> 1997. On the x-axis time is reported in steps of 3 *h*. The time window then covers the whole sequence, until October 31<sup>th</sup> 1997. On the y-axis is reported the number of events, modeled or registered, in the study area ( $\approx 400 \text{ km}^2$ ).

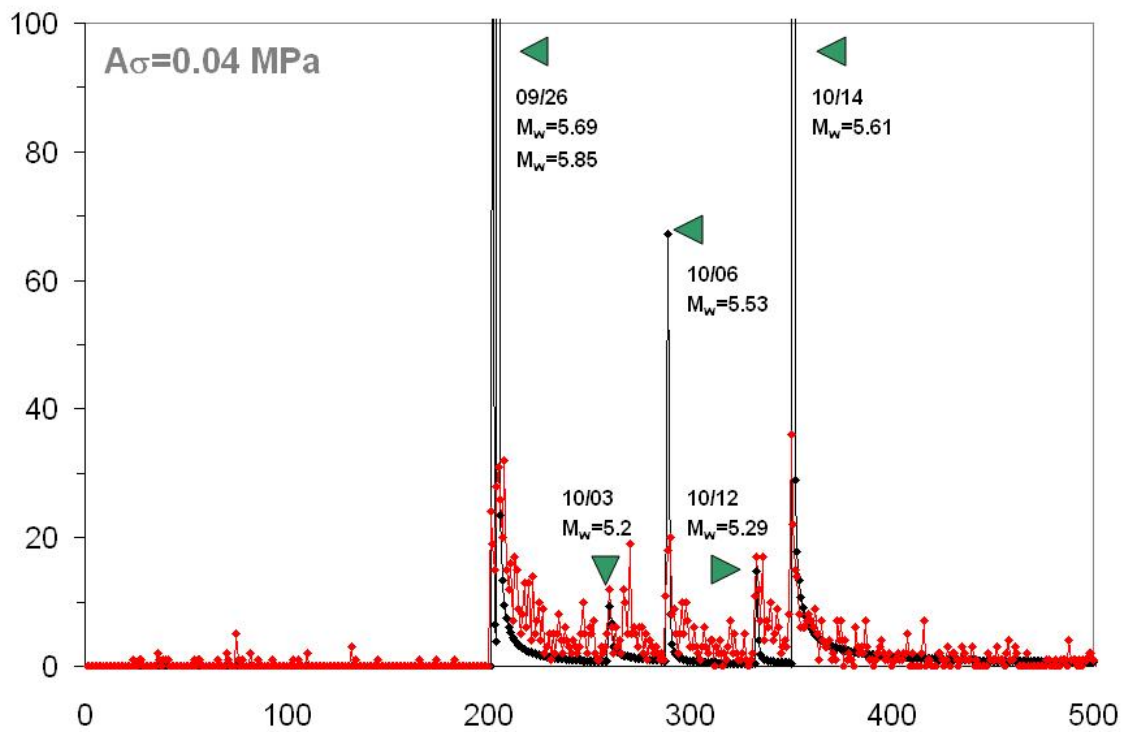


Figure 3.18: Trend of the modeled temporal behavior for  $A\sigma = 0.04 \text{ MPa}$  compared with the observed trend. This figure is the same of panel 2 of figure (3.16) with a cut in the y-axis. On the y-axis is reported the number of events, modeled or registered, in the study area ( $\approx 400 \text{ km}^2$ ).

you can also observe how, with such a high value, one can not still distinguish the different decay episodes (the Omori type decays); to the other hand, the maximum values relative to this case are closer to the real ones, rather than those with smaller  $A\sigma$ . However, we believe that the behavior shown in the second panel of figure (3.16), relative to the best fitted value of  $A\sigma = 0.04$  *MPa*, is in good agreement with real data, considering as an explanation for the discrepancy in the peak values that after a big event it is practically difficult to register the real large amount of events.

Observing the zoom of this diagram, shown in figure (3.18), you can see a satisfactory agreement between observed and modeled temporal evolution. The total number of the events expected during the time interval is comparable to the observed number for  $A\sigma = 0.04$  *MPa*: respectively 1951 and 1677.

Looking at figures (3.19) and (3.20), which show the same data in a much longer scale, it can be noted that the positive effect of the stress change dominates the overall aftershock production only for a limited period of time (approximately more than 20 *years* for  $A\sigma = 0.04$  *MPa*), after which the seismic activity drops below the background level (quiescence). Inversely, the negative effect lasts for a much longer time. In figures (3.19) and (3.20) we highlight the importance of such parameter in controlling the length and the shape of the quiescence and the averaged characteristic time  $t_a$  over a very long period. We can conclude that, in general, the period of quiescence seems longer than that of increasing seismicity. Let us remember that, anyway, the total number of expected events tends to 0 for  $\Delta t \rightarrow \infty$ , as we have already discussed in chapter (1). Figures (3.19) and (3.20), in fact, can be compared to figure (1.5): over such long time scale these diagrams agree with that representing the response to a single stress change, because one can imagine that each event is occurred at  $t = 0$ .

### 3.6 Probability estimates

As we anticipated in the Introduction and in section (2.5), we are interested in translating seismicity rates into probabilities of occurrence, using relation (2.27).

In spite of the attentive and critical work we did to make possible such computations, we acknowledge that the results presented in this section are in an early stage. Our aim in the next future is to consolidate the presented procedure, considering more different applications and deepening the role of the parameters involved in the model, resolving their effective weight.

What we do like to highlight here is exactly the influence that the choice of the model parameters has in the final results. In our case we refer in particular to the discussed about parameter  $A\sigma$ . For this purpose we have calculated the probabilities with four different values of  $A\sigma$ : 0.01, 0.04, 0.08 and 0.34 *MPa* (the same values we have used in section (3.4.1)) in different areas. In figure (3.21) it

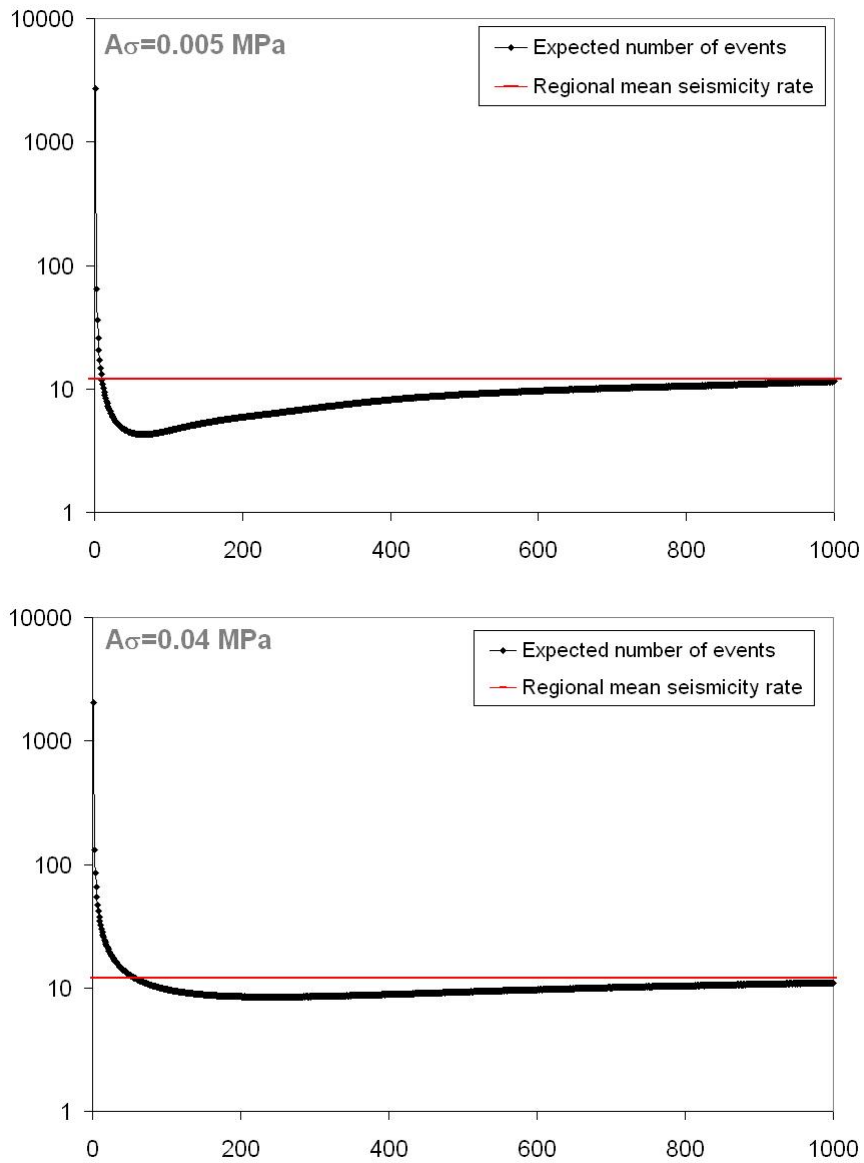


Figure 3.19: Trend of the modeled temporal behavior for different values of  $A\sigma$  for a long time period: 1000 years from September 1<sup>st</sup> 1997. The x-axis represents the time steps in years. The red line represents the mean seismicity rate for the whole study region ( $\approx 400 \text{ km}^2$ ) and temporal window.

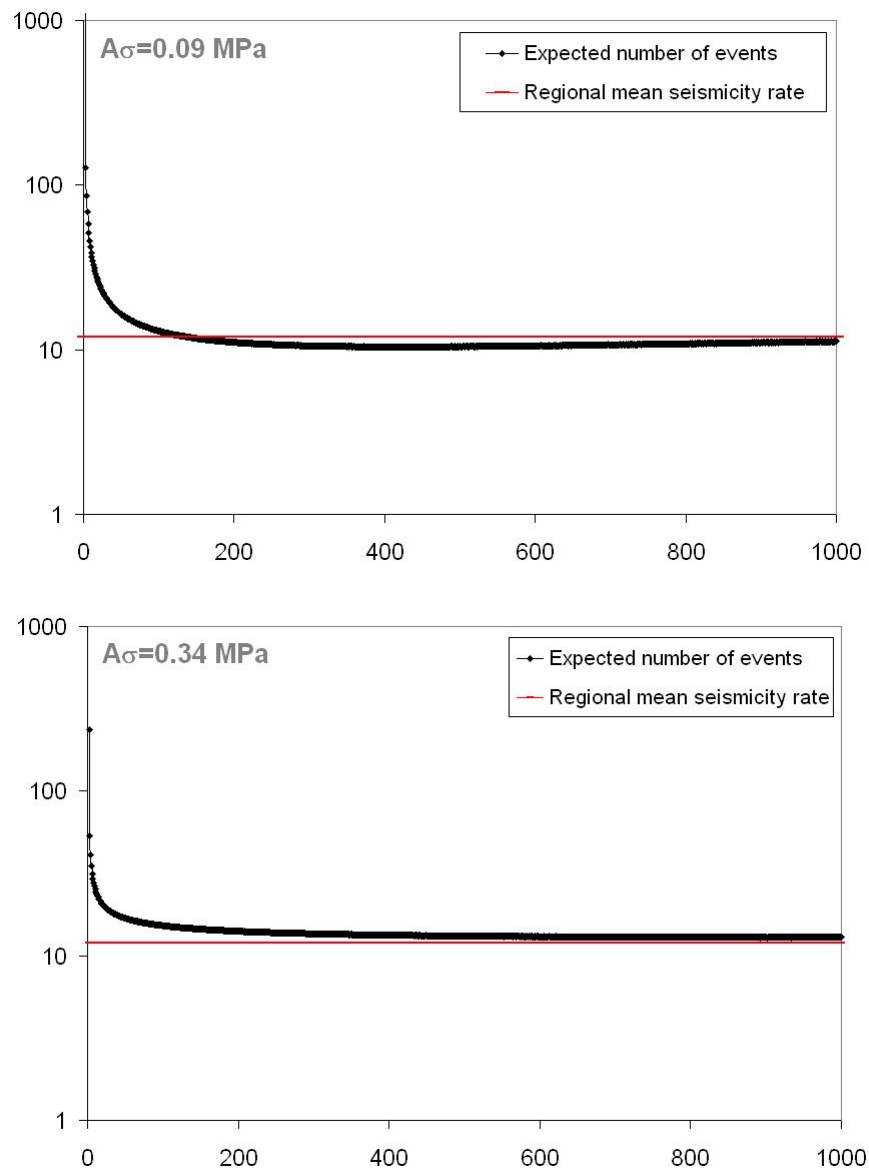


Figure 3.20: Trend of the modeled temporal behavior for different values of  $A\sigma$  for a long time period: 1000 *years* from September 1<sup>st</sup> 1997. The x-axis represents the time steps in years. The red line represents the mean seismicity rate for the whole study region ( $\approx 400 \text{ km}^2$ ) and temporal window.

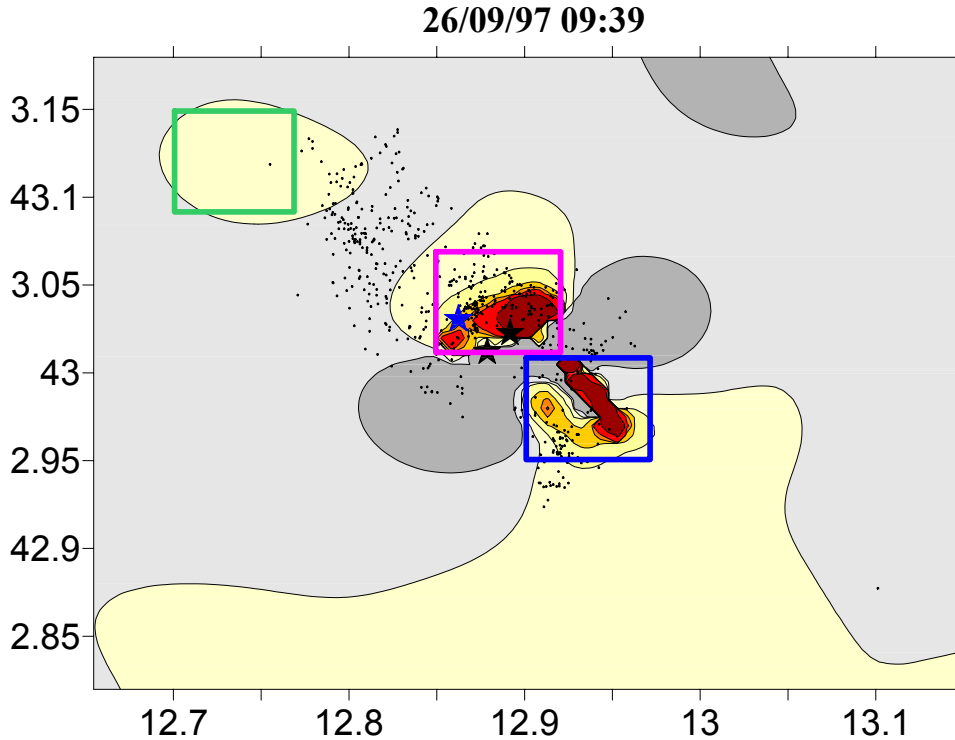


Figure 3.21: Reference map for the evaluation of the probabilities of earthquake occurrence. The map refers to September 26<sup>th</sup> (09:39 UTM) with  $A\sigma = 0.04 \text{ MPa}$  and  $\mu = 0.05$ .

is shown the map to which we refer for our exercise in calculating probabilities.

We imagine to have the updated rates at September 26<sup>th</sup> (09:39 UTM) (just before the third big event at 09:40 UTM) and to select three areas (of the same size), the pink, the blue and the green one, where we want estimate the future probability of occurrence. In table (3.4) are listed the results for the different areas of figure (3.21) and for different values of  $\bar{m}$ . The interval time  $\Delta T$  adopted to calculate  $P$  is fixed at 7 days.

These results show clearly the considerable influence of  $A\sigma$  in probability evaluations. For the pink area and for  $\bar{m} = 3.0$ , the variation in probability between  $A\sigma = 0.01$  and  $A\sigma = 0.04 \text{ MPa}$  is of the order of 12%; and between  $A\sigma = 0.01$  and  $A\sigma = 0.08 \text{ MPa}$  is of the order of 30%. There is even a leap in probability between  $A\sigma = 0.01$  and  $A\sigma = 0.34 \text{ MPa}$ : the variation in probability is higher than 70%. We can also observe that the bigger the minimum magnitude, the lower the probability and the differences among different values of  $A\sigma$ . The blue area results show a particular behavior, highlighted also in figure (3.22): the decrease of probabilities with respect of  $A\sigma$  is not monotonic. We would try to

Table 3.4: Probabilities  $P(\Delta S, \Delta T, m \geq \bar{m})$  evaluated in the pink, blue and green areas of figure (3.21) for different values of the reference magnitude  $\bar{m}$  and of the parameter  $A\sigma$ . The interval time  $\Delta T$  is fixed at the value of 7 days.

$\bar{m}$	$A\sigma$ [MPa]	$P_{pink}$ [%]	$P_{blue}$ [%]	$P_{green}$ [%]
3.0	0.01	94.6	87.5	< 1
4.0	0.01	20.6	15.1	< 1
5.0	0.01	1.8	1.3	< 1
6.0	0.01	< 1	< 1	< 1
3.0	0.04	82.4	57.7	< 1
4.0	0.04	12.8	6.6	< 1
5.0	0.04	1.1	< 1	< 1
6.0	0.04	< 1	< 1	< 1
3.0	0.08	65.5	67.0	< 1
4.0	0.08	8.1	8.6	< 1
5.0	0.08	< 1	< 1	< 1
6.0	0.08	< 1	< 1	< 1
3.0	0.34	< 1	14.1	< 1
4.0	0.34	< 1	1.2	< 1
5.0	0.34	< 1	< 1	< 1
6.0	0.34	< 1	< 1	< 1

give here a reasonable explanation of such phenomenon, but highlighting again the early stage of our study about probability estimates. Our explanation is connected to the consideration of two different factors: the first, the probability estimate in this case depends on the influence of a spatially variable CFF; then, we have to consider the superposition of different stress changes; the second, we remember the double role of  $A\sigma$  in the RSM: it influences both the initial value of  $R$  and the expected temporal behavior of the rate of earthquake occurrence. Moreover, observe that only for the blue area the value  $A\sigma = 0.34$  MPa leads to probabilities higher than 1%. Finally, observing table (3.4), one can note that, as we expect, the probabilities in the pink area are higher than those in the blue one; and the probabilities in the green area are always unimportant. Obviously, enlarging  $\Delta T$  the probabilities increase consequently from some units to a few tens of percentage. Theoretically, when  $\Delta T \rightarrow \infty$  follows that  $P \rightarrow 1$ .

In figure (3.22) we show the trend of  $P$  versus  $A\sigma$  in the three selected areas. The range of  $A\sigma$  is that proposed by *Harris (1998)*, the largest founded in literature. One can observe, for the pink and the blue areas, that the trends are not regular and they have some fluctuations. We are out to investigate whether

Table 3.5: Probabilities  $P(\Delta S, \Delta T, m \geq \bar{m})$  evaluated in the pink, blue and green areas of figure (3.21) for different values of the reference magnitude  $\bar{m}$  and of the effective friction coefficient  $\tilde{\mu}$ . The interval time  $\Delta T$  is fixed at the value of 7 days.

$\bar{m}$	$\tilde{\mu}$	$P_{pink}$ [%]	$P_{blue}$ [%]	$P_{green}$ [%]
3.0	0.75	78.6	58.1	< 1
4.0	0.75	11.5	6.6	< 1
5.0	0.75	< 1	< 1	< 1
6.0	0.75	< 1	< 1	< 1
3.0	0.70	79.3	57.7	< 1
4.0	0.70	11.7	6.6	< 1
5.0	0.70	< 1	< 1	< 1
6.0	0.70	< 1	< 1	< 1
3.0	0.60	80.8	57.7	< 1
4.0	0.60	12.2	6.6	< 1
5.0	0.60	1.0	< 1	< 1
6.0	0.60	< 1	< 1	< 1
3.0	0.50	82.4	57.7	< 1
4.0	0.50	12.8	6.6	< 1
5.0	0.50	1.1	< 1	< 1
6.0	0.50	< 1	< 1	< 1
3.0	0.40	83.9	63.9	< 1
4.0	0.40	13.4	7.7	< 1
5.0	0.40	1.1	< 1	< 1
6.0	0.40	< 1	< 1	< 1

such fluctuations have a physical meaning or they can be associated to the error in estimating the probability. As we have just observed above, the trend relative to the blue area is also not monotone.

We want now consider also the influence that the effective friction coefficient  $\tilde{\mu} = \mu - \alpha$  has in probability estimates. We still take as reference the three areas shown in figure (3.21). We summarize the results in table (3.5). One can see that considering the two more drastic solution,  $\alpha = 0.00$  ( $\tilde{\mu} = 0.75$ ) and  $\alpha = 0.25$  ( $\tilde{\mu} = 0.35$ ) the probabilities in the pink and blue areas vary by about 5 – 6 %.

We can so conclude that, also in probability computations,  $\tilde{\mu}$  shows a minor influence than  $A\sigma$ .  $A\sigma$ , to the other hand, shows a great influence in such computations that should be taken into account.

We are conscious that, for the moment, our efforts to analyze the probability behavior versus the two parameters  $A\sigma$  and  $\tilde{\mu}$  must be improved to be fully

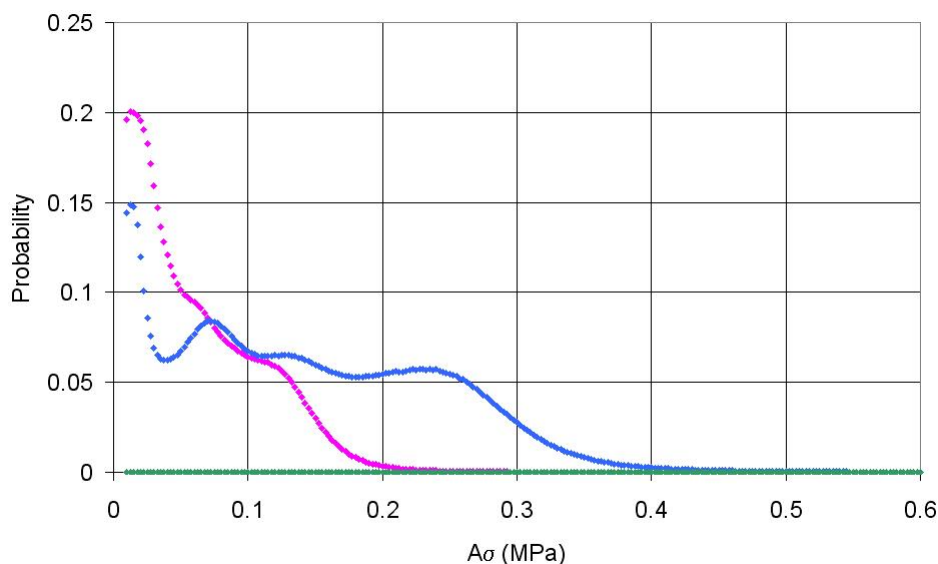


Figure 3.22: Trend of the probabilities (the colors refer to the rectangles in figure (3.21) versus  $A\sigma$ .

statistically substantiated. We mean that the procedure should be backed by a sufficient number of directly observed successes and failures to establish its performance at some agreed level and evaluate its variability (the difficulties to accumulate the information necessary to such a validation could be overcome with synthetic catalogs). This is more stringent than having general evidence in favor of the theory or from retrospective analysis. Anyhow, we believe that such initial elaborations can represent an inception of future deeper studies.

We strongly believe that to make a realistic and reliable seismic forecast with the RSM we must first deepen the role of the most important parameters and their involvement in probability computations and variability.

### 3.7 Discussion and conclusions

We have applied the developed RSM to compute seismicity rate changes caused by the repeated occurrence of moderate magnitude earthquakes, during a seismic sequence which struck central Italy in 1997. There were two main features of this sequence of normal faulting main shocks that we attempted to model in terms of changes in the rate of earthquake production: the occurrence of normal faulting aftershocks on the hanging wall of the main rupture planes and the southwestward migration of seismicity.

Our modeling results reveal that the seismicity rate changes, calculated from the stress perturbations caused solely by the largest magnitude main shocks, cannot provide an explanation to the seismicity shadow on the hanging wall as well as to the evident spatio-temporal migration of seismicity. In other words, our modeling of seismicity rate changes furnishes the same results obtained by *Nostro et al.* (2005) who modeled only static stress changes. However, both the temporal behavior represented by the Omori-like decay following each mainshock and the total number of aftershocks are quantitatively well described by the model. The unexpectedly long duration of the quiescence phase is a feature not easily observed on real catalogs, because of their shortness.

The failure in forecasting the migration of seismicity does not prove that the RSM is incorrect. On the contrary, it demonstrates that the stress time history perturbing the fault population within the seismogenic volume is much more complex than that simulated only through static coseismic stress changes.

Fluid flow can certainly explain seismicity migration (see *Antonoli et al.* (2006) and references therein). Furthermore, pore pressure relaxation can give an explanation to the presence of normal faulting earthquakes on the hanging wall of normal faults. *Miller et al.* (2004) proposed that seismicity on the hanging wall of normal faults is promoted by a pressure pulse originating (co-seismically) from this known deep source of trapped high-pressure  $CO_2$  and propagating into the damage region created by the earthquake. Therefore, the poroelastic response of the medium can contribute to explain the temporal evolution of stress perturbations. The heterogeneity of the spatial pattern of stress perturbations can also be associated to geometrical complexity of the pre-existing fracture pattern. This is consistent with the findings of *Marsan* (2006) and *Helmstetter and Shaw* (2006) who proposed that stress heterogeneity can remove seismicity shadows.

We cannot exclude that a more accurate choice of the reference seismicity could really improve the results of the model. We believe that the background seismicity is an essential ingredient of such a model and a choice to be evaluated in a more accurate way. However, it is unlikely that in an area characterized by a low regional rate of earthquake production the spatial variability of the reference rate can explain the observed southwestward migration. In this sense, we have tried to enlarge the time window for smoothing the most previous seismicity and we have include also in the model two big earthquakes of the past; but the so obtained results have not showed very different outcomes. We rely on the spatial and temporal stress heterogeneity and we emphasize that this should be taken into account for the applications of seismicity rate changes to assess earthquake probability.

During the work, the will to deal only with information given by a catalog, led us to reduce the free parameters of the model to only one. We have so

introduced an original relation to estimate the reference shear stressing rate from the reference seismicity rate. Theoretically it is a great improvement of such a model, together with the introduction of the log-likelihood method to perform the unique free parameter. However, facing with the real information we have at our disposal for this region, we have recognized an internal bias of the procedure when information on reference seismicity is lacking. In fact, in this case, also the evaluation of the reference shear stressing rate and of the characteristic time are consequently biased. We anyway have overcome this problem imposing a reasonable, uniform value to the seismicity reference rate.

This application has also allowed us to perform the best value of the unique free parameter  $A\sigma$  and to test the variability of the model. The best value we found for  $A\sigma$  is consistent with those proposed in literature.

We have demonstrated that the seismicity rate and probability estimates exhibit an important variability with respect to  $A\sigma$  values. For this reason we believe that our effort to perform its best value with a statistical method is very important, also because  $A\sigma$  is not directly observable.

We can conclude that the development and application of the presented model have been achieved investigating any aspects that could have influence on the final outcomes, obtaining original and interesting results that represent to us the clues for the future progress of such procedure.



## 4

# An overview on the possibility of unifying the epidemic and the rate-state models

The phenomenon of earthquake clustering, i.e. the increase of occurrence probability for seismic events close in space and time to other previous earthquakes, has been modeled both by physical and statistical processes.

In the previous chapters we have extensively described a physical model of such phenomenon. The RSM is considered as one of the most powerful model of earthquake interactions.

In this last chapter we present some results regarding our attempt to merge in an unique model a physical approach as that we have presented during the work, and a purely statistical one.

From a statistical viewpoint the so-called epidemic model (ETAS, Epidemic Type Aftershock Sequences) introduced by *Ogata* (1988), and its variations, have become fairly well known in the seismological community. Tests on real seismicity and comparison with the plain time-independent Poissonian model through likelihood-based methods have reliably proved its validity. But a purely stochastic model as ETAS ignores the physical interpretation of earthquakes.

To the other hand, the RSM, in the way we have used it, does not completely model the epidemic behavior of triggering process. Let us remember in fact that in our application in chapter (3) we imagined that just a few number of main events interact.

From these observations grew up our wish to investigate the performances of a hybrid model, that here we will call ERS model (Epidemic Rate and State). We were also interested to test the ERS model and for this purpose we applied it to real seismicity in Japan and in California. The application to the seismicity of Japan from 1970 to 2003 showed that the new ERS model preserves the capability of describing the observations with high likelihood, slightly higher then those obtained by purely epidemic models. To the other hand, the application to the seismicity of California did not match the same result. However, we can justify this deficiency of the ERS model make some observations about its main characteristics.

In the chapter we will first review the principles of stochastic models for earthquake clustering. Then we will introduce a new formulation of the RSM that

allows its application to modeling earthquake clustering fully epidemically (i.e., *each* source is supposed capable of increasing the probability of new earthquakes).

#### 4.1 Stochastic model for earthquake clustering

In a stochastic model earthquakes are regarded as the realization of a point process. Each event is characterized by its spatio-temporal-magnitude coordinates  $x, y, z, t, m$  (here  $z$  is fixed). We assume that the Gutenberg-Richter law describes the magnitude distribution of all the earthquakes in a sample, with a constant  $b$ -value, independently of the space coordinates.

If we neglect the interactions between events, and assuming that the earthquake occurrence is a stochastic process with no memory, the space density of earthquakes of magnitude equal to or larger than  $m$  is expressed as

$$\mu(x, y, m) = \mu_0(x, y)e^{-\beta(m-m_0)}, \quad (4.1)$$

where  $\mu_0(x, y) = \mu(x, y, m_0)$  is the space density of earthquakes of magnitude equal to or larger than  $m_0$ .  $\mu_0(x, y)$  represents exactly what we mean for *reference seismicity*. The density magnitude distribution of earthquakes under the same hypothesis (no memory stochastic process), obtained from equation (4.1), is:

$$\lambda_0(x, y, m) = \mu_0(x, y)\beta e^{-\beta(m-m_0)}. \quad (4.2)$$

In both equations (4.1) and (4.2) the choice of  $m_0$  is not critical, provided that the set of data is complete above it.

Taking into account the influence of the previous inducing earthquakes, the expected rate density of seismic events can be written more in general as (*Ogata*, 1988; *Console and Murru*, 2001; *Console et al.*, 2003):

$$\lambda(x, y, t, m) = f_r \lambda_0(x, y, m) + \sum_{i=1}^N H(t - t_i) \lambda_i(x, y, t, m), \quad (4.3)$$

where  $f_r$  is the failure rate (i.e., the fraction of events that occurs spontaneously),  $\lambda_0(x, y, m)$  represents the distribution of seismicity expressed as in (4.2),  $t_i$  is the occurrence time of the earthquakes, the total number of which is  $N$ ,  $H(t)$  is the step function, and  $\lambda_i(x, y, t, m)$  is the single contribution of the previous earthquakes. The term  $f_r \mu_0(x, y, m)$  is the *background seismicity* that substantially expresses the spontaneous rate of earthquake considering the process time independent and the absence of clusters. During the work we have just discussed about the difference between background seismicity and reference seismicity. The unperturbed term  $f_r \mu_0(x, y, m)$  of the ETAS model (neglecting the magnitude

distribution  $\beta e^{-\beta(m-m_0)}$ ) represents precisely what commonly is meant for background, while the only  $\mu_0(x, y, m)$  represents the reference seismicity which can include also clusters.

Equation (4.3) expresses the popular concept of the ETAS model (*Ogata, 1988*). The seismicity rate corresponding to any earthquake is constituted by the superposition of the first (the background) and the second (the effect of each perturbation) terms on the right-hand of (4.3). In this way, as in an epidemic system, no earthquake is claimed to be fully linked to any other earthquake in particular, but rather to all previous events and to the background seismicity, with different weights.

We hypothesized that the contribution of any previous earthquake  $(x_i, y_i, t_i, m_i)$  to the occurrence rate density of the subsequent earthquakes is decomposable (for  $t > t_i$ ) into three terms, respectively representing the *time*, the *magnitude* and the *space distribution*, as:

$$\lambda_i(x, y, t, m) = Kh(t - t_i)\beta e^{-\beta(m-m_i)}f(x - x_i, y - y_i), \quad (4.4)$$

where  $K$  is a constant parameter, while  $h(t)$  and  $f(x, y)$  are the time and space distributions, respectively. In a more general way, the magnitude distribution of induced events (or *aftershock productivity*) is expressed by the relation:

$$N(m) = e^{\alpha m_i} e^{-\beta m}, \quad (4.5)$$

where the term  $e^{\alpha m_i}$  is commonly recognized as proportional to the number of aftershocks produced by a mainshock with magnitude  $m_i$ . The  $\alpha$  parameter in this context has not to be confused neither with the Linker parameter introduced in chapters (2) and (3) to correct the friction coefficient for the nucleation solution; nor with the  $\alpha = a \ln(10)$  parameter of the Gutenberg-Richter law. But here it represents a parameter which describes the relation between the number of induced events ( $m$ ) and the magnitude of the inducing event ( $m_i$ ). We would here preserve the symbol  $\alpha$  for consistency with several works in the literature that deal with the aftershock productivity, as *Ogata (1989, 1994)*; *Console et al. (2003)*; *Zhuang et al. (2004)*; *Helmstetter et al. (2005)*; *Gasparini and Lolli (2006)* and references therein. In equation (4.4) we implicitly assumed the hypothesis that  $\alpha = \beta$  (*Reasenber and Jones, 1989*).

For the time dependence we adopted the so-called modified Omori law (*Ogata, 1983*):

$$h(t) = (p - 1)c^{(p-1)}(t + c)^{-p} \quad (p > 1), \quad (4.6)$$

where  $c$  and  $p$  are characteristic parameters of the process, and the expression is normalized, so that:

$$\int_0^\infty h(t)dt = 1. \quad (4.7)$$

In this context, equation (4.6) is used not only for the first generation of aftershocks, but also for secondary aftershocks triggered by subsequent earthquakes.

For the spatial distribution of the induced seismicity we have considered two different forms. The first is represented by a function, normalized to 1, with circular symmetry around the point of coordinates  $(x_i, y_i)$ . This function, translated in polar coordinates  $(r, \theta)$ , can be written as:

$$f(r, \theta) = \frac{q-1}{\pi} \frac{d^{2(q-1)}}{(r^2 + d^2)^q}, \quad (4.8)$$

where  $r$  is the distance from the point  $(x_i, y_i)$  and  $d$  and  $q$  are two free parameters (*Console et al.*, 2003). The second form is still represented by an isotropic inverse power of the distance, with circular symmetry around the epicenter of the triggering earthquake. But it includes the dependence on the magnitude of the previous events by scaling the parameter  $d$  with the magnitude:

$$f(r, \theta) = \frac{d_i^2}{(r^2 + d_i^2)^q}, \quad (4.9)$$

where  $d_i = d_0 e^{\alpha(m_i - m_0)}$ . In this case  $f(r, \theta)$  is not normalized, so  $m_i$  in equation (4.4) must be substituted with  $m_0$ . The parameter  $\alpha$  in this case is introduced again in the modeling, then for the ETAS-b model the *Reasenber and Jones* (1989) hypothesis does not hold.

Equations (4.4), (4.6), and (4.8) and (4.9) define the stochastic model ETAS; we will distinguish between an ETAS-a and an ETAS-b according to the use of equation (4.8) or (4.9) respectively. The free parameters for model ETAS-a are  $K$ ,  $c$ ,  $p$  of the generalized Omori formula, and  $d$  and  $q$  of the space distribution of triggered events. In model ETAS-b the further free parameter  $\alpha$  is added (*Zhuang et al.*, 2004).  $\beta$  (or  $b$ ) is obtained from the catalog data by the maximum likelihood method, independently of the other adjustable parameters.

## 4.2 The Epidemic Rate-and-State (ERS) model

In the previous section we have reviewed the principles which define a pure stochastic model for earthquake clustering, the ETAS model (that we distinguished into two forms depending on the spatial distribution assumed).

Now we would build up a new clustering model also considering the rate-and-state theory, so introducing a physical description of the phenomenon. In the ERS model we assume that the temporal behavior of the seismicity triggered by a shear stress change is described by the *Dieterich* (1994) model by the relation (1.5). This procedure will allow the computation of the likelihood of a seismic catalog also under the new hybrid model.

In general, the shear stress change  $\Delta\tau$  to be substituted in  $R(t)$ , equation (1.5), caused at any point by any earthquake, should be computed taking into account the focal parameters and the source mechanism of each earthquake. But this information is not usually contained in an earthquake catalog. Here we introduce a shortcut that allows the use of the most common catalog information constituted just by the origin time, the epicentral coordinates and the magnitude. So, empirically we hypothesize that the stress change produced by an earthquake is given by:

$$\Delta\tau = \Delta\tau_0 \left( \frac{d_i^2}{r^2 + d_i^2} \right)^q, \quad (4.10)$$

where  $r$ ,  $d_i$  and  $q$  have the same meaning as in equation (4.8) and  $\Delta\tau_0$  is a free parameter representing the maximum shear stress produced by the fault at its epicenter. Equation (4.10) implies a strong simplification of the stress pattern, ignoring the typical azimuthal dependence which presents also negative lobes. This rather crude assumption can be used as a first approximation, taking into account the experimental difficulties found in observing stress shadows and the importance of location errors for the computation of the stress change induced by small ( $m < 5$ ) earthquakes (*Marsan, 2003; Helmstetter et al., 2005*).

Let us give some more general remarks on the procedure adopted here to include the rate-and-state theory in an epidemic model. We have already proposed above a very simplified stress pattern in comparison with that computed in chapter (3). We now completely ignore the contribution of the normal stress change considered in the CFF computations.

We would highlight that to develop and apply an epidemic model it is necessary having information on all the interacting events; therefore it is unrealistic taking into account for each event all the characteristics considered for the CFF computation in the previous chapter (where just a few events were supposed to interact each other). Moreover, let us remember that the likelihood computation places far too much weight on the least probable events (see section (2.4)); then, in the case of an epidemic model, considering also the stress shadows could lead to misleading results because of the location errors.

The circular symmetry expressed by equation (4.8) and (4.9) is retained in equation (4.10). Note that if  $q = 1.5$ , equation (4.10) is consistent with the physical requirement of the  $1/r^3$  decay of the stress for  $r \rightarrow \infty$ , expected for a double couple source in an elastic medium (see also *Dieterich (1995)*). We guess that  $d_i$  is related to the magnitude  $m$  of the earthquake and we make the hypothesis that

$$d_i^2 = d_0^2 10^{m_i - m_0}, \quad (4.11)$$

where  $d_0$  is the radius of a circular fault of magnitude  $m_0$ . The  $b$  value is imposed equal to 1. Equation (4.11) can be simply derived by the combination of the expressions of the seismic moment for a circular fault in terms of stress drop and

source radius (*Keilis-Borok*, 1959):

$$M_0 = \frac{16}{7} \Delta\sigma d^3, \quad (4.12)$$

and that of the seismic moment and the magnitude  $m$  of an earthquake:

$$M_0 = M_0^* 10^{1.5(m-m_0)}, \quad (4.13)$$

where  $M_0^*$  is the seismic moment released by an event of magnitude  $m_0$ . Integrating the expected rate of earthquakes  $R(t)$  as in (1.8), over the whole  $(x, y)$  plane, and considering relation (4.10), we obtain that the total number of aftershocks triggered by an earthquake is:

$$N_{tot} = \frac{r}{\dot{\tau}} \int \int_{-\infty}^{+\infty} \Delta\tau dx dy = r \frac{\Delta\tau_0}{\dot{\tau}} \frac{\pi}{q-1} d^2. \quad (4.14)$$

The total number of aftershocks is so proportional to the source area and, as a consequence of equations (4.12) and (4.13), to  $10^m$  or to  $10^{\frac{2}{3}M_0}$ , assuming a bidimensional distribution of sources as discussed by *Helmstetter et al.* (2005). This result is consistent with that shown in chapter (1), section (1.4), for the application of the RSM to a rectangular fault. It is also in agreement with some empirical observations as those reported by *Vere-Jones* (1969); *Helmstetter and Sornette* (2001) and *Felzer et al.* (2002).

Then, assuming the stress pattern (4.10), we can finally reformulate the epidemic model of equation (4.3) replacing  $\lambda_i(x, y, t, m)$  with the net triggered occurrence density rate obtained multiplying  $\mathcal{R} = R - r$  by  $\beta$  for each earthquake of the catalog occurring at the time  $t_i$ .

For the numerical applications that we are going to show in the next sections it remains only to define the value of the various parameters involved in the procedure.

The parameters  $\Delta\tau$  and  $q$  can be fixed guessing their values by the experience:  $\Delta\tau = 2.5 \text{ MPa}$ , as fixed also by *Dieterich* (1995);  $q = 1.5$  for consistency with the theory of elasticity.

The reference seismicity  $r$ , also used in the ETAS model and represented by  $\mu_0$ , has been estimated again by smoothing the seismicity over a time period. For the application in Japan we smoothed the seismicity on the period January 1<sup>st</sup> 1970-December 31<sup>th</sup> 1993 (which we will call the learning period) using 20 km for the correlation distance  $c$ . For this purpose we selected all the events with magnitude  $m \geq 4.5$  and depth  $z \leq 70 \text{ km}$  from the Japan Metereological Agency (JMA) catalog in the time window selected. Figure (4.1) shows an example of smoothing the seismicity on the whole time window considered in Japan (1970-2003). Otherwise, for the application in California we smoothed seismicity on the period 1984-1992 using 11 km for the correlation distance  $c$  (see *Frankel* (1995)

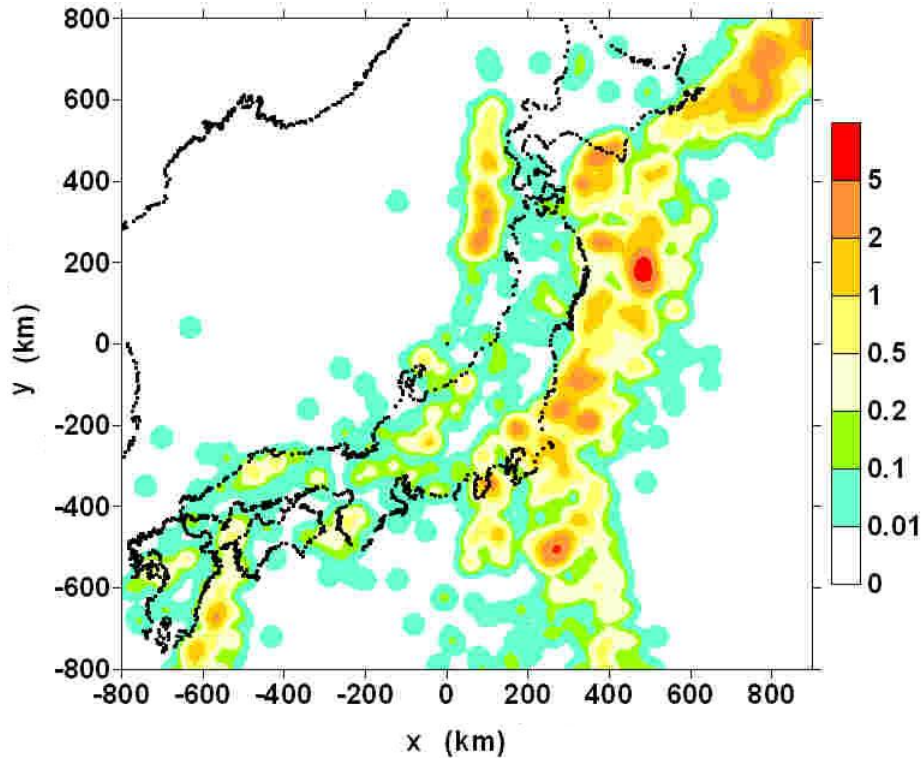


Figure 4.1: Smoothed seismicity of Japan and of the surrounding area during the years 1970-2003. The color scale represents the average number of earthquake with  $m \geq 4.0$  in an area of  $100 \text{ km}^2$ .

for the smoothing method) and selecting all the events with  $m \geq 3.0$  and  $z \leq 30 \text{ km}$ .

Let us remember that also in this chapter we make use of the relation (2.25) which introduces the  $b$ ,  $m_0$  and  $m_{max}$  free parameters in the model.  $m_{max}$  and  $m_0$  can be deduced by catalog information.  $d_0$  can be derived by the  $m_0$  value through the *Kanamori and Anderson* (1975) relation. So, we have left only  $\Delta\tau_0$  and  $A\sigma$  as free parameters of the new model, to be determined by the maximum likelihood best fit.

### 4.3 Testing the ERS model through the Japanese seismicity

In this section we would test the new ERS model on the Japanese seismicity in comparison with the pure stochastic ETAS model (in the two different forms, ETAS-a and ETAS-b, introduced in section (4.1)). The procedure is the same de-

scribed in section (2.4) and consists in searching for the maximum log-likelihood function for the realization of seismic events described by a catalog. But now the goals and the procedure are pretty different than those of the test in chapter (3).

Here we aim to establish the predictive power of the models for earthquakes of significant impact on the population. In this sense we do not want to limit the use of the epidemic model to forecast just conventional aftershock activity soon after main shocks, but we want to emphasize also its capacity of forecasting main shocks that occur after foreshocks. We therefore decided to consider the likelihood of the observed earthquakes under the respective models taking as target events only the strongest ones, and we arbitrarily selected for them the magnitude threshold  $\bar{m} = 6.5$ . In this way, the sum in the first member of the right side of equation (2.26) and the integral in the second member are computed only for the earthquakes with magnitude  $\bar{m} \geq 6.5$ , but the expected rate density is computed taking into account the triggering effect of all the earthquakes exceeding magnitude  $m_0$ .

The method has been implemented on the seismic catalog collected by the Japan Meteorological Agency (JMA) from January 1<sup>st</sup> 1970 to December 31<sup>th</sup> 2003, which contains 33,346 earthquakes of magnitude equal to or larger than 4.0. On the basis of an analysis of completeness, we have selected the events with magnitude  $m \geq 4.5$  and depth  $h \leq 70$  km contained in the polygon 30-46°N and 128-150°E. This selection reduces the data set to a number of 7,467 events. The largest recorded magnitude is  $m_{max} = 8.2$ . The extent of the geographical region used in this exercise reflects the generality of the epidemic algorithm, which is capable of fitting the seismicity in various situations, without the necessity of being tuned on the features of specific environments.

The catalog has been divided in two parts: a learning period from 1970 to 1993 and a test period from 1994 to 2003. This choice has been guided by the criterion that each of the periods included enough events to achieve a good reliability of the results. Let us note that it is the proper procedure for testing a model. It is easily applicable in a catalog as that of the Japan (or California), but it is not applicable to a catalog as that we treated in chapter (3) because of its paucity of data.

The first part of the catalog (*the learning data set*), containing 4,671 events of magnitude  $m \geq 4.5$  and 43 events of magnitude  $m \geq 6.5$ , has been used for the best fit of the free parameters characterizing models ETAS-a, ETAS-b and ERS respectively. The maximum-likelihood b-value of the learning data set is  $0.924 \pm 0.011$ , with the error computed using the formula suggested by *Shi and Bolt* (1982).

The second part (*the testing data set*), containing 2,796 events of magnitude  $m \geq 4.5$  and 28 events of magnitude  $m \geq 6.5$ , has been used for the evaluation

of the likelihood for the three models in a forward-retrospective way. Therefore, the statistical requirement that the test is carried out on a data set independent of that on which the hypothesis is formulated is fulfilled.

The maximum-likelihood best fit for model ETAS-a, ETAS-b and ERS on the learning data set has provided the results shown in table (4.1). For the ERS

Table 4.1: Best fit values of the parameters of models ETAS-a, ETAS-b and ERS obtained on the learning period of the Japanese catalog.

<b>ETAS-a</b>	<b>ETAS-b</b>	<b>ERS</b>
$K = 0.0076 \text{ days}^{p-1}$	$K = 0.00057 \text{ days}^{p-1}$	$\Delta\tau_0 = 0.75 \text{ MPa}$
$d = 5.91 \text{ km}$	$d_0 = 2.52 \text{ km}$	$A\sigma = 0.012 \text{ MPa}$
$q = 1.757$	$q = 1.989$	$f_r = 0.437$
$c = 0.0158 \text{ days}$	$c = 0.0143 \text{ days}$	$\ln L = 299.91$
$p = 1.244$	$p = 1.244$	
$f_r = 0.58$	$\alpha = 0.87$	
$\ln L = 305.44$	$f_r = 0.57$	
	$\ln L = 308.88$	

model we initially choose  $m_0 = 4.5$  (from which derives  $M_0^* = 7.06 \cdot 10^{15} \text{ Nm}$  and  $d_0 = 1.07 \text{ km}$ ), and we imposed  $\alpha = \beta$ . Observe that the log-likelihood for the ERS model is slightly lower than those for models ETAS-a and ETAS-b. The difference is of the order of few units, not enough to reject any of the three hypotheses in favor of the other, according to the Akaike Information Criterion (*Akaike*, 1977). In fact, let us remember that in such a case one has to take into account also the number of the free parameters of a model. In the ERS model the free parameters are fewer than in the two ETAS ones, so weakening the performance capacity of the procedure. Note also that the log-likelihood under a time-independent Poisson model on the same catalog is only  $\ln L = 228.02$ , so as to fully allow rejecting this hypothesis in favor of the others.

The test is otherwise carried out on a different and independent data set (1994-2003): the testing data set. In the test we run the algorithm for the likelihood computation without looking for a best fit, but using the parameters obtained from the learning phase. The effective number of free parameters in the test is zero for all the models, so that the Akaike Information Criterion is now not applicable. The results for the different models are:

- **Poisson:**  $\ln L = 111.54$
- **ETAS-a:**  $\ln L = 165.30$
- **ETAS-b:**  $\ln L = 169.81$

- **ERS:**  $\ln L = 171.24$

So, on the testing period, the ERS model yields a likelihood value slightly larger than those of the ETAS-a and ETAS-b ones.

A more detailed analysis of the single contribution of each target event (those of magnitude  $m > 6.5$ ) to the final value of the log-likelihood can be made by considering the rate density  $\lambda_0(x_j, y_j, m_j)$  of the Poisson model in comparison with the rate density  $\lambda(x_j, y_j, m_j)$  of the clustering models for each target events. These rates are reported in table (4.2) for the whole test period (1994-2003). In this case we considered only the purely epidemic-model ETAS-b.

Table (4.2) shows that for 9 out of the 28 events the rate density computed by both clustering models is by some orders of magnitude larger than that computed by the Poisson model. These events (marked by a star in the first column of table (4.2)) can be considered as forecasted by the clustering algorithms. However, 6 of these 9 forecasted events occurred in the influence space-time volume of previous larger earthquakes, making them aftershocks rather than mainshocks triggered by foreshocks. This was the case of both the clusters occurred in 1994 and of the cluster occurred in 2003. In the three first cases, the two October 5<sup>th</sup> and the 9<sup>th</sup> events of  $m = 6.8$ ,  $m = 6.6$  and  $m = 7.3$  respectively, were preceded by the October 4<sup>th</sup>, 1994 main shock,  $m = 8.2$ , off the east coast of Hokkaido. In the same year, the two December 29<sup>th</sup> events, both  $m = 6.5$ , were preceded by the December 28<sup>th</sup>, 1994 main shock,  $m = 7.6$ , off the east coast of Tohoku. Finally, the September 26<sup>th</sup>, 2003 event,  $m = 7.1$  east of Hokkaido, had been preceded by the  $m = 8.0$  main shock, occurred about one hour before. In the case of other two earthquakes, respectively the October 19<sup>th</sup>, 1996 main shock,  $m = 6.9$  east of Kyushu, and the July 1<sup>st</sup>, 2000 main shock,  $m = 6.5$  south of Tokyo, no larger magnitude earthquakes had been recorded in a short space-time interval before them. Finally, another earthquake of the same magnitude and a high rate density has followed the latter main shock at an epicentral distance of 30 km, after one month. There are, otherwise, 16 earthquakes for which the Poisson rate is larger or similar to the clustering model rate density: these cases can be called failures of predicting. The January 17<sup>th</sup>, 1995,  $m = 7.3$  Kobe earthquake is among them.

The last column of table (4.2) reports the ratio between the rate densities of model ERS and model ETAS-b, respectively. The ratio is larger than 1 if the occurrence rate predicted by model ERS is larger than that predicted by model ETAS-b. Though the number of cases for which this ratio is smaller or larger than 1 is about the same, the overall better performance of model ERS is due to a few earthquakes for which it achieves a rate several times larger than model ETAS-b. This circumstance applies to earthquakes that occurred later in time and longer on distance from the triggering event, as it can be seen in table (4.2) for the earthquakes whose value of  $\lambda_{ERS}/\lambda_b$  is higher than 2.0.

Table 4.2: List of the 28 target events of  $m > 6.5$  and their occurrence rate density ( $events/day/km^2$ ) under the Poisson ( $\lambda_0$ ), ETAS-b ( $\lambda_b$ ) and ERS ( $\lambda_{ERS}$ ) models respectively.

Date	Coordinates	m	$\lambda_0$	$\lambda_b$	$\lambda_{ERS}$	$\lambda_{ERS}/\lambda_0$
08/04/1994	40.568,143.957	6.5	6.1E-08	3.5E-08	3.3E-08	0.932
04/10/1994	43.372,147.678	8.2	2.6E-09	1.6E-09	1.5E-09	0.943
<b>05/10/1994*</b>	43.270,148.468	<b>6.8</b>	<b>1.5E-08</b>	<b>2.1E-05</b>	<b>5.5E-05</b>	2.676
<b>05/10/1994*</b>	43.322,148.370	<i>6.6</i>	<b>2.3E-08</b>	<b>8.7E-04</b>	<b>3.4E-04</b>	0.391
<b>09/10/1994*</b>	43.555,147.807	<b>7.3</b>	<b>1.7E-08</b>	<b>2.6E-06</b>	<b>2.3E-06</b>	0.866
28/12/1994	40.427,143.748	7.6	6.0E-09	3.7E-09	5.8E-09	1.583
<b>29/12/1994*</b>	40.113,143.023	<b>6.5</b>	<b>4.9E-08</b>	<b>3.0E-06</b>	<b>8.9E-06</b>	2.911
<b>29/12/1994*</b>	40.315,143.815	<b>6.5</b>	<b>7.2E-08</b>	<b>1.6E-04</b>	<b>3.3E-05</b>	0.205
07/01/1995	40.220,142.308	7.2	2.4E-08	2.1E-08	7.8E-08	3.662
17/01/1995	34.595,135.037	7.3	5.4E-11	3.4E-11	3.0E-11	0.882
29/04/1995	43.707,147.887	6.7	6.8E-08	1.0E-07	3.8E-07	3.635
25/11/1995	44.565,149.363	6.8	4.9E-08	2.9E-08	2.8E-08	0.969
30/12/1995	40.697,143.755	6.5	3.3E-08	2.8E-08	7.5E-08	2.716
17/02/1996	37.305,142.550	6.8	7.3E-09	4.3E-09	5.0E-09	1.158
<b>19/10/1996*</b>	31.795,132.010	<b>6.9</b>	<b>3.8E-08</b>	<b>8.8E-05</b>	<b>1.1E-04</b>	1.241
03/12/1996	31.765,131.682	6.7	1.5E-08	1.6E-08	1.3E-07	8.025
26/03/1997	31.968,130.360	6.6	8.9E-10	6.0E-10	1.2E-09	2.067
25/06/1997	34.438,131.668	6.6	8.7E-10	5.1E-10	5.2E-10	1.018
28/01/2000	43.005,146.748	7.0	2.9E-08	1.8E-08	1.6E-08	0.899
01/07/2000*	34.187,139.197	6.5	1.7E-08	1.5E-05	5.8E-06	0.402
30/07/2000*	33.967,139.413	6.5	2.9E-08	1.6E-05	1.7E-05	1.067
06/10/2000	35.270,133.352	7.3	5.5E-09	3.5E-09	3.3E-09	0.924
24/03/2001	34.128,132.695	6.7	2.1E-09	1.2E-09	2.2E-09	1.764
25/05/2001	44.313,148.817	6.9	2.5E-08	1.5E-08	1.4E-08	0.979
26/09/2003	41.775,144.082	8.0	1.1E-09	6.2E-10	6.1E-10	0.994
<b>26/09/2003*</b>	41.707,143.695	<b>7.1</b>	<b>5.7E-09</b>	<b>1.6E-04</b>	<b>4.7E-05</b>	0.287
29/09/2003	42.357,144.557	6.5	1.4E-08	5.7E-07	2.7E-06	4.668
31/10/2003	37.828,142.698	6.8	9.8E-09	6.8E-09	1.7E-08	2.548

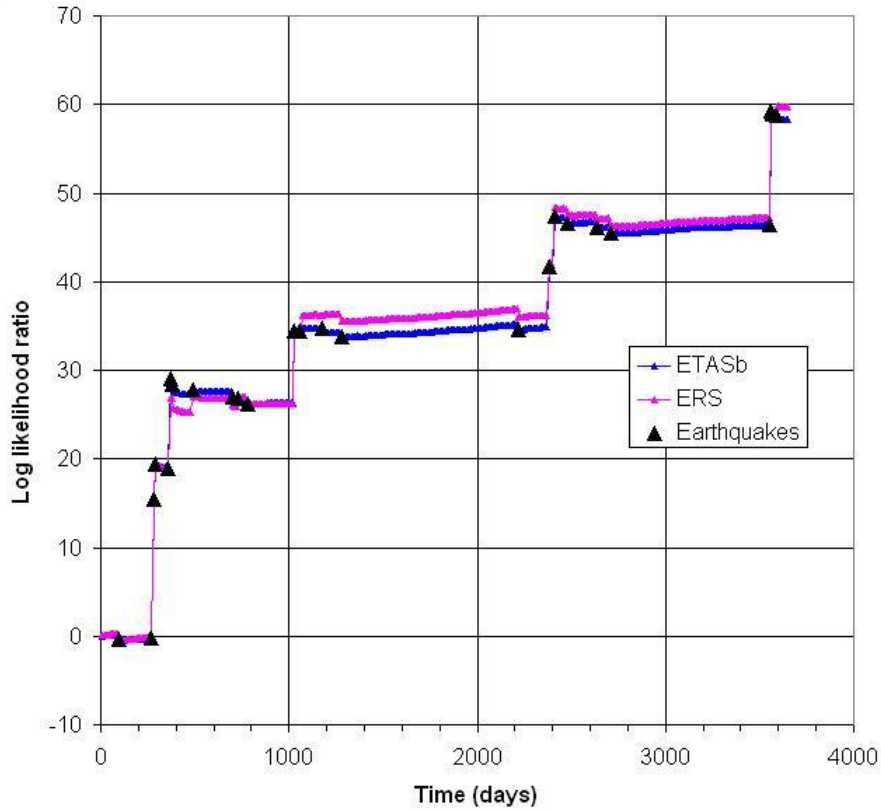


Figure 4.2: Log-performance factors  $\ln(\lambda_b/\lambda_0)$  and  $\ln(\lambda_{ERS}/\lambda_0)$  achieved by the ETAS-b and ERS models respectively, against the Poisson one. The temporal window comprises the whole testing period; the origin time is January 1<sup>st</sup>, 1994 at 00:00 UTC. The black triangles represent the target events with  $m > 6.5$ .

Figure (4.2) shows the plot of the log-performance factor (that is the difference of the log-likelihood values) for both models ETAS-b and ERS against the time independent Poisson model, versus time for the ten-year test period. Each of the events with magnitude equal to or larger than 6.5 (black triangles) produces a sharp step in the performance factor. The step is positive when the occurrence rate expected by the epidemic model is larger than that expected by the Poisson model. Observe the difference in the size of these steps between the two epidemic models. Besides the information contained in table (4.2), figure (4.2) puts in evidence also the trend of the performance factor in the time periods between the target events. This trend is positive if the occurrence rate expected by the Poisson model for the whole target area is smaller than that expected by the epidemic models, as it is generally the case.

Figures (4.3) show an example of how the ERS model displays the changes of the expected occurrence rate density. Panel (a) shows the expected rate of earthquakes the day before the October 19<sup>th</sup>, 1996 event (31.83  $N$ -132.01  $E$ ,  $m = 6.9$ , 23:44 UTC) within a square of  $100 \times 100$  km. Panel (b) shows the situation just before the event, after the occurrence of few precursory events. Note that the occurrence rate density before the sequence is not zero but ranges from  $1 \cdot 10^{-4}$  to  $5 \cdot 10^{-4}$ . The values of the parameters are those obtained by the maximum log-likelihood best fit.

Let us make a general observation. Considering a simplified stress pattern, as in equation (4.10) (to practically merge the RSM with the ETAS model), rather than a complex one, as we did in chapter (3), leads to mask the variable geometry of the triggering phenomenon. In fact, in the two panels of figure (4.3), we can not observe neither the negative lobes of stress change, nor the directivity of the triggering. The whole information is simplified and so reduced using equation (4.10).

#### 4.4 Testing the ERS model through the seismicity of California

For this test on Californian seismicity, we consider the likelihood of the observed earthquakes under models ETAS-a and ERS using only earthquakes with magnitude equal to or larger than 4.0 as target events. This is the same threshold considered for California in the *Regional Earthquake Likelihood Models* (RELM) test exercise (visit <http://www.earthquake.ethz.ch/docs/presentations/talk-schorlemmer2005.pdf>). The procedure adopted in this section is exactly the same described in the previous section, but here we focus our attention only on model ETAS-a and model ERS, both assuming the hypothesis  $\alpha = \beta$ .

The method has been implemented on the (undeclustered) California seismic catalog collected for the RELM test exercise (*Schorlemmer et al.*, 2004) from January 1984 to December 2004, containing 14,823 earthquakes of magnitude equal to or larger than 3 with depth  $z \leq 30$  km. We have selected the events contained in the rectangle of  $1,800 \times 1,800$  km centered on the point of coordinates  $36.5^\circ N$  and  $-119^\circ E$ , including the entire state of California. This selection reduces the data set to 14,699 events. The largest recorded magnitude is  $m_{max} = 7.3$ .

Again the catalog has been divided in two parts: a learning period from January 1984 to September 1992 and a testing period from October 1992 to December 2004. Also in this case, as in the previous section, this choice has been guided by the criterion that each of the periods would include enough events to achieve a good reliability of the results.

The first part of the catalog (the learning data set), containing 7,346 events of magnitude  $m \geq 3.0$  and 953 events of magnitude  $m \geq 4.0$ , has been used for the

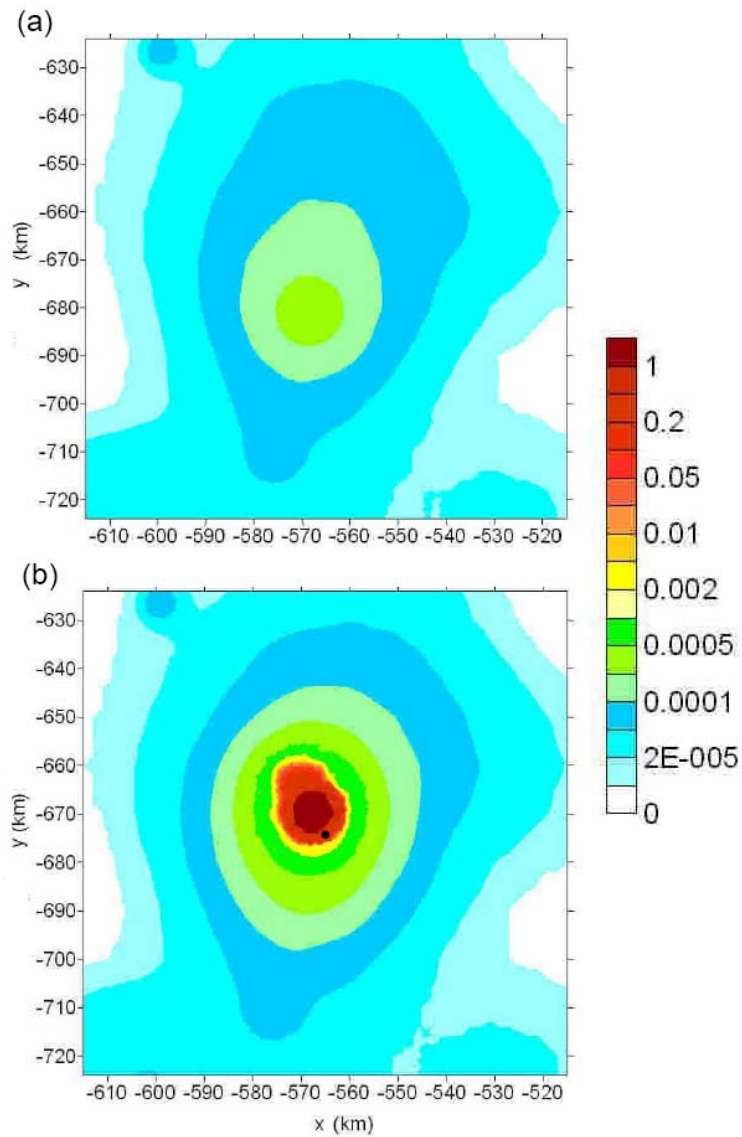


Figure 4.3: Modeled rate density expected before the October 19<sup>th</sup>, 1996 event before (a) and after (b) few precursory events. The color scale represent the number of earthquake per day and per 100  $Km^2$

best fit of the free parameters characterizing both the models and for estimating the reference seismicity  $\mu_0(x, y)$ , with the parameter of the correlation distance  $c = 11 \text{ km}$ . We fixed  $q = 1.5$ . The maximum-likelihood b-value of the learning data set is  $0.859 \pm 0.01$ . The values of the best fitted parameters and for the likelihoods for the two models on the learning period is shown in table (4.3).

Table 4.3: Best fit values of the parameters of models ETAS-a and ERS obtained on the learning period of the Californian catalog.

<b>ETAS-a</b>	<b>ERS</b>
$K = 0.0029 \text{ days}^{p-1}$	$\Delta\tau_0 = 0.17 \text{ MPa}$
$d = 1.57 \text{ km}$	$A\sigma = 0.0057 \text{ MPa}$
$c = 0.0044 \text{ days}$	$f_r = 0.288$
$p = 1.146$	$\ln L = 13393.21$
$f_r = 0.39$	
$\ln L = 12857.06$	

The second part of the catalog (the testing data set), containing 7,352 events of magnitude  $m \geq 3.0$  and 940 events of magnitude  $m \geq 4.0$ , has been used for the evaluation of the likelihood for the two models in forward-retrospective way:

- **Poisson:**  $\ln L = 10435.50$
- **ETAS-a:**  $\ln L = 12597.26$
- **ERS:**  $\ln L = 11717.30$

Note that the log-likelihood for model ERS is lower than that for model ETAS-a. The difference is of the order of 536, so large enough to reject the physically constrained hypothesis in favor of the stochastic model, according to the Akaike Information Criterion (*Akaike*, 1974). Note also that the log-likelihood under a time-independent Poisson model on the same catalog is only 10435.50, so as to allow rejecting this null hypothesis in favor of the ETAS and ERS models.

Figure (4.4) shows the temporal variation of the log-performance factor for both models ETAS-a and ERS with respect to the time-independent Poisson model for the testing period. Each of the events with magnitude equal to or larger than 4.0 produces a sharp step in the performance factor. The step is positive when the occurrence rate expected by the epidemic model is larger than that expected by the Poisson model. Note the difference in the size of these steps between the two models considered. In general, the ETAS-a model achieves larger steps for all the earthquakes. Figure (4.4) shows the trend of the performance factor in the time periods between the target events. This trend is positive if

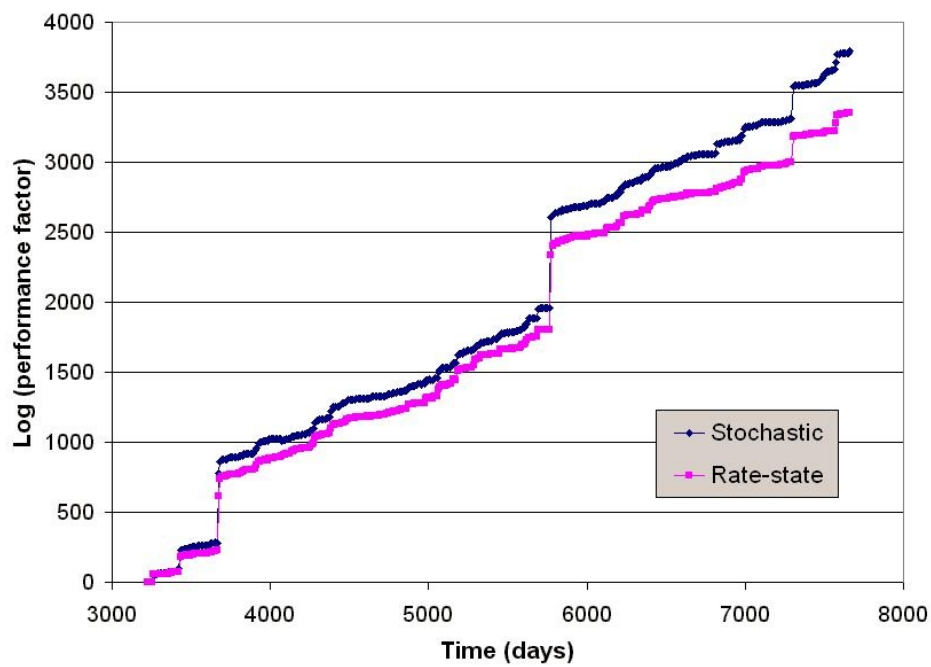


Figure 4.4: Log-performance factors  $\ln(\lambda_a/\lambda_0)$  and  $\ln(\lambda_{ERS}/\lambda_0)$  achieved by the ETAS-a and ERS models respectively, against the Poisson one. The temporal window comprises the whole testing period; the origin time is arbitrary.

the occurrence rate expected by the Poisson model for the whole target area is smaller than that expected by the epidemic model, as is generally the case.

The strong difference in the spatial distribution modeled by the ETAS-a and ERS models may help explain the better performance of the former when applied to the seismicity of California. The ETAS-a model contains the  $d$  parameter, which can be adjusted to account for the location errors of the epicenters in the catalog, typically of the order of magnitude of several kilometers. In this respect model ERS is much more rigid, as the spatial distribution does not depend on any free parameter, but is constrained by the relation between the magnitude and the source size. Because the source size for magnitudes as small as 3.0 is smaller than 200 m (*Kagan, 2002*), the much larger spread introduced by the location errors affects the likelihood of the catalog to a large extent. This circumstance also explains why the ERS model exhibits a better performance with the Japanese catalog, for which we consider only magnitudes larger than 4.5.

## 4.5 Discussion on the ERS model achievements and final remarks

We have shown how a previously existing purely epidemic model (the ETAS model) can be modified by the application of the rate-and-state theory. This application has allowed to reduce the number of the free parameters of the model, giving at the same time a physical meaning to each of them. Otherwise, the new modeling has allowed the generalization of the RSM toward a really epidemic procedure.

The time dependence of the ETAS model, commonly described by the Omori law, has been substituted by the more general temporal trend modeled by *Dieterich* (1994) for a population of faults. We have already discussed in this work how the temporal trend expected by the RSM gives a more complex information than that of the Omori law (chapter(1)).

The application of both the stochastic and the ERS model to the computation of the likelihood of earthquake catalogs implies considerable simplifications of the seismic processes.

The most limiting simplification assumed in the ERS model is the circular symmetry of the triggering effects. A similar simplified and approximate representation has been used also by *Dieterich* (1995). We have shown before, in chapters (2) and (3), a more complex and realistic solution, but such complex stress pattern is unrealistically applicable in an epidemic model. In fact there is no doubt that the stress change computation made by a physical model (as the CFF) of each earthquake source would improve the results significantly, but the information needed to compute such stress change is not currently available in a typical seismic catalog.

Note that in model ETAS-a equation (4.8) gives directly the density distribution of triggered events, where  $d$  is a constant independent of the magnitude of the triggering earthquake. The best fit of  $d$  may reflect the location error of the events in the catalog, especially for small magnitudes. The same applies to  $d_0$  for equation (4.9) in model ETAS-b. For model ERS the parameter  $d_0$  depends on the magnitude through equation (4.11), and it is no longer a free parameter.

The three models ETAS-a, ETAS-b and their modified version ERS have been initially tested by the seismic catalog reported by JMA for Japan. This test has shown that the likelihood of the data set under the new epidemic-physical model ERS is better than that obtained under the purely stochastic models. The analysis has confirmed also that the ERS model (as in general any epidemic model) performs better when applied to an ongoing cluster, and not in forecasting a real foreshock.

With respect to the number of events triggered by a previous earthquake, called aftershock productivity, we have supposed that this number is proportional to  $e^{\alpha m_i}$ , with  $\alpha = \beta$ , both for models ETAS-a and ERS. Model ETAS-b is the only one where  $\alpha$  is introduced again and obtained by a maximum likelihood best fit. The value so estimated, nearly three times smaller than  $\beta$ , appears unrealistically small. If this circumstance was real, it would mean as a consequence that small events dominate the process of triggering aftershocks. It seems that this feature is typical of the cases when  $\alpha$  is obtained by the maximum likelihood best fit of a catalog (*Helmstetter et al.*, 2005). For instance, *Console et al.* (2003) obtained 1.0 for the Italian seismicity; *Gasperini and Lolli* (2006) verified that assuming a coefficient for mainshock magnitude  $\alpha = 2/3\beta$  improves the ability to forecast the behavior of the Italian sequences; and *Zhuang et al.* (2004) obtained a value around 1.35 for the JMA catalog. There are at least two different possible explanations of such results: one of them might be the lack of aftershocks reported in the catalogs soon after a strong earthquake; the other could be thought as a mathematical artifact caused by the strong correlation between  $K$  and  $\alpha$  in the best fit regression (*Gasperini and Lolli*, 2006).

Model ETAS-a and ERS have been then tested by the Californian catalog too. The outcomes of this application show that the log-likelihood for model ERS is lower than that for model ETAS-a. The difference is large enough to reject the physically constrained hypothesis in favor of the stochastic model, according to the AIC (*Akaike*, 1974). However, the likelihood value obtained under the Poisson model allows to reject this null hypothesis in favor of both the ETAS-a and ERS models. We found a possible justification of such result in the rigidity of the ERS model with respect of its dependence to the spatial distribution.

Let us now consider the physical implications of the values obtained for the parameters. For Japanese seismicity, we found  $\Delta\tau_0 = 0.17 MPa$ , a value smaller

than the value of the constant stress drop commonly assumed ( $\approx 3 \text{ MPa}$ ) in the source model. We must consider that the value obtained from the best fit is an average result of extremely complex real situations. These situations may include strong stress change variations over the fault area, from negative values of the order of  $\Delta\sigma$ , where the stress drop is total, to larger positive values, in correspondence of barriers. The same happens for seismicity of California, for which we found  $\Delta\tau_0 = 0.75 \text{ MPa}$ .

To the other hand, our result for  $A\sigma$  in the first application ( $0.012 \text{ MPa}$ ) is smaller but comparable with that obtained in chapter (3), and so comparable with those more commonly reported in literature. Otherwise, the value obtained for California ( $0.0057 \text{ MPa}$ ) is even smaller, so it is not comparable with the previous values; but it is however comprised in the range proposed by *Harris* (1998). Let us give some other important remarks on this outcome. According to *Dieterich* (1995), who assumed values of  $A$  ranging from 0.00001 to 0.007 in his simulations, our result leads to a normal stress  $\sigma$  ranging from 0.8 to 570  $\text{MPa}$  in the seismogenic layer. The upper limit of this range is consistent with the lithostatic pressure existing in the seismogenic layer at a depth of 5 – 10  $\text{km}$ . Moreover, a conversion of the mean background rate into the average stress rate leads to the value  $\dot{\tau} = 47.4 \text{ Pa/day}$  for the California seismic catalog over the entire seismogenic area. Dividing  $A\sigma = 0.0057 \text{ MPa}$  by  $\dot{\tau} = 47.4 \text{ Pa/day}$ , we obtain a characteristic time  $t_a = 120 \text{ days}$ , which is a reasonable value for the average duration of aftershock sequences according to the analysis of the catalog. However, one has to consider that the best fit of  $A\sigma$  has not been the main goal of the applications presented in this section. In fact, to properly perform the best value of  $A\sigma$  it could be better consider the whole catalog, including the major sequences on it.

We would like to conclude highlighting the most important reached goals with this new procedure:

- the introduction of relatively simple physical constraints allowed a substantial reduction in the number of free parameters necessary in the formulation of the ETAS model;
- the new Epidemic Rate-and-State model performs better (or at least the results are comparable) than the purely ETAS one on Japanese seismicity.
- we must consider the rigid dependence of the ERS model to the spatial distribution when we deal with small magnitude values: the consequent small values of the source size lead to a much spread of the locations errors on likelihoods.



## Final remarks and speculations on the future

In this work we have deepened, revised and improved a rate and state model. Beginning with a theoretical analysis in chapter (1), that led us to some new insights on the modeling, we have delivered then a more complex and realistic procedure with the intent to apply it in real cases, aiming to contribute to seismic hazard assessments (chapters (2) and (3)).

During the application to the 1997 Umbria-Marche sequence, we investigated the model capabilities with the criticism necessary to perform an objective and exhaustive analysis. We have also tried, in chapter (4), to unify such physical model with the pure statistical ETAS model. Testing the new hybrid model, the Epidemic Rate and State (ERS) model, on real seismicity in Japan and California, we analyzed its capacities and its limits.

With the purpose of studying both the spatial and the temporal behavior of the phenomenon of clustering we merged the strengthened Coulomb Failure Function (CFF) model with the Rate-and-State one (RSM). The more important novelties introduced with a rate-and-state model are:

- the physical properties of the faults are even taken into account, explaining some important features of the earthquake interaction phenomenon, as the delay in triggering response or the clock advance of the close-to-failure faults;
- it is a time dependent model capable to justify the aftershock decay rate and the time delay between interacting events;
- the phenomenon of triggering is explained in probabilistic terms (not deterministic) allowing a rigorous testing procedure on the model.

Analyzing minutely the spatio-temporal behavior predicted by the RSM we found in chapter (1) several new findings; the most important are (regarding an application to a rectangular fault):

- the total number of triggered events per unit area is proportional to the shear stress change if interactions among events are neglected;

- many earthquakes of small magnitude can produce, in total, a number of aftershocks comparable to that of fewer larger earthquakes;
- the seismic activity is very intense during the first few hours or days after the occurrence of the primary earthquake, in the proximity of the edges of the fault;
- for longer time (several years) the total number of triggered events in the external zone becomes comparable with that of the most internal one, so becoming significantly large;
- the regional reference seismicity could be so interpreted as a sort of noise, or memory, due to the superposition of the effect of many older earthquakes;
- the time decay described by the popular Omori law could be interpreted as an apparent average result of the contribution from the various areas on the plane containing the primary fault;
- the seismic activity inside the fault drops to negligible values at the occurrence of the primary earthquake and returns to normal values only after a time much longer than the characteristic time (several tens of years in our simulations);
- the seismicity rate changes in space and time, but it does not have influence on the rate averaged over very large space-time intervals: a null net balance is lastly reached as a sort of conservative natural law.

Developing and improving such a forecasting tool, with the purpose of applying it in real time making use only of a catalog information, we have enabled the algorithm to manage with a real seismic sequence and we have introduced some original skills in the model:

- we introduced an original relationship between the reference seismicity rate and the shear stressing rate;
- we reduced the free parameters to one;
- we allowed to perform the unique free parameter through a log-likelihood method.

Some important and unexplored topics have been deepened during the model developing and application:

- we pointed out the correction needed in computing the friction coefficient when used in a nucleation solution, and its weight in rates and probabilities computations;

- we analyzed the role of the free parameter value, the reference seismicity rate and the stress heterogeneity on rates and probabilities estimates;
- we modeled also the temporal behavior of expected seismicity rates finding a good accordance with real observations.

At this point the algorithm was ready to be tested in a real application. For this reason we selected a particular sequence as that of Umbria-Marche, 1997, with the aim to investigate if such a model can justify the migration of seismicity from northwest toward southeast, and the presence of normal faulting aftershocks on the hanging wall of the main shock fault planes, and the consequent lack of seismicity on the footwall. The application revealed that the seismicity rate changes, computed with our procedure, can not provide such desired explanations. But the failure in forecasting the migration of seismicity does not prove that the RSM is incorrect; rather, we believe that it demonstrated that the stress time history perturbing the fault population is much more complex than that simulated only through static coseismic stress changes. We have recognized three important factors that can justify this lack of the RSM defining better the stress time history:

- the fluid flow and the pore pressure relaxation can contribute to explain the temporal evolution of stress perturbations;
- stress heterogeneity, and the associated geometrical complexity of the pre-existing fault, can remove seismicity shadows;
- a more accurate evaluation of the reference seismicity rate can refine the outcomes of the model.

With respect to the role of the parameters on the outcomes of the model, we have demonstrated that the  $A\sigma$  parameter has an important influence both in seismicity rates and in occurrence probabilities. Such influence can not be ignored in hazard assessments.

Also the applications and tests of the hybrid ERS model highlighted some interesting results:

- the introduction of the rate-and-state laws allowed a substantial reduction in the number of the free parameters necessary in the formulation of the ETAS model, bringing also a physical description of the phenomenon;
- to practically apply a rate-and-state type model as a pure epidemic one, one needs to make some simplifications for using only information contained in a catalog;

- the new ERS model performs better than the purely ETAS one on Japanese seismicity. It was not true for Californian seismicity;
- we must consider the simplified rigid dependence of the ERS model to the spatial distribution when we deal with relative small magnitude values (such as those used in the California test): the consequent small values of the source size lead to a much spread of the locations errors on likelihoods.

We believe that the preliminary study we have made on this type of new hybrid model could lead in future to some other interesting developments and results.

Much progress has been made in the last decade on the topics of stress transfer, earthquake triggering, and time dependent seismic hazard. But, at the moment, there is no general agreement on which is the most appropriate model to be used for time-varying forecasts.

In this work we presented some preliminary outcomes in estimating probability of earthquake occurrence with the RSM. The most important and original result that we found is that:

- Probability of earthquake occurrence shows an important dependence on the free parameter  $A\sigma$  of the rate-and state procedure.

We strongly believe that this topic has to be deepened in the next future.

In general we believe that the next step in probability estimations must regard a robust procedure for testing models and predictions, to develop their performances and become conscious of their reliability.

In the domain of time varying hazard and its testing procedures several problems arise (*Vere-Jones, 1995*). The estimates are likely to be strongly model dependent. An advantage is taken reducing the number of the parameters to be estimated (as we did), thus allowing the existing data to be used more effectively. We also faced with the problem of the paucity of data in the region we selected for our case study.

An ideal, proper sequence in a testing procedure is: i) model development and model validation; ii) development of time-varying risk forecasts based on the model; iii) development of earthquake alerts based on the risk forecasts to be compared with the real data. This procedure can identify the models that, despite their imperfections, can provide reliable guidelines to initiate an early warning activity.

With these aims the presented work will be undertaken in the SAFER-NERIES projects ([www.saferproject.net](http://www.saferproject.net) and [www.neriesproject.net](http://www.neriesproject.net)). The scientific issues of these projects are in full accordance with our future designs. These can be summarized as follows:

- a consensus should be found in defining background and reference seismicity and carefully analyze how to compute them as fundamental parts of triggering models.

We have just observed that the *background seismicity* should be evaluated in a fixed time window and on a declustered catalog (or on a catalog which is believed not to contain aftershock sequences). Instead, *reference seismicity* should be the seismicity rate evaluated always in a certain time window but on an undeclustered catalog. Despite the first definition is widely used in literature, we have just observed that long lasting, secondary triggering make it very difficult identifying a catalog without aftershock sequences.

- A strategy for models calibration has to be selected, that could be: a posteriori tests on real seismicity; tests on synthetic catalogs; a priori real-time applications.
- Make probability estimates obtaining comparable results (also with different models).



# Bibliography

- Akaike, H. (1974), On entropy maximization principle, *IEEE Trans. Autom. Control.*, *19*, 716–722.
- Akaike, H. (1977), *A new look at the statistical model identification*, P.R. Krishnaiah ed., 27-41 pp., Amsterdam and New York: North Holland Pub. Co.
- Aki, K., and P. Richards (1980), *Quantitative seismology, theory and methods*, vol. 1, W.H. Freeman and Company, San Francisco.
- Antonoli, A., M. Belardinelli, A. Bizzarri, and K. S. Vogfjord (2006), Evidence of instantaneous dynamic triggering during the seismic sequence of year 2000 in south Iceland, *J. Geophys. Res.*, *111*(B03302), doi:10.1029/2005JB003935.
- Beeler, N. M., R. W. Simpson, D. A. Lockner, and S. H. Hickman (2000), Pore-fluid pressure, apparent friction and Coulomb failure, *J. Geophys. Res.*, *105*, 25,533–25,554.
- Belardinelli, M., M. Cocco, O. Coutant, and F. Cotton (1999), Redistribution of dynamic stress during coseismic ruptures: evidence for fault interaction and earthquake triggering, *J. Geophys. Res.*, *104*(B7), 14,925–14,945.
- Belardinelli, M., A. Bizzarri, and M. Cocco (2003), Earthquake triggering by static and dynamic stress change, *J. Geophys. Res.*, *108*(B3), 2135, doi: 10.1029/2002JB001779.
- Boatwright, J., and M. Cocco (1996), Frictional constraints on crustal faulting, *J. Geophys. Res.*, *101*(10), 13,895–13,910.
- Bonafede, M., and A. Neri (2000), Effects induced by an earthquake on its fault plane: a boundary element study, *Geophys. J. Int.*, *141*(1), 43–56, doi: 10.1046/j.1365-246X.2000.00074.x.
- Catalli, F. (2006), Sorgenti sismiche: rappresentazione matematica ed applicazione al calcolo degli spostamenti, *Quaderni di Geofisica*, in print.

- Catalli, F., R. Console, M. Cocco, and L. Chiaraluze (2006), An application of the rate-state model for seismicity rate changes to the 1997 Umbria-Marche, Central Italy, seismic sequence, in prep.
- Chiarabba, C., and A. Amato (2003),  $v_p$  and  $v_p/v_s$  images in the  $m_w$  6.0 Colfiorito fault region (central Italy): a contribution to the understanding of seismotectonic and seismogenic processes, *J. Geophys. Res.*, *108*(B5), 2248, doi:10.1029/2001JB001665.
- Chiarabba, C., L. Jovine, and R. D. Stefano (2005), A new view of Italian seismicity using 20 years of instrumental recordings, *Tectonophysics*, *395*, 251–268.
- Chiaraluze, L. (2004), Complex normal faulting in the Apennines thrust and fold belt: the 1997 seismic sequence in the central Italy, *Bull. Seismol. Soc. Am.*, *94*, 99–116.
- Chiaraluze, L., W. ELLsworth, C. Chiarabba, and M. Cocco (2003), Imaging the complexity of an active normal fault system: the 1997 Colfiorito (central Italy) case study, *J. Geophys. Res.*, *108*(B6), 2294, doi:10.1029/2002JB002166.
- Chinnery, M. (1961), The deformation of the ground around surface faults, *Bull. Seism. Soc. Am.*, *51*, 355–372, doi:10.1046/j.1365-246X.2000.00074.x.
- Cocco, M., and J. Rice (2002), Pore pressure and poroelasticity effects in coulomb stress analysis of earthquake interactions, *J. Geophys. Res.*, *107*(B2), 2468, doi:10.1029/2002JB002130.
- Collettini, C., L. Chiaraluze, S. Pucci, M. Barchi, and M. Cocco (2005), Looking at fault inversion matching structural geology and seismology data, *J. Struct. Geol.*, *27*(5), 937–942.
- Console, R., and F. Catalli (2006), A physical model for aftershocks triggered by dislocation on a rectangular fault, in print.
- Console, R., and M. Murru (2001), A simple and testable model for earthquake cluster, *J. Geophys. Res.*, *106*, 8699–8711.
- Console, R., M. Murru, and A. Lombardi (2003), Refining earthquake clustering models, *J. Geophys. Res.*, *108*(B10), 2468, doi:10.1029/2002JB002130.
- Console, R., M. Murru, and F. Catalli (2006), Physical and stochastic models of earthquake clustering, *Tectonophysics*, *417*, 141–153.
- Cramer, C., M. Petersen, T. Cao, T. Topozada, and M. Reichle (2000), A time-dependent probabilistic seismic-hazard model for California, *Bull. Seismol. Soc. Am.*, *90*, 1–21.

- Dechamps, A., G. Iannaccone, and R. Scarpa (1983), The Umbrian earthquake (Italy) of 19 September 1979, *Annales Geophysicae*, *2*, 1,29–36.
- Dieterich, J. (1986), A model for the nucleation of earthquake slip, *Geophy. Monogr. Ser.*, *37*, 36–49.
- Dieterich, J. (1992), Earthquake nucleation on faults with rate and state dependent strenght, *Tectonophysics*, *211*, 115–134.
- Dieterich, J. (1994), A constitutive law for rate of earthquake production and its application to earthquake clustering, *J. Geophys. Res.*, *99*(18), 2601–2618.
- Dieterich, J. (1995), Earthquake simulations with time-dependent nucleation and long-range interactions, *Nonlinear Processes in Geophysics*, *2*, 109–120.
- Dieterich, J. (2000), Earthquake nucleation and its relationship to earthquake clustering, *Tech. rep.*, U.S. Geological Survey.
- Ekstrom, G., A. Morelli, E. Boschi, and A. Dzievonski (1998), Moment tensor analysis of the central Italy earthquake sequence of September-October 1997, *Geophys. Res. Lett.*, *25*, 1971–1974.
- Enescu, B., and K. Ito (2002), Spatial analysis of the frequency-magnitude distribution and decay rate of aftershock activity of the 2000 Western Tottori earthquake, *Earth Planet Space*, *54*, 847–859.
- et al., A. A. (1998), The 1997 Umbria-Marche , Italy, earthquake sequence: a first look at the main shocks and aftershocks, *Geophys. Res. Lett.*, *25*, 2861–2864.
- Felzer, K., T. W. Becker, R. E. Abercrombie, G. Ekstrom, and J. R. Rice (2002), Triggering of the 1999  $M_W$  7.1 Hector Mine earthquake by aftershocks of the 1992  $M_W$  7.3 Landers earthquake, *J. Geophys. Res.*, *107*(B9), 2190, doi: 10.1029/2001JB000911.
- Felzer, K., E. Abercrombie, and G. Ekstrom (2003), Secondary aftershocks and their importance for aftershocks forecasting, *Bull. Seismol. Soc. Am.*, *93*, 1433–1448.
- Frankel, A. (1995), Mapping seismic hazard in the central and eastern United States, *Seis. Res. Lett.*, *66*(4), 8–21.
- Gasperini, P., and G. Ferrari (2000), Deriving numerical estimates from descriptive information: the computation of earthquake parameters, *Annali di Geofisica*, *43*, 729–246.

- Gasparini, P., and B. Lolli (2006), Correlation between the parameters of the aftershock rate equation: implications for the forecasting of future sequences, *Physics of the Earth and Planetary Interiors*, 156, 41–58.
- Gomberg, J., N. Beeler, M. Blanpied, and P. Bodin (1998), Earthquake triggering by transient and static deformations, *J. Geophys. Res.*, 103(12), 24,411–24,426.
- Gomberg, J., N. Beeler, and M. Blanpied (2000), On rate-state and Coulomb failure models, *J. Geophys. Res.*, 105(14), 7857–7872.
- Gomberg, J., P. Reasenberg, P. Bodin, and R. Harris (2001), Earthquake triggering by seismic waves following the Landers and Hector Mine earthquakes, *Nature*, 411, 462–466.
- Gomberg, J., P. Reasenberg, N. Beeler, M. Cocco, and M. Belardinelli (2005a), A frictional population model of seismicity rate change, *J. Geophys. Res.*, 110(B05S03), doi:10.1029/2004JB003404.
- Gomberg, J., P. Reasenberg, N. Beeler, M. Cocco, and M. Belardinelli (2005b), Time-dependent earthquake probabilities based on population models, *J. Geophys. Res.*, 110(B05S04), doi:10.1029/2004JB003405.
- Gross, S. (2001), A model of tectonic stress state and rate using the 1994 Northridge earthquake sequence, *Bull. Seismol. Soc. Am.*, 91, 263–275.
- Gross, S., and C. Kisslinger (1997), Estimating tectonic stress rate and state with Landers aftershocks, *J. Geophys. Res.*, 102(B4), 7603–7612.
- Guatteri, M., P. Spudich, and G. Beroza (2001), Inferring rate and state friction parameters from a rupture model of the 1995 Hyogo-ken Nanbu (Kobe) Japan earthquake, *J. Geophys. Res.*, 106(B11), 26,511–26,522, doi:10.1029/2001JB000294.
- Hainzl, S., and Y. Ogata (2005), Detecting fluid signals in seismicity data through statistical earthquake modeling, *J. Geophys. Res.*, 110(B05S07), doi:10.1029/2004JB003247.
- Hardebeck, J. (2004), Stress triggering and earthquake probability estimates, *J. Geophys. Res.*, 109(B04310), doi:10.1029/2003JB002437.
- Harris, R. (1998), Introduction to special section: Stress triggers, stress shadows, and implications for seismic hazard, *J. Geophys. Res.*, 103(12), 24,347–24,358.
- Helmstetter, A. (2003), Is earthquake triggering driven by small earthquakes?, *Phys. Res. Lett.*, 91(058501).

- Helmstetter, A., and B. E. Shaw (2006), Relation between stress heterogeneity and aftershock rate in the rate-and-state model, *J. Geophys. Res.*, *111*(B07304), doi:10.1029/2005JB004077.
- Helmstetter, A., and D. Sornette (2001), Sub-critical and super-critical regimes in epidemic models of earthquake aftershocks, *AGU Fall Meeting Abstracts*.
- Helmstetter, A., Y. Kagan, and D. Jackson (2005), Importance of small earthquakes for stress transfers and earthquakes triggering, *J. Geophys. Res.*, *110*(B05S08), doi:10.1029/2004JB003286.
- Hernandez, B., M. Cocco, F. Cotton, S. Stramondo, O. Scotti, F. Courboulex, and M. Campillo (2004), Rupture history of the 1997 Umbria-Marche (central Italy) largest earthquakes from inversion of GPS, DInSAR and near field seismological data, *Ann. Geophys.*, *47*, 1355–1376.
- Iwasaki, T., and R. Sato (1979), Strain field in a semi-infinite medium due to an inclined rectangular fault, *J. Phys. Earth*, *27*, 117–123.
- Kagan, Y. Y. (2002), Aftershock zone scaling, *Bull. Seism. Soc. Am.*, *92*, 641–655, doi:10.1785/0120010172.
- Kagan, Y. Y., and D. D. Jackson (1991), Long-term earthquake clustering, *Geophys. J. Int.*, *104*, 117–133.
- Kagan, Y. Y., and D. D. Jackson (2000), Probabilistic forecasting of earthquakes, *Geophys. J. Int.*, *143*, 438–453.
- Kagan, Y. Y., D. D. Jackson, and Z. Liu (2005), Stress and earthquakes in southern California, 1850–2004, *J. Geophys. Res.*, *110*(B05S14), doi:10.1029/2004JB003313.
- Kanamori, H., and D. L. Anderson (1975), Theoretical basis for some empirical relations in seismology, *Bull. Seism. Soc. Am.*, *65*, 1073–1095.
- Keilis-Borok, V. (1959), On estimation of the displacement in an earthquake source and of source dimensions, *Annali di Geofisica*, *12*, 2,205–2,214.
- Kilb, D., J. Gomberg, and P. Bodin (2002), Aftershock triggering by complete coulomb stress changes, *J. Geophys. Res.*, *107*, doi:10.1029/2001JB0002002.
- King, G., and M. Cocco (2001), Fault interaction by elastic stress changes: New clues from earthquake sequences, *Adv. Geophys.*, *44*, 1–39.
- King, G., R. Stein, and J. Lin (1994), Static stress change and the triggering of earthquakes, *Bull. Seismol. Soc. Am.*, *84*, 935–953.

- Knopoff, L. (1957), Energy release in earthquake, *Tech. Rep. 90*, Institute of Geophysics, University of California, U.S.A.
- Kostrov, B., and S. Das (1998), *Principles of earthquake source mechanics*, Cambridge University Press.
- Kostrov, V. (1974), Seismic moment and energy of earthquakes, and seismic flow of rocks, *Izv. Acad. Sci. USSR Phys., Solid Earth*, *1*, 23–44.
- Linker, J., and J. Dieterich (1992), Effects of variable normal stress on rock friction: observations and constitutive equations, *J. Geophys. Res.*, *97*, 4923–4940.
- Lombardi, A., and W. Marzocchi (2007), Evidence of clustering and nonstationarity in the time distribution of large worldwide earthquakes, *J. Geophys. Res.*, *112*(B02303), doi:10.1029/2006JB004568.
- Lombardi, A., W. Marzocchi, and J. Selva (2006), Exploring the evolution of a volcanic seismic swarm: the case of the 2000 Izu Islands swarm, *Geophys. Res. Lett.*, *33*(L07310), doi:10.1029/2005GL025157.
- Marsan, D. (2003), Triggering of seismicity at short timescales following Californian earthquakes, *J. Geophys. Res.*, *108*(B5), 2266, doi:10.1029/2002JB001946.
- Marsan, D. (2006), Can coseismic stress variability suppress seismicity shadows? insights from a rate-and-state friction model, *J. Geophys. Res. (Solid Earth)*, *111*(B10), 6305, doi:10.1029/2005JB004060.
- Marsan, D., and S. Nalbant (2005), Methods for measuring seismicity rate changes: a review and a study of how the  $m_w$  7.3 Landers earthquake affected the aftershock sequence of the  $m_w$  6.1 Joshua Tree earthquake, *Pure Appl. Geophys.*, *162*, 1151–1185, doi:10.1007/s00024-004-2665-4.
- Mendoza, C., and S. Hartzell (1988), Aftershock patterns and main shock faulting, *Bull. Seism. Soc. Am.*, *78*, 1438–1449.
- Miller, S. A., C. Collettini, L. Chiaraluce, M. Cocco, M. Barchi, and B. Kaus (2004), Aftershocks driven by a high pressure  $CO_2$  source at depth, *Nature*, *427*, 724–727, doi:10.1038/nature02251.
- Murru, M., R. Console, and A. Lisi (2004), Seismicity and mean magnitude variations correlated to the strongest earthquakes of the 1997 Umbria-Marche sequence (central Italy), *J. Geophys. Res.*, *109*(B01304), doi:10.1029/2002JB002276.

- Nostro, C., M. Cocco, and M. Belardinelli (1997), Static stress changes in extensional regimes: an application to southern Apennines (Italy), *Bull. Seism. Soc. Am.*, *87*(1), 234–248.
- Nostro, C., L. Chiaraluce, M. Cocco, D. Baumont, and O. Scotti (2005), Coulomb stress changes caused by repeated normal faulting earthquakes during the 1997 Umbria-Marche (central Italy) seismic sequence, *J. Geophys. Res.*, *110*(B05S20), doi:10.1029/2004JB003386.
- Ogata, Y. (2005), Detection of anomalous seismicity as a stress change sensor, *J. Geophys. Res.*, *110*(B05S06), doi:10.1029/2004JB003245.
- Ogata, Y. (1983), Estimations of the parameters in the modified Omori formula for aftershock frequencies by the maximum likelihood procedure, *J. Phys. Earth*, *31*, 115–124.
- Ogata, Y. (1988), Statistical models for earthquake occurrence and residual analysis for point processes, *J. Amer. Statist. Assoc.*, *83*, 9–27.
- Ogata, Y. (1989), Statistical models for standard seismicity and detection of anomalies by residual analysis, *Tectonophysics*, *169*, 159–174.
- Ogata, Y. (1994), Detection of precursory relative quiescence before great earthquakes through a statistical model, *J. Geophys. Res.*, *97*, 19,845–19,871.
- Ogata, Y. (1998), Space-time point-process models for earthquake occurrences, *Ann. Inst. Statist. Math.*, *50*, 379–402.
- Okada, Y. (1985), Surface deformation due to shear and tensile faults in a half-space, *Bull. Seism. Soc. Am.*, *75*(4), 1135–1154.
- Okada, Y. (1992), Internal deformation due to shear and tensile faults in a half-space, *Bull. Seism. Soc. Am.*, *82*(2), 1018–1040.
- Papadimitriou, E., C. Papazachos, and T. Tsapanos (2001), Test and application of the time and magnitude predictable model to the intermediate and deep focus earthquakes in the subduction zones of the Circum-Pacific Belt, *Tectonophysics*, *330*, 45–68.
- Parsons, T. (2005), Significance of stress transfer in time-dependent earthquake probability calculations, *J. Geophys. Res.*, *110*(B05S02), doi:10.1029/2004JB003190.
- Reasenber, P., and L. Jones (1989), Earthquake hazard after a mainshock in California, *Science*, *243*, 1173–1176.

- Reasenber, P., T. Hanks, and W. Bakun (2003), An empirical model for earthquake probabilities in the San Francisco bay region, 2002-2031, *Bull. Seism. Soc. Am.*, *93*, 1–13.
- Ruina, A. (1983), Slip instability and state variable friction laws, *J. Geophys. Res.*, *88*(B12), 10,359–10,370.
- Schorlemmer, D., M. Gerstenberger, S. Wiemer, L. Field, L. Jones, and D. D. Jackson (2004), T-relm testing center: Rigorous testing of probabilistic earthquake forecast models, Seismological Society of America meeting, Lake Tahoe.
- Serpelloni, E., M. Anzidei, P. Baldi, G. Casula, and A. Galvani (2005), Crustal velocity and strain-rate fields in Italy and surrounding region: new results from the analysis of permanent and non-permanent GPS fields., *Geophys. J. Int.*, *161*, 861–880, doi:10.1111/j.1365-246X.2005.02618.x.
- Shi, Y., and A. Bolt (1982), The standard error of the magnitude-frequency b value, *Bull. Seism. Soc. Am.*, *72*(B12), 1677–1687.
- Stacy, S., S. Nalbant, J. McCloskey, C. Nostro, O. Scotti, and D. Beaumont (2005), Onto what planes should Coulomb stress perturbations be resolved?, *J. Geophys. Res.*, *110*(B05S15), doi:10.1029/2004JB003356.
- Stein, R. (1999), The role of stress transfer in earthquake occurrence, *Nature*, *402*, 605–609.
- Stein, R., A. Barka, and J. Dieterich (1997), Progressive failure on the North Anatolian fault since 1939 by earthquake stress triggering, *Geophys. J. Int.*, *128*, 594–604.
- Stein, S., and M. Wysession (2002), *An introduction to seismology, earthquakes, and Earth structures*, Blackwell Publishing.
- Team Task 4.7-S2 (2005-2007), Variazioni temporali della probabilità di accadimento di forti terremoti sulle principali strutture sismogenetiche del territorio italiano, Istituto Nazionale di Geofisica e Vulcanologia.
- Toda, S., and R. Stein (2000), Did stress triggering cause the large off-fault aftershocks of the 25 March 1998 Mw=8.1 Antarctic plate earthquake?, *Geophys. Res. Lett.*, *27*(15), 2301–2304.
- Toda, S., and R. Stein (2003), Toggling of seismicity by the 1997 Kagoshima earthquake couplet: a demonstration of time-dependent stress transfer, *J. Geophys. Res.*, *108*(B12), 2567, doi:10.1029/2003JB002527.

- Toda, S., R. Stein, P. Reasenberg, J. Dieterich, and A. Yoshida (1998), Stress transferred by the 1995 Mw=6.9 Kobe, Japan, shock: Effect on aftershocks and future earthquake probabilities, *J. Geophys. Res.*, *103*(B10), 24,543–24,566.
- Toda, S., R. Stein, K. Richards-Dinger, and S. Bozkurt (2005), Forecasting the evolution of seismicity in southern California: animations built on earthquake stress transfer, *J. Geophys. Res.*, *110*(B05S16), doi:10.1029/2004JB003415.
- Udias, A. (1999), *Principles of seismology*, Cambridge University Press.
- Utsu, T. (1969), Aftershocks and earthquake statistics (i) – investigation of aftershocks and other earthquake sequences based on a new classification of earthquake sequences, *J. of Faculty of Science, Hokkaido Univ., Series VII (Geophysics)*, *3*.
- Utsu, T., Y. Ogata, and R. Matsuura (1995), The centenary of the Omori formula for a decay law of aftershock activity, *J. Phys. Earth*, *43*, 1–33.
- Vere-Jones, D. (1969), A note on the statistical interpretation of bath's law, *Bull. Seism. Soc. Am.*, *59*, 1535–1541.
- Vere-Jones, D. (1995), Forecasting earthquakes and earthquake risk, *Int. J. of Forecasting*, *11*, 503–538.
- Westaway, R., R. Gawthorpe, and M. Tozzi (1989), Seismological and field observation of the 1984 Lazio-Abruzzo earthquakes: implications of the active tectonics of Italy, *Geophys. J. Int.*, *98*, 489–514.
- Wiemer, S. (2000), Introducing probabilistic aftershock hazard mapping, *Geophys. Res. Lett.*, *27*(20), 3405–3408.
- Wiemer, S., and K. Katsumata (1999), Spatial variability of seismicity parameters in aftershock zones, *J. Geophys. Res.*, *104*(B6), 13,135–13,152.
- Wiemer, S., and M. Wyss (2002), Spatial and temporal variability of the b-value in seismogenic volumes, *Adv. Geophysics*, *45*, 259–302.
- Wiemer, S., M. Gerstenberger, and E. Hauksson (2002), Properties of the Aftershock Sequence of the 1999 Mw 7.1 Hector Mine Earthquake: implications for aftershock hazard, *Bull. Seism. Soc. Am.*, *92*(4), 1127–1240.
- Wiemer, S., M. Cocco, G. Gruenthal, I. Main, W. Marzocchi, M. Gerstenberger, and D. Schorlemmer (2005), Towards an European framework for testing earthquakes forecasts, *Tech. Rep. 23*, ISM report on Research and Education.

- 
- Yamanaka, Y., and K. Shimazaki (1990), Scaling relationship between the number of aftershocks and the size of the mainshock, *J. Phys. Earth.*, *38*, 305–324.
- Zhuang, J., Y. Ogata, and D. Vere-Jones (2004), Analyzing earthquake clustering features by using stochastic reconstruction, *J. Geophys. Res.*, *109*(B05031), doi:10.1029/2003JB002879.
- Ziv, A., and A. Rubin (2000), Static stress transfer and earthquake triggering; no lower threshold insight?, *J. of Geophys. Res.*, *105*, 13,631–13,642.
- Ziv, A., and A. M. Rubin (2003), Implications of rate-and-state friction for properties of aftershock sequence: Quasi-static inherently discrete simulations, *J. of Geophys. Res.*, *108*, 2051, doi:10.1029/2001JB001219.

# Curriculum Vitae

- **Contact Information**

Flaminia Catalli

*Office*

Dipartimento di Sismologia e Tettonofisica  
Istituto Nazionale di Geofisica e Vulcanologia  
Via di Vigna Murata 605, 00142, Roma, Italy

Tel.: +39 06 51860571

E-mail: catalli@ingv.it

*Home*

Viale Pico della Mirandola 129 F, 00142, Roma, Italy

Tel.: +39 06 54602416

- **Biographical Data**

Birth date: March 14, 1977

Place of birth: Roma, Italy

Citizenship: Italian

Languages: Italian (mother tongue), English (good knowledge), French (fluent)

- **Education**

*January 2004 - Present*

PhD student, Department of Physics, Sector of Geophysics,

*Università di Bologna Alma Mater Studiorum*

Supervisors: Dr. Massimo Cocco and Dr. Rodolfo Console Supervising

Professor: Prof. Maria Elina Belardinelli Chairperson of the PhD School:  
Prof. Michele Dragoni

*September 2003*

Degree in Physics, 101/110,

*Università degli Studi di Roma Tre*

Title of the final year dissertation (Tesi di Laurea):

*Un modello fisico di interazione fra terremoti*

Supervisor: Dr. Rodolfo Console

*A.A. 1999-2000*

ERASMUS fellow

*Université Joseph Fourier, Grenoble, France*

I attended and passed the exams (in French language) of the following courses: Mathématique, Climat, Géophysique, Télédétection, Travaux Pratiques du Terrain. I also conducted an intership at the Institute de Recherche pour l'Ingénierie de l'Agriculture et de l'Environnement (CEMAGREF), Grenoble, France, and I produced a thesis entitled: *Etude Préliminaire de la Répartition Spatiale des Précipitation Liquides sur le Bassin Glaciaire de Sarennes* (A Preliminary Study on the Spatial Repartition of Rainfall in the Sarennes Glacial Basin )

*July 1996*

Leaving Certificate (Diploma di Maturità Classica) obtained at

*Liceo Terenzio Mamiani, Rome,*

grade 48/60

- **Additional Education**

*October 18-24, 2006*

School of Geophysics, 26° Erice workshop: “Earthquake and shaking probabilities: helping the society to make the right choice”, organized at the Ettore Majorana Foundation and Centre for Scientific Culture, Erice (PA), Italy

*January 9-13, 2006*

The 4th International Workshop on Statistical Seismology (Statsei4), Japan. See <http://www.ism.ac.jp/ogata/Statsei4/index.html>

*January-March, 2005*

Course “Modelli Numerici in Fisica (Numerical Models in Physics)” at Department of Physics E. Amaldi, Roma Tre University, Rome, Italy (60

hours)

*15-20 April, 2005*

European Geosciences Union, General Assembly in Vienna, Austria

*15-18 February, 2005*

Course “Elementi di Dinamica non Lineare: Stabilità, Biforcazioni e Caos (Nonlinear Dynamics and Chaos)”, organized by Società Italiana Caos e Complessità (SICC) at Fondazione Eni Enrico Mattei (FEEM), in collaboration with the Department of Information Science and Electronic of Politecnico di Milano, Milano, Italy

*12-13 May, 2004*

Workshop: “Non Linear Models and Statistical Analysis in Seismology: Chaos, Fractals and Self-Organization”, Cetraro (CS), Italy

- **Teaching Experience**

*Present*

Teaching assistant,  
Department of Physics,  
Università degli Studi di Roma Tre  
Course: “Seismology”  
Supervisor: Dr. Rodolfo Console

*A.A. 2005-2006*

Teaching assistant (20 hours),  
Department of Physics,  
Università degli Studi di Roma Tre  
Course: “Seismology”  
Supervisor: Dr. Rodolfo Console

*14-19 March 2005*

Collaborated to the “XV Settimana Scientifica e Tecnologica” at Istituto Nazionale di Geofisica e Vulcanologia (INGV) promoted by the MIUR (Ministero Istruzione Università e Ricerca)

*January-May 2005*

Collaborated to the project “ASTROSCI” for the teaching and the divulgation of the Astronomy and the Natural Sciences in the schools in collaboration with Department of Physics E. Amaldi of Roma Tre University,

Rome, Italy, and Ministero Istruzione Università e Ricerca (MIUR).

- **Publications**

1. Catalli F.,  
*Sorgenti Sismiche: rappresentazione matematica ed applicazione al calcolo degli spostamenti*,  
Quaderni di Geofisica, in print.
2. Console R. and Catalli F.,  
*A rate-state model for aftershocks triggered by dislocation on a rectangular fault: a review and new insights*,  
Annals of Geophysics, in print.
3. Console R. , Murru M. , Catalli F. and Falcone G.,  
*Real time forecasts through an earthquake clustering model constrained by the rate-and-state constitutive law compared with a purely stochastic ETAS model*,  
Seismological Research Letters,  
preprint available <http://www.RELM.org>.
4. Console R. , Murru M. and Catalli F.,  
*Physical and stochastic models of earthquake clustering*,  
Tectonophysics 417 (2006) 141-153.
5. Catalli F., Console R., Cocco M. and Chiaraluce L.,  
*An application of the rate-state model for seismicity rate changes to the 1997 Umbria-Marche, Central Italy, seismic sequence*, in prep.
6. Console R., Murru M., Falcone G. and Catalli F.,  
*Effect of stress interaction on the probability of occurrence of characteristic earthquakes in Central Appennines*, in prep.

- **Proceedings**

1. Catalli F. and Console R.,  
*An application of the Dieterich model for seismicity rate change to the 1997 Umbria-Marche, central Italy, seismic sequence*,  
ISM Report on Research and Education No.23, January 2006.
2. Console R., Murru M. and Catalli F.,  
*Applying the rate-and-state friction law to an epidemic model of earthquake clustering*,  
ISM Report on Research and Education No.23, January 2006.
3. Murru M., Console R., Catalli F. and Falcone G.,  
*Application of physical and stochastic models of earthquake clustering*

- to regional catalogs,*  
ISM Report on Research and Education No.23, January 2006.
4. Cocco M., Chiaraluce L. and Catalli F.,  
*Seismicity migration and time-dependent stress transfer: supporting and conflicting evidence from Umbria-Marche (Central Italy) seismic sequence,*  
ISM Report on Research and Education No.23, January 2006.
  5. Console R. and Catalli F., *A physical model for aftershocks triggered by dislocation on a fault,*  
Geophysical Research Abstracts, Vol. 7, 05503, 2005,  
SRef-ID: 1607-7962/gra/EGU05-A-05503  
European Geosciences Union 2005.
  6. Console R. , Murru M. and Catalli F.,  
*Optimizing the Parameters of the Rate-and-State Constitutive Law in an Earthquake Clustering Model*  
2004 Eos Trans. AGU 85(47), Fall Meet. Suppl., Abstract S21C-06.
  7. Console R., Catalli F, Leggeri M. and Colangelo A., *Effect of stress interaction on the probability of occurrence of characteristic earthquakes in southern appennines,*  
2006 AGU, Abstract 7223.
  8. Falcone G., Murru M, Console R. and Catalli F., *Probabilità di occorrenza di un grande terremoto con l'ausilio di modelli fisici*  
GNGTS 2006.